AALBORG UNIVERSITY

MASTER'S THESIS

Elasto-plastic concrete beam analysis by 1-dimensional Finite Element Method

Authors:
Niels F. Overgaard
Martin B. Andreasen

Supervisors:
Johan Clausen
Lars V. Andersen

A thesis submitted in fulfilment of the requirements for the degree of M.Sc. in Engineering

in the

Department of Civil Engineering

June 6, 2016

School of Engineering and Science
Study board of Civil Engineering
Fibigerstræde 10
9220 Aalborg Øst
Phone: 99 40 84 84
http://www.byggeri.aau.dk

AALBORG UNIVERSITY
STUDENT REPORT

Title: Elasto-plastic concrete beam analysis by 1-dimensional Finite Element Method
Project period: Fall 2015 to spring 2016
Supervisors: Lars Vabbersgaard Andersen
Johan Clausen

Number of pages: 92
Delivered: 08-06-2016

Synopsis:
This project focuses on analysis of reinforced concrete beams using the finite element method. A program developed in MatLab is compared with the commercial software program Abaqus in the study of a reinforced concrete beam structure. The comparison showed good results for the MatLab program, which ability to evaluate reinforced concrete structures was promising as the deviation between the programs results were minor.
The dynamic study showed the difference between analysing a structure purely elastic and implementing plasticity in the calculations. This analysis showed a dissipation in energy when the material is becoming plastic, decreasing the vibrations created from the load.

Martin Bundgaard Andreasen

Niels Færch Overgaard

Preface

This report presents the master thesis from the master program in *Structural and Civil Engineering* at Aalborg University. The report is written by Niels Færch Overgaard and Martin Bundgaard Andreasen. The subject is "*Elasto-plastic concrete beam analysis by 1-dimensional Finite Element Method*". The project was done over two semesters during the fall semester 2015 and the spring semester 2016 and delivered on 10.06.2016. The project was supervised by Johan Clausen and Lars Andersen.

Reading guidelines

The bibliography is a collection of the references used throughout the report and can be found in the back of the report. Here, all sources are presented with the needed information. Sources are presented via the *Harvard Method*. A reference is given as: [Author, Year].

For each chapter in the main report, tables, figures and equations are given reference numbers corresponding to the current chapter. For better understanding of the reader, commentary text is added to each table and figure.

Appendices, for a better understanding of parts of the main report, are found in the back of the report. Further, a digital appendix is placed on a CD, attached to the report. The digital appendix consist of MatLab scripts and the report as a PDF version.

Notations

A	Area
$[\mathbf{B}]$	Strain interpolation matrix
$[\mathbf{c}]$	Damping matrix
C_y	Centroid
$[\mathbf{D}]$	Constitutive matrix
$\{d\}$	displacement vector
E	Young's modulus
F	Force
$\{f\}$	Force vector
f_c	Yield stress in comression
f_t	Yield stress in tension
f_u	Ultimate stress
f_y	Yield stress
I	Moment of inertia
I_1	First invariant of the stress tensor
J_2	Second invariant of the deviatoric stress tensor
$[\mathbf{k}]$	Stiffness matrix
L	Length
M	Moment
$[\mathbf{m}]$	Mass matrix
N	Axial force
np_x	Integration points in x direction
np_y	Integration points in y direction
q	Transverse force
q_z	Line load
R	Restoring force
r	Residual force

$[\mathbf{T}]$	Transformation matrix
t	Time
x_e	local x coordinate
V	Shear force
v	Transverse displacement
u	Displacement
u_0	Axial deformation at beam axis
$\dot{u}$	Velocity
$\ddot{u}$	Acceleration
y_0	y coordinate of neutral axis
y_e	local y coordinate
σ	Stress
σ_0	Uniaxial yield stress
σ_m	Mean stress
σ_e	Equivalent stress
σ_1	Stress in principal direction 1
σ_2	Stress in principal direction 2
ε	Strain
ε_c	Strain at yield stress in compression
ε_u	Strain at ultimate stress
ε_t	Strain at yield stress in tension
ε_0	Strain at beam axis
θ	Rotation
κ	Curvature
κ_{el}	Maximum elastic curvature
α	Material parameter
Φ	Shape function
ξ	Local coordinate system for element
β	Parameter for Newmark-β method
γ	Parameter for Newmark-β method
ρ	Density

ν	Poisson's ratio

Contents

Chapter 1

Introduction

In practical engineering, time is the one of the most important factors in designing structures, foundations, etc. The time of an engineer should be spend efficiently, avoiding waiting for longer periods on results from software calculations. This problem is easily resolved by granting the engineer more computational power, but this is often expensive and limited by today's technology. Instead, the modelling of the structure should be assessed in terms of efficiency, which could be computational time versus accuracy. Thus, it is advantageous to develop models with a certain degree of accuracy living up to today's expectations of good engineering practice, but time efficient so that the waiting for results is minimized.

Concrete is a worldwide used construction material, which the construction industry has good experience with. Concrete has widely different strength characteristics for compression and tension, which is why it is often reinforced with steel bars. This combination makes a complex behaviour of reinforced concrete structures as concrete is a nonlinear behaving material and steel has a relatively large range of linear elastic material behaviour. As a consequence, reinforced concrete structures is often designed based on an elastic distribution of forces. This project will illuminate a method of dealing with elasto-plastic calculations of e.g. concrete structures, without performing heavy calculations in complex 3D models.

It was mentioned, that concrete has a nonlinear behaviour, but concrete is also a plastic material, which means some of the deformation is permanent and cannot be restored. An example of concrete behaviour is sketched in Figure 1.1.

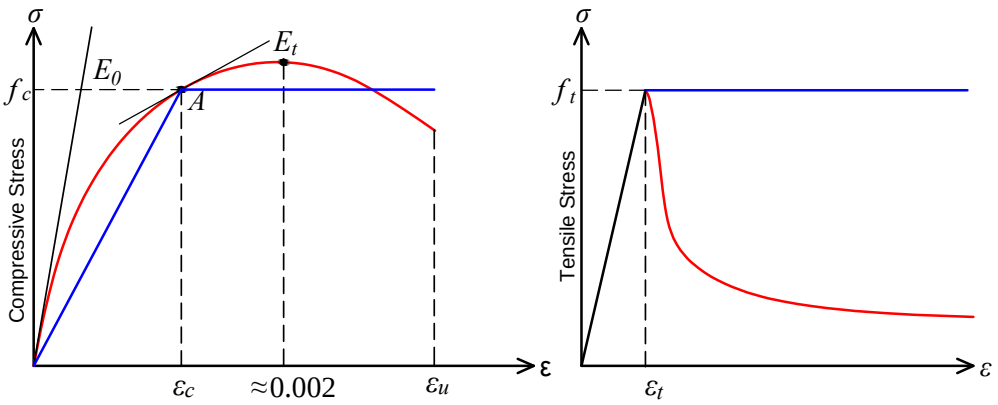

Figure 1.1: Stress - strain curves, Concrete.

The real behaviour of concrete is indicated by the red lines, where the blue lines are simplifications. First, the simplifications are applied to model the behaviour of concrete. Later on, the real behaviour is modelled via more complex material models like Drucker-Prager.

Steel has a more tangible behaviour with a pure elastic region and a pure plastic region. This is not the real behaviour of steel but is though a good estimate of steel behaviour. This is sketched in Figure 1.2.

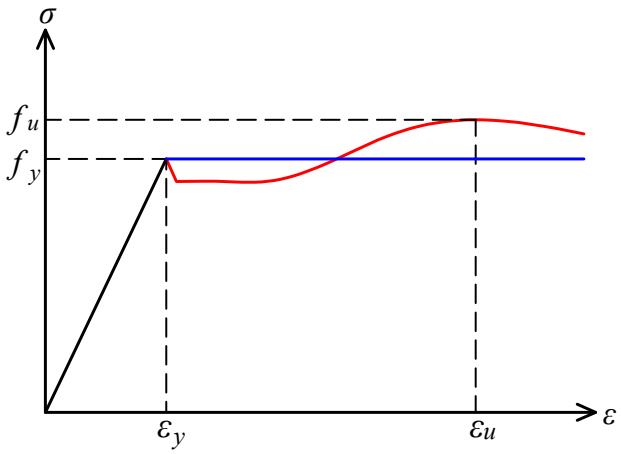

Figure 1.2: Stress - strain curve, Steel.

The real σ-ε curve for steel, indicated by the red line, has an ultimate strength due to strain hardening. The estimation, indicated by the blue line, is a perfect elasto-plastic approximation which do not consider any change in stresses once yielding has occurred.

The design basis of reinforced concrete structures can be carried out analytically

as well as for many other types of materials. Analytical solutions are often faster executed and easier to handle than complex numerical models. Also, analytical approaches are widely used and accepted as applicable methods of designing structures.

The material models shown earlier are not normally applicable in the beam element method. Thus, an elasto-plastic beam element is implemented to handle plastic behaviour. This beam element also includes the possibility of applying asymmetric cross sections.

Project description

This project can roughly be divided into two parts. Firstly, the main part is developing a program in MatLab capable of calculating reinforced concrete structures by use of one-dimensional finite element models. one-dimensional models are often carried out by use of beam elements in terms of Bernoulli-Euler or Timoshenko assumptions, and this is also the case in this project.

The MatLab program will then be compared with other methods of analysing reinforced concrete structures. These other approaches will be an analytical method and a numerical three-dimensional method by using Abaqus, which is a commercial software for analysing structures by the finite element method.

The comparison will be carried out for a simply supported beam as illustrated in Figure 1.3.

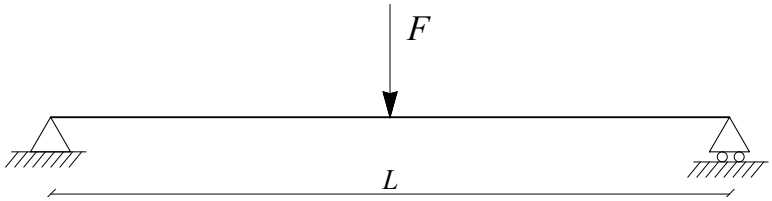

Figure 1.3: Simple supported beam.

This system is chosen for the simplicity. Comparing two models with different complexity gives more reliable results if the model is as simple as possible. The considered cross section of the beam is a rectangular reinforced concrete cross section as illustrated in Figure 1.4.

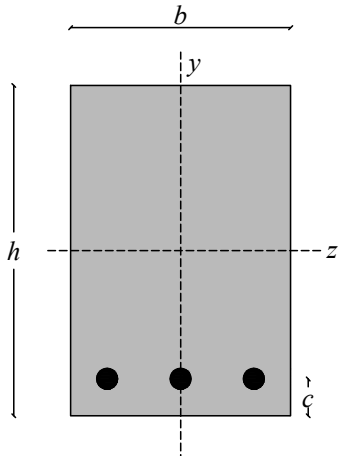

Figure 1.4: Beam cross section.

The simple rectangular cross section is chosen for the same reason as the system, namely to make the model as simple as possible. The benchmark cross section values chosen for all calculations throughout the report, are given in Table 1.1.

Height, h	300 mm
Width, b	200 mm
Length, L	3000 mm
Reinforcement bars	3 ø12
Distance from bar to bottom, c	50 mm

Table 1.1: Benchmark cross section values.

Part I

Static finite-element analysis

Chapter 2

Beam theory

The Bernoulli-Euler beam theory forms the basic foundation of the calculations made throughout most of this report.

2.1 Bernoulli-Euler beam theory

In this section the Bernoulli-Euler beam theory in incremental formulation with an arbitrary beam axis is present. First of all the basic assumption is stated that plane sections remain plane and perpendicular to the neutral axis. Thus, no shear deformation is considered.

Equilibrium

The equilibrium equations consists of two equations, namely vertical- and moment equilibrium, see Figure 2.1. Vertical equilibrium:

$$q_z = \frac{dV}{dx}. \tag{2.1}$$

Moment equilibrium:

$$V = \frac{dM}{dx}. \tag{2.2}$$

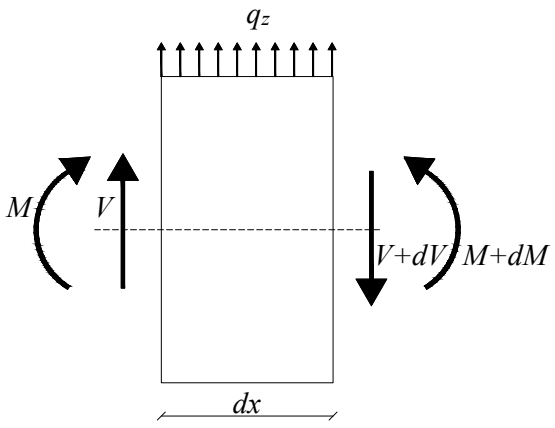

Figure 2.1: Vertical- and moment equilibrium for small beam element.

Normal strains

Considering a small section of the beam, as illustrated in Figure 2.2, with a rectangular cross section and the x axis placed in the beam axis going through the neutral point of the cross section.

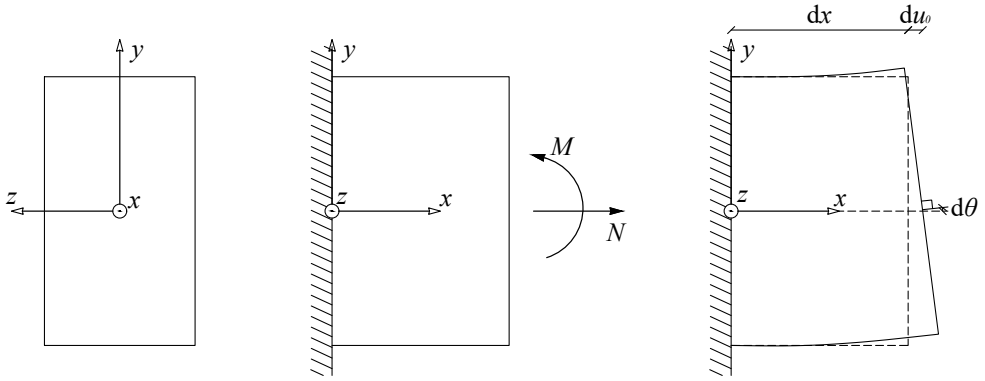

Figure 2.2: Cross section, beam section with internal forces and beam section with deformation.

The beam axis can be positioned as wished in the beam element, so the coordinate system can be defined in any way. In this project, the Cartesian coordinate system is used, where the beam axis is located at the x axis ($y = 0$ and $z = 0$). This is illustrated in Figure 2.3.

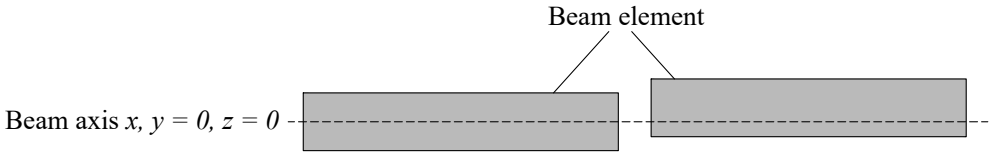

Figure 2.3: Location of beam axis in beam element.

Considering the two different approaches in Figure 2.3, the deformation at the beam axis will change depending on the position of the coordinate system. In this project the beam axis will be positioned in the elastic neutral point of the cross section.

The relation between strains and deformations is described by Poulsen og Olesen [2015] and is presented in the following. The axial deformation can be written as

the displacement at the right edge of the beam section:

$$\mathrm{d}u_x(y) = \mathrm{d}u_0 - \mathrm{d}\theta\, y. \tag{2.3}$$

Where $\mathrm{d}u_0$ is the displacement increment at the beam axis, and $\mathrm{d}\theta$ is the angle increment, which the cross section is rotated from the original cross section. The strain of a beam fibre is found as

$$\varepsilon_x(y) = \frac{\mathrm{d}u_x}{\mathrm{d}x} = \frac{\mathrm{d}u_0}{\mathrm{d}x} - \frac{\mathrm{d}\theta}{\mathrm{d}x}\, y. \tag{2.4}$$

The derivatives of u_0 and θ are called beam strains and are indicated by ε_0 and κ respectively. The rotation can generally be described as

$$\theta = \frac{\mathrm{d}u_y}{\mathrm{d}x}. \tag{2.5}$$

The curvature is the change in rotation per longitude unit. With the definition from Eq. (2.5) the curvature can be defined as

$$\kappa = \frac{\mathrm{d}^2 u_y}{\mathrm{d}x^2}. \tag{2.6}$$

The normal strain is found as

$$\varepsilon_x(y) = \varepsilon_0 - \kappa\, y. \tag{2.7}$$

This linear strain increment is only valid for small strains. The strain increments are distributed as illustrated in Figure 2.4.

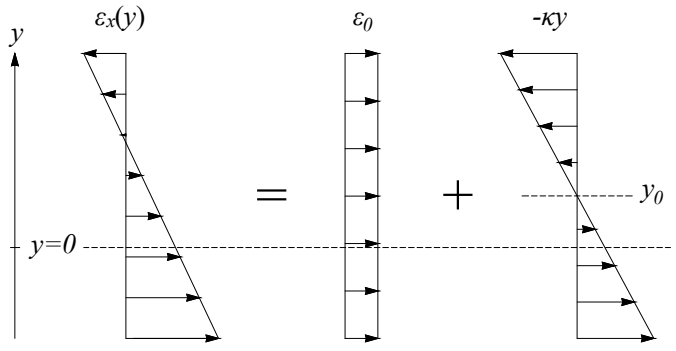

Figure 2.4: Distribution of normal strains for arbitrary beam axis.

As said, the beam axis $y = 0$ is set to the elastic neutral axis when the calculations

are initiated. This implies that $y_0 = 0$, when the behaviour is elastic. When the material starts yielding y_0 will differ from zero.

Normal stresses

For a linear elastic material the stress is given by Hooke's law. The stress in a beam fibre can then be described as

$$\sigma_x(y) = E(y)\,\varepsilon_x(y) = E(y)\left(\frac{\mathrm{d}u_x}{\mathrm{d}x} - \frac{\mathrm{d}\theta_z}{\mathrm{d}x}y\right) = E(y)\,\varepsilon_0 - E(y)\,\kappa y. \tag{2.8}$$

The stress distribution in the beam section is represented by the internal force increments N and M, see Figure 2.5.

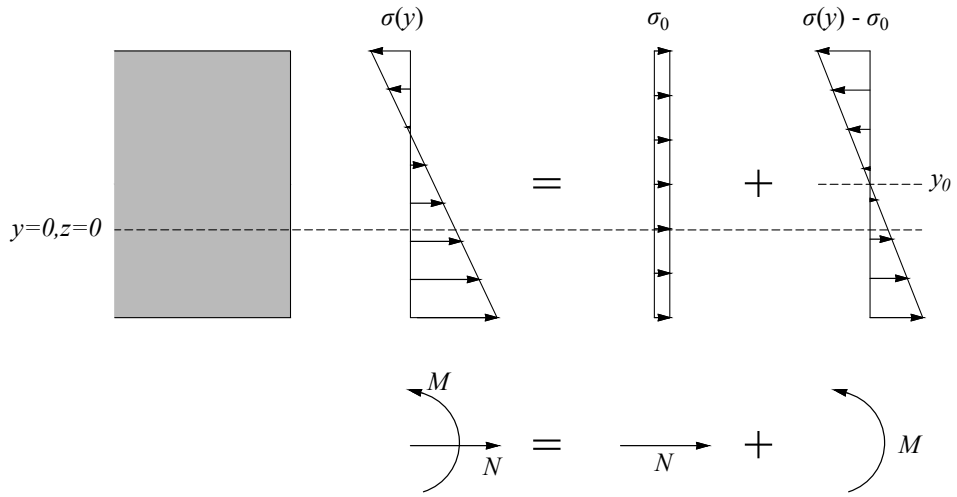

Figure 2.5: Distribution of normal stresses from normal force and moment.

Cross section integration

To obtain the equivalent state of normal stresses and internal forces, the integral of the normal stresses over the cross section must be equal to the normal forces and the integral of the normal stresses moment around the z axis, which is determined by the choice of the location of the beam axis, see Figure 2.2. The integral is done over the cross sectional area:

$$N = \int_A \sigma_x(y)\,\mathrm{d}A = \int_y\int_z \sigma_x(y)\,\mathrm{d}z\,\mathrm{d}y \tag{2.9}$$

$$M = \int_A \sigma_x(y)\,y\,\mathrm{d}A = \int_y\int_z \sigma_x(y)\,y\,\mathrm{d}z\,\mathrm{d}y \tag{2.10}$$

For elastic cases, the relations can be expanded to

$$\begin{aligned} N &= \int_y \int_z (E\ \varepsilon_0 - E\ \kappa y)\ \mathrm{d}z\ \mathrm{d}y \\ &= \left(E\ A \frac{\mathrm{d}u_x}{\mathrm{d}x} - \int_A E\ y\ \mathrm{d}A \frac{\mathrm{d}\theta_z}{\mathrm{d}x} \right), \end{aligned} \tag{2.11}$$

$$\begin{aligned} M &= \int_y \int_z (E\ \varepsilon_0 - E\ \kappa y)\ y\ \mathrm{d}z\ \mathrm{d}y \\ &= \left(- \int_A E\ y\ \mathrm{d}A \frac{\mathrm{d}u_x}{\mathrm{d}x} - \int_A E\ y^2\ \mathrm{d}A \frac{\mathrm{d}\theta_z}{\mathrm{d}x} \right). \end{aligned} \tag{2.12}$$

For plastic cases, an incremental formulation can be applied:

$$\mathrm{d}N = \int_y \int_z (E_t\ \mathrm{d}\varepsilon_0 - E_t\ \mathrm{d}\kappa\ y)\ \mathrm{d}z\ \mathrm{d}y \tag{2.13}$$

$$\mathrm{d}M = \int_y \int_z (E_t\ \mathrm{d}\varepsilon_0 - E_t\ \mathrm{d}\kappa\ y)\ y\ \mathrm{d}z\ \mathrm{d}y. \tag{2.14}$$

Only normal force $\mathrm{d}N$ and bending moment $\mathrm{d}M$ are found. The shear force must be found be equilibrium and is not related to the beam strains.

The integral of the stresses caused by bending must be equal to zero:

$$\int_A (\sigma_x(y) - \sigma_0)\ \mathrm{d}A = \int_A E_t\ (-\kappa\ y)\ \mathrm{d}A = 0, \tag{2.15}$$

where σ_0 is the stress at the beam axis $y = 0$. The integral of the stresses caused by axial deformation must be equal to the normal force:

$$\mathrm{d}N = \int_A E_t\ \mathrm{d}\varepsilon_0\ \mathrm{d}A. \tag{2.16}$$

Governing equations

Combining the above relations and definitions of equilibrium, cross section integration, material law and kinematics, the governing equation for the beam can be

expressed as:

$$\text{Rotation (Kinematic condition):}\quad \theta = \frac{\mathrm{d}u_y}{\mathrm{d}x}, \tag{2.17}$$

$$\text{Bending moment (Static equivalence):}\quad M = \int_y E\, y^2\, \mathrm{d}y\, \frac{\mathrm{d}^2 u_y}{\mathrm{d}x^2}, \tag{2.18}$$

$$\text{Shear force (Static equivalence):}\quad V = \int_y E\, y^2\, \mathrm{d}y\, \frac{\mathrm{d}^3 u_y}{\mathrm{d}x^3}, \tag{2.19}$$

$$\text{Loading (Differential equation):}\quad q_z = \int_y E\, y^2\, \mathrm{d}y\, \frac{\mathrm{d}^4 u_y}{\mathrm{d}x^4}. \tag{2.20}$$

On matrix form this can be presented as

$$\begin{Bmatrix} N \\ M \end{Bmatrix} = \begin{bmatrix} \int_A E\, \mathrm{d}A & -\int_A Ey\, \mathrm{d}A \\ -\int_A Ey\, \mathrm{d}A & \int_A Ey^2\, \mathrm{d}A \end{bmatrix} \begin{Bmatrix} \frac{\mathrm{d}u_x}{\mathrm{d}x} \\ \frac{\mathrm{d}\theta_z}{\mathrm{d}x} \end{Bmatrix}. \tag{2.21}$$

With these equations it is possible to analyse a beam by a fully analytical approach.

Material law and material models

Plasticity is described as non-recoveable deformation of the material and leaves permanent strains in the beam when it is unloaded. Thus, Hooke's law is not sufficient to describe the behaviour. An assumption can be made, as mentioned in Chapter 1, to describe the material elasto-plasticly. The material now behaves linear elastic until yielding and then becomes perfect plastic. This is a good way of describing steel behaviour without drifting to far from the real behaviour. For concrete, it is still a rough assumption to assume linear elastic - perfectly plastic behaviour.

Drucker-Prager criterion

Constructing more realistic material models for concrete can be done by use of material models like Drucker-Prager. Krabbenhøft [2002] describes the Drucker-Prager criterion as a modified von Mises criterion:

$$f(I_1,J_2) = \sqrt{J_2} + \alpha I_1 - k. \tag{2.22}$$

Where I_1 and J_2 are invariants and α, k are material parameters. The Drucker-Prager may also be written in terms of stresses:

$$f(\sigma) = \sigma_e + \alpha\sigma_m - \sigma_0. \tag{2.23}$$

Where σ_e is the equivalent stress, σ_0 is uniaxial yield stress and σ_m is the mean stress. The mean stress is given by:

$$\sigma_m = I_1 = \frac{1}{3}(\sigma_x + \sigma_y + \sigma_z). \tag{2.24}$$

The modification compared to the von Mises criterion allows setting a limit for positive mean stresses, which is tensile stresses. The material is on the other hand strengthened by superposition of the negative mean stress.

Yield surface

As said, plasticity is considered when the material is yielding. This can be described using Figure 2.6.

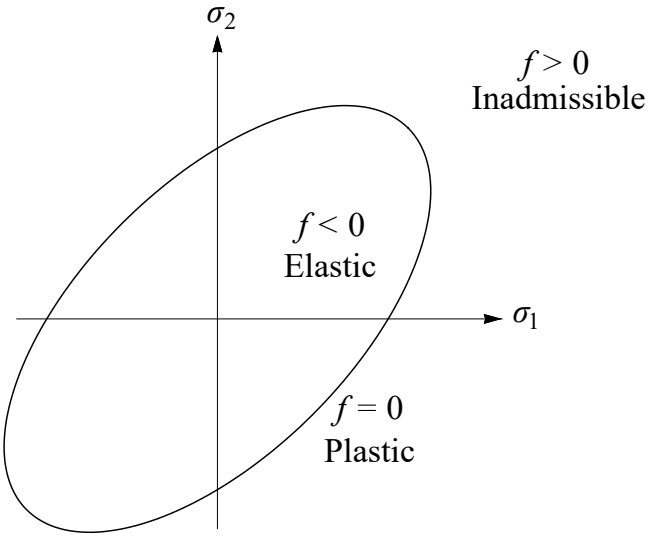

Figure 2.6: Yield surface.

The yield surface is defined as a function f, which has three possible outcomes, as seen in Figure 2.6. For $f < 0$, the behaviour is elastic and is located inside the yield surface. For $f > 0$, outside the yield surface, is an inadmissible state which cannot occur. For $f = 0$, the behaviour is plastic. [Krabbenhøft, 2002]

In this report, the yield surface is simplified even more. For 1-dimensional yield-

ing, the uniaxial yielding limits are sufficient to describe the behaviour. Thus, only compressive yielding and tensile yielding are needed to defined the yielding "surface". Thus, the Drucker-Prager criterion is not applied directly, but only the concept is used to model the material behaviour in this project.

2.2 Elasto-plastic bending

When beams are loaded beyond their yield strength, plastic behaviour will occur as stated earlier, see Figure 1.2. The simplest case of yielding is obtained by observing an axially loaded bar. In this case all points in the bar are subjected to the same stress, which leads to simultaneous yielding throughout the bar.

The case is different for beam members subjected to bending. Now the stresses vary across the cross section and, depending on the applied load, along the length. The variation of stresses across the cross section is sketched in Figure 2.7.

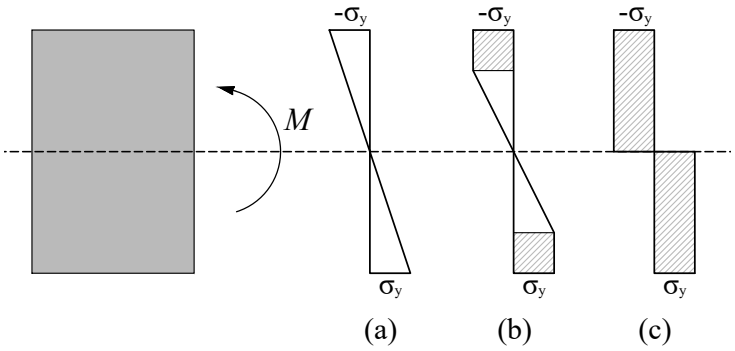

Figure 2.7: Stages in yield of a cross section.

As long as the stress has not reached the yield stress f_y, the stresses vary linearly as stage (a) indicates. Here the stresses at the top and bottom has just reached the yield stress. If further loading is applied, the stress variation will grow into stage (b). The hatched part indicates constant stress in the outer yielded region, the inner region still has a linear variation of stresses which has an elastic behaviour. At some point the entire cross section will yield and is not able to sustain any further increase in moment. Stage (c) is fully plastic, the corresponding moment is called the plastic moment M_p.

2.2.1 Plastic moment

When the stress in a single point of the cross section reaches yielding, the use of the elastic bending stiffness *EI* to analyse bending stresses is no longer valid

as the assumption of complete linear elastic cross section is violated. Instead, the moments of the cross section are used to analyse the bending stresses. This section is based on [Williams og Todd, 1999].

The stress diagram can for partially yielded sections be divided into a triangular parts and rectangular parts, see Figure 2.8. These parts are as earlier stated the elastic and plastic part, respectively.

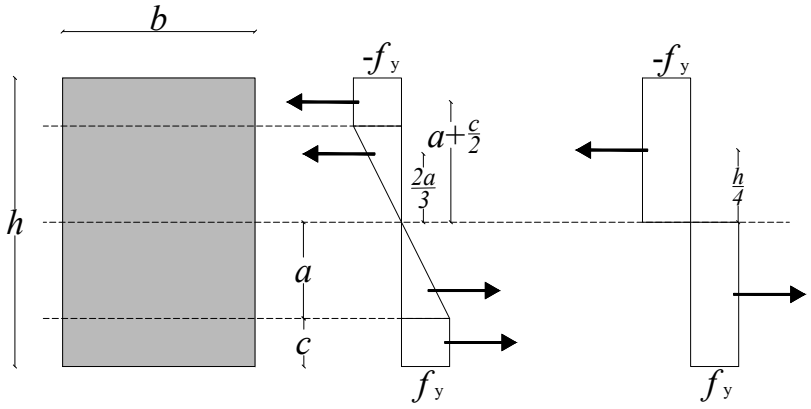

Figure 2.8: Stresses in partially- and fully yielded symmetric cross section.

Taking moment of the forces around the neutral axis gives

$$M = \int_A \sigma_x \, y \, \mathrm{d}A = \left[\frac{f_y ab}{2} \frac{2a}{3} + f_y cb \, \left(a + \frac{c}{2} \right) \right]. \tag{2.25}$$

For fully yielded rectangular cross sections, the moment simplifies to

$$M_p = 2 \, \frac{f_y bh}{2} \, \frac{h}{4} = f_y \frac{bh^4}{4}. \tag{2.26}$$

Figure 2.9 shows the behaviour of a beam with the dimensions b = 200 mm, h = 300 mm, f_y = 235 MPa and $E = 2.1 \times 10^6$ MPa. Here M is the bending moment and κ is the curvature.

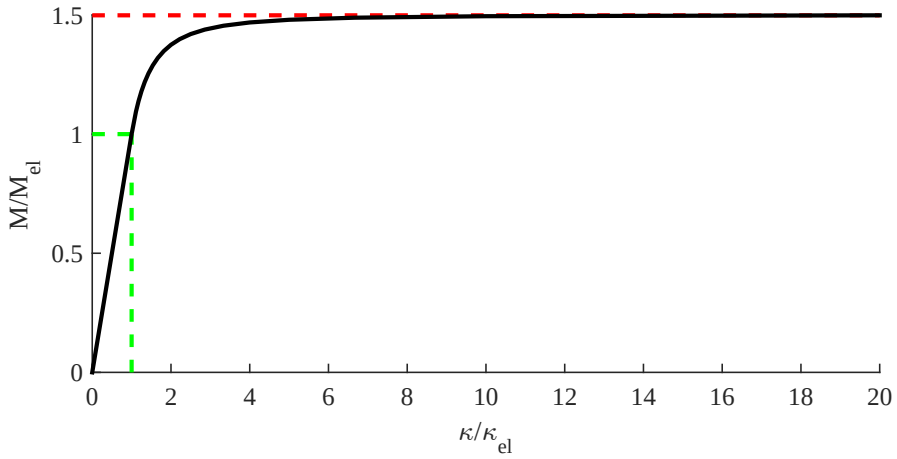

Figure 2.9: M - κ curve normalized.

For the given cross section, the behaviour until the curve reaches the dotted green lines, indicating the yielding moment of the material, is fully linear elastic. After reaching yielding, the behaviour is a combination of elastic and plastic deformation. The red dotted lines indicates some final value of yielding, in this case the cross section is fully plastic.

The maximum moment is used to find the maximum force which a simple supported beam with a perfect elasto-plastic continuous material can be subjected to. This force is then used as a benchmark for future numerical FE calculations to compare the MatLab program to analytical solutions. The plastic moment and the ultimate force capacity are given in table 2.1.

Table 2.1: Results from analytical calculations on elasto-plastic cross section.

Plastic moment, M_p	10.6×10^8 Nmm
Maximum force capacity, F	14.1×10^5 N

2.3 Bending capacity of reinforced concrete beams

The bending capacity of a reinforced beam is found analytically and used as a benchmark for the numerical calculations. In the calculations, no safety factors will be applied in any of the models. This section is based on [Jensen, 2012].

For the chosen cross section seen in Figure 1.4 (p. 4), the following specifications are applied:

Table 2.2: Beam properties.

	Yield strength f_c/f_t	Young's modulus E
Concrete	30 MPa / 3 MPa	30×10^3 MPa
Steel	550 MPa	210×10^3 MPa

First, the elastic neutral axis is found as illustrated in Figure 2.10.

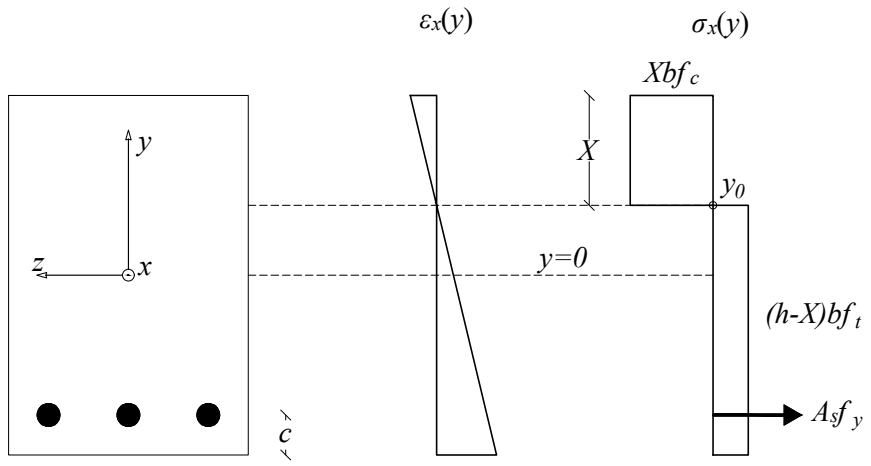

Figure 2.10: Horizontal equilibrium of concrete cross section subjected to pure bending.

Next, the horizontal equilibrium is set up to find the compressive zone x:

$$Xbf_c = (h-X)bf_t + A_s f_y, \tag{2.27}$$

$$X = \frac{A_s f_y + bhf_t}{bf_c + bf_t}. \tag{2.28}$$

The plastic moment is then found from taking moment around the elastic neutral axis:

$$M_p = A_s f_y (y_0 - c) + (y_0 b f_t)\frac{y_0}{2} - ((h - y_0 - X)\, b f_t)\frac{h - y_0 - X}{2} - \left(Xbf_c\,(h - y_0 - X) + \frac{X}{2}\right). \tag{2.29}$$

The maximum force capacity of the benchmark beam is then found from simple statics:

$$F = \frac{2M_p}{\frac{L}{2}}. \tag{2.30}$$

The force F is the benchmark for the future numerical calculations on a concrete FE beam. Using the beam properties stated in Table 2.2, the compressive zone, plastic moment and maximum force capacity are calculated. The values are stated in Table 2.3.

Table 2.3: Results from analytical calculations.

Compressive zone, X	55.5 mm
Plastic moment, M_p	6.3×10^7 Nmm
Maximum force capacity, F	8.5×10^4 N

Chapter 3

Finite element modelling

Modelling structures of materials like concrete and consider the plastic behaviour, the numerical models are often done in three dimensions. Thus, the stresses and strains are functions of x, y and z. This is illustrated in Figure 3.1.

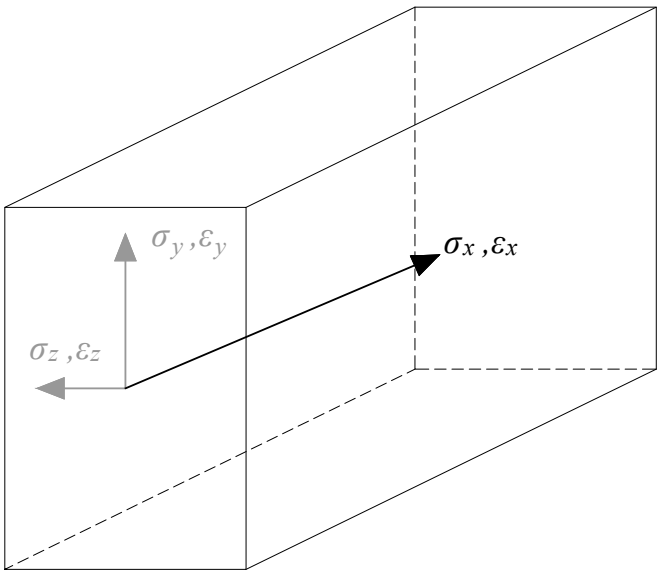

Figure 3.1: Three-dimensional beam.

The goal is to create a finite element formulation capable of handling plasticity using one-dimensional elements. Thus, the stress and strain states in the y and z direction are based on assumptions from basic beam theory as presented in Chapter 2. With elasto-plastic one-dimensional beam elements, the computational time should decrease drastically compared to three-dimensional solid or shell elements, but still have a reasonable accuracy.

3.1 Basic 1-D FEM theory

In this project a concrete beam is modeled using beam FE, the element used is a rod element. The rod element is composed of a bar element to account for displacement in the axial direction, and a beam element based on Bernoulli-Euler

beam theory which account for the transversal displacement and rotation. A bar and beam element is illustrated in Figure 3.2, with the annotations used.

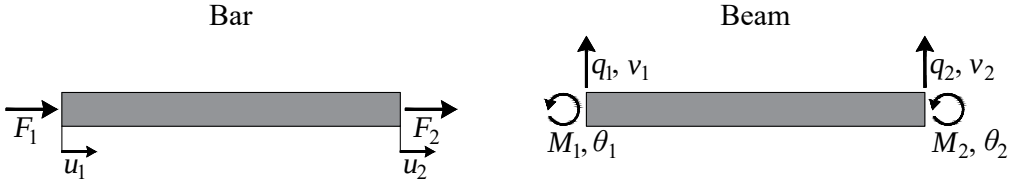

Figure 3.2: Bar and beam element.

Where:

F_i	Axial force at element node i
u_i	Axial displacement at element node i
q_i	Transversal force at element node i
v_i	Transversal displacement at element node i
M_i	Moment at element node i
θ_i	Rotation at element node i

In the concrete beam nonlinear behaviour is taken into account. When doing nonlinear FE using beam theory, it is necessary to use a finer mesh than what would be required in the linear case. In linear beam FE only nodes at supports and where forces are applied is required. When considering plasticity a number of extra nodes are required, to model the behaviour of the beam during yielding. One of the effects of plasticity starting to develop, is that the curvature, κ, stops being continuous between elements in the FE model. Thus, more elements are necessary to obtain accurate results.

As a rod element has three degrees of freedom (d.o.f) at each node, the element has six shape functions. The shape functions are illustrated in Figure 3.3.

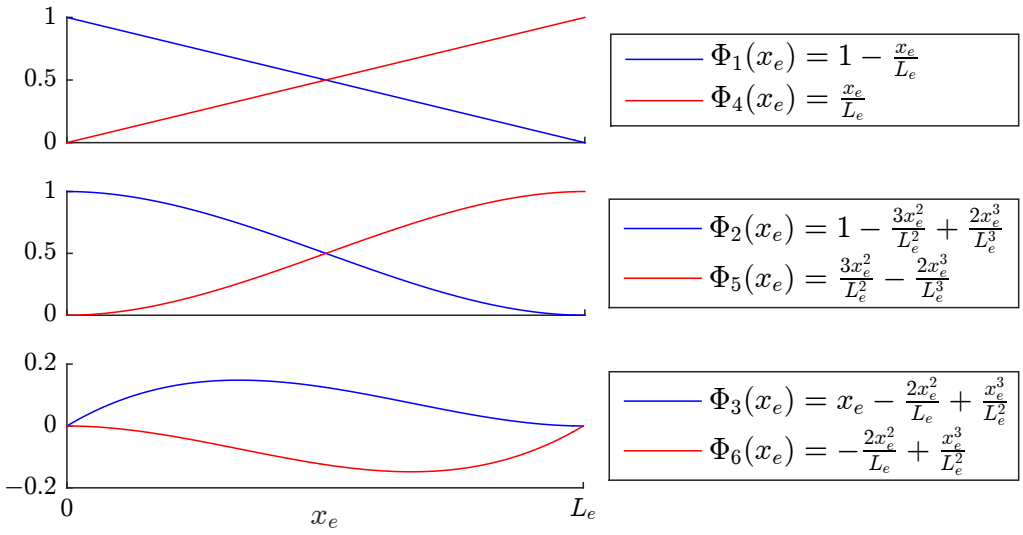

Figure 3.3: Shape function of the rod element.

Where the numbering of the shape functions correspond to the location in the displacement vector, which is

$$\{d\} = \begin{Bmatrix} d_1 \\ d_2 \\ d_3 \\ d_4 \\ d_5 \\ d_6 \end{Bmatrix} = \begin{Bmatrix} u_1 \\ v_1 \\ \theta_1 \\ u_2 \\ v_2 \\ \theta_2 \end{Bmatrix}. \tag{3.1}$$

3.1.1 Bar element

The stiffness of the bar element is derived using the Galerkin approach [Andersen, 2014]. First the strong form is established

$$D_{Bar}\frac{\mathrm{d}^2\Delta u(x_e)}{\mathrm{d}x_e^2} + \Delta f(x_e) = 0, \tag{3.2}$$

where the axial stiffness is $D_{Bar} = \int_A E(y)\mathrm{d}A$ and f is the external force.
The Galerkin approach can be divided into three steps:

1. Apply discretization and interpolation of displacement field:

$$\Delta u(x_e) = \{\Phi(x_e)\}\{\Delta d\}$$

$$D_{Bar}\frac{\mathrm{d}^2\{\Phi(x_e)\}}{\mathrm{d}x_e^2}\{\Delta d\} + \Delta f(x_e) = 0. \tag{3.3}$$

Here only the shape functions corresponding to the bar element are used, $\{\Phi(x_e)\} = \{\Phi_1(x_e)\ \Phi_4(x_e)\}$.

2. Premultiply strong form by weight function: $\{\Phi(x_e)\}^T$

$$\{\Phi(x_e)\}^T\left(D_{Bar}\frac{\mathrm{d}^2\{\Phi(x_e)\}}{\mathrm{d}x_e^2}\{\Delta d\} + \Delta f(x_e)\right) = \{\Phi(x_e)\}^T 0. \tag{3.4}$$

3. Integrate by parts over the element length

$$\begin{aligned}\int_0^{L_e}\{\Phi(x_e)\}^T\left(D_{Bar}\frac{\mathrm{d}^2\{\Phi(x_e)\}}{\mathrm{d}x_e^2}\{\Delta d\} + \Delta f(x_e)\right)\mathrm{d}x = \\ \int_0^{L_e}\{\Phi(x_e)\}^T 0\,\mathrm{d}x. \Rightarrow \\ \left[\{\Phi(x_e)\}^T D_{Bar}\frac{\mathrm{d}\{\Phi(x_e)\}}{\mathrm{d}x_e}\right]_0^{L_e}\{\Delta d\} - \\ \int_0^{L_e}\frac{\mathrm{d}\{\Phi(x_e)\}^T}{\mathrm{d}x_e}D_{Bar}\frac{\mathrm{d}\{\Phi(x_e)\}}{\mathrm{d}x_e}\{\Delta d\}\,\mathrm{d}x + \\ \int_0^{L_e}\{\Phi(x_e)\}^T\Delta f(x_e)\mathrm{d}x = \{0\}\end{aligned} \tag{3.5}$$

The physical interpretation of the second term in Equation (3.5) is $[k]\{\Delta d\}$, so the stiffness becomes

$$[k_{Bar}] = \int_0^{L_e}\frac{\mathrm{d}\{\Phi(x_e)\}^T}{\mathrm{d}x_e}D_{Bar}\frac{\mathrm{d}\{\Phi(x_e)\}}{\mathrm{d}x_e}\,\mathrm{d}x. \tag{3.6}$$

This can be simplified to

$$[k_{Bar}] = \int_0^{L_e}\{B_{Bar}\}^T D_{Bar}\{B_{Bar}\}\,\mathrm{d}x \tag{3.7}$$

Where $\{B_{Bar}\}$ is the strain interpolation vector of a bar element and D_{Bar} is the constitutive relation in the bar. The first term in Equation (3.5) is the boundary

load.

$$\{f_B\} = \left[\{\Phi(x_e)\}^T D_{Bar} \frac{\mathrm{d}\{\Phi(x_e)\}}{\mathrm{d}x_e}\right]_0^{L_e} \{\Delta d\} \tag{3.8}$$

The third term is the consistent nodal loads, used to apply line loads.

$$\{f_C\} = \int_0^{L_e} \{\Phi(x_e)\}^T \Delta f(x_e) \mathrm{d}x \tag{3.9}$$

The total load is the sum of the boundary load and the consistent nodal load,

$$\{f_T\} = \{f_B\} + \{f_C\}. \tag{3.10}$$

3.1.2 Beam element

The stiffness matrix of the beam element is derived using the Galerkin approach [Andersen, 2014]. First the strong form is established

$$D_{Beam} \frac{\mathrm{d}^4 \Delta v(x_e)}{\mathrm{d}x_e^4} = \Delta f(x_e), \tag{3.11}$$

where the bending stiffness is $D_{Beam} = \int_A E(y)\, y^2 \, \mathrm{d}A$.

The Galerkin approach can be divided into three steps:

1. Apply discretization and interpolation of displacement field:
   $\Delta v(x_e) = \{\Phi(x_e)\}\{\Delta d\}$

   $$D_{Beam} \frac{\mathrm{d}^4 \{\Phi(x_e)\}}{\mathrm{d}x_e^4} \{\Delta d\} - \Delta f(x_e) = 0. \tag{3.12}$$

   Here only the shape function corresponding to the beam element is used, which is rotation and transversal displacement,
   $\{\Phi(x_e)\} = \{\Phi_2(x_e)\ \Phi_3(x_e)\ \Phi_5(x_e)\ \Phi_6(x_e)\}$.

2. Premultiply strong form by weight function: $\{\Phi(x_e)\}^T$

   $$\{\Phi(x_e)\}^T \left(D_{Beam} \frac{\mathrm{d}^4 \{\Phi(x_e)\}}{\mathrm{d}x_e^4} \{\Delta d\} - \Delta f(x_e) \right) = \{\Phi(x_e)\}^T 0. \tag{3.13}$$

3. Integrate by parts over the element length

$$\begin{aligned}\int_0^{L_e}\{\Phi(x_e)\}^T\left(D_{Beam}\frac{\mathrm{d}^4\{\Phi(x_e)\}}{\mathrm{d}x_e^4}\{\Delta d\}-\Delta f(x_e)\right)\mathrm{d}x = \\ \int_0^{L_e}\{\Phi(x_e)\}^T 0\,\mathrm{d}x \Rightarrow \\ \left[\{\Phi(x_e)\}^T D_{Beam}\frac{\mathrm{d}^3\{\Phi(x_e)\}}{\mathrm{d}x_e^3}\right]_0^{L_e}\{\Delta d\}+ \\ \left[\{\Phi(x_e)\}^T D_{Beam}\frac{\mathrm{d}^2\{\Phi(x_e)\}}{\mathrm{d}x_e^2}\right]_0^{L_e}\{\Delta d\}- \\ \int_0^{L_e}\frac{\mathrm{d}^2\{\Phi(x_e)\}^T}{\mathrm{d}x_e^2}D_{Beam}\frac{\mathrm{d}^2\{\Phi(x_e)\}}{\mathrm{d}x_e^2}\mathrm{d}x\{\Delta d\}- \\ \int_0^{L_e}\{\Phi(x_e)\}^T\Delta f(x_e)\mathrm{d}x=\{0\}\end{aligned} \tag{3.14}$$

The physical interpretation of the third term in Eq. (3.14) is $[k]\{d\}$, so the stiffness becomes

$$[k_{Beam}]=\int_0^{L_e}\frac{\mathrm{d}^2\{\Phi(x_e)\}^T}{\mathrm{d}x_e^2}D_{Beam}\frac{\mathrm{d}^2\{\Phi(x_e)\}}{\mathrm{d}x_e^2}\mathrm{d}x \tag{3.15}$$

This can be simplified to

$$[k_{Beam}]=\int_0^{L_e}\{B_{Beam}\}^T D_{Beam}\{B_{Beam}\}\,\mathrm{d}x \tag{3.16}$$

Where $\{B_{Beam}\}$ is the strain interpolation vector of a beam element and D_{Beam} is the constitutive relation in the beam. The first and second term in Eq. (3.14) is the boundary loads.

$$\begin{aligned}\{f_B\}=&\left[\{\Phi(x_e)\}^T D_{Beam}\frac{\mathrm{d}^3\{\Phi(x_e)\}}{\mathrm{d}x_e^3}\right]_0^{L_e}\{\Delta d\}\\ &+\left[\{\Phi(x_e)\}^T D_{Beam}\frac{\mathrm{d}^2\{\Phi(x_e)\}}{\mathrm{d}x_e^2}\right]_0^{L_e}\{\Delta d\}\end{aligned} \tag{3.17}$$

The fourth term is the consistent nodal loads, used to apply line loads.

$$\{f_C\}=\int_0^{L_e}\{\Phi(x_e)\}^T\Delta f(x_e)\mathrm{d}x \tag{3.18}$$

The total load is the sum of the boundary load and the consistent nodal load,

$$\{f_T\} = \{f_B\} + \{f_C\}. \tag{3.19}$$

3.1.3 Rod element

To calculate the stiffness matrix for the rod element, the strain interpolation matrix and the constitutive matrix is needed. The strain interpolation vector of the bar and beam element, is combined into a strain interpolation matrix for the rod element.

$$B = \begin{bmatrix} B_{Bar}(1) & 0 & 0 & B_{Bar}(2) & 0 & 0 \\ 0 & B_{Beam}(1) & B_{Beam}(2) & 0 & B_{Beam}(3) & B_{Beam}(4) \end{bmatrix} \tag{3.20}$$

The constitutive matrix for the rod element consist of the constitutive relation form the bar and beam element, to account for a arbitrary beam axis a diagonal term is added.

$$[D] = \begin{bmatrix} D_{Bar} & -\int_A E(y)\, y \, \mathrm{d}A \\ -\int_A E(y)\, y \, \mathrm{d}A & D_{Beam} \end{bmatrix} \tag{3.21}$$

The stiffness matrix for the rod element is

$$[k] = \int_0^{L_e} [B]^T [D][B] \, \mathrm{d}x. \tag{3.22}$$

3.1.4 Quadrature methods

The choice of numerical integration method is a part of the program which has influence on the accuracy and computing time. In this project two methods are used to handle numerical integration tasks. This being the trapezoidal rule and Gauss integration. The difference is roughly sketched in Figure 3.4.

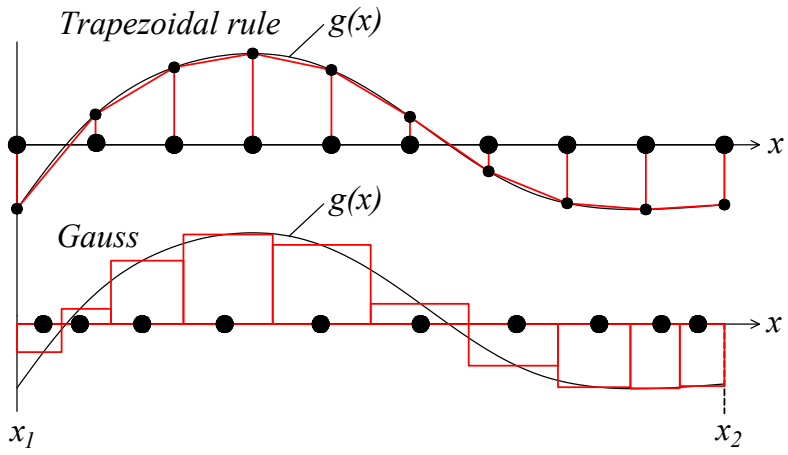

Figure 3.4: Quadrature methods sketch.

The Gauss integration method has a tendency to push the observed points to the edges of the element. The trapezoidal rule method is dividing the element and places the observation points with equal distance between them.

The integral for an element is then:

$$J = \int_{x_1}^{x_2} g(x)\,\mathrm{d}x. \tag{3.23}$$

To account for asymmetry and plasticity, it is necessary to include cross section integration as well.

Using Gauss integration, polynomials of degree $2n-1$ can be fitted exactly by a n degree Gauss integral. Gauss integration picks optimal points and weights to numerically estimate the integral of a function $g(x)$.

Weighting

The weight is described as the area or distance belonging to each integration point. These weights change for each point in a Gauss integration, but are constant for the the trapezoidal rule.

It is observed, that the further away from the center the smaller weight is assigned the integration point. This tendency could mean more accurate prediction of strains and stresses at the edges, as the integration is done over smaller areas or distances.

For plasticity, this is a promising quality, as the first sign of plastic behaviour is located at the edges of the cross section, whereas elastic behaviour can be predicted

exact and the need for integration points and weights are less.

Element integration

By substituting, the limits (x_1, x_2) with $\xi = -1$ and $\xi = 1$, a local coordinate system is used for the element, now the function is called ϕ. The integral becomes:

$$J = \int_{-1}^{1} \phi \, d\xi. \tag{3.24}$$

Plasticity requires integration over the cross sectional area and therefore a number of points are placed along the y-axis. Further, to get a more accurate integration of stresses, a number of points are used along the ξ-axis of each element. The final integration of an element is illustrated in Figure 3.5.

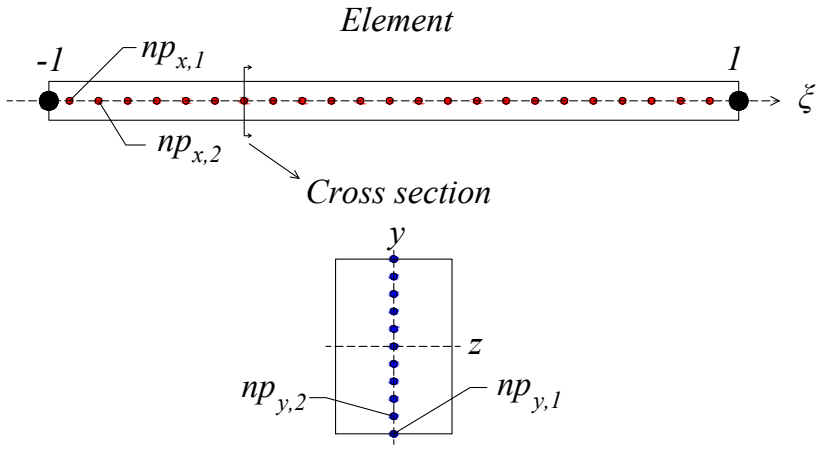

Figure 3.5: Linear integration of a beam element.

For every integration point in the element ξ-axis, an integration is done over the cross sectional area. Now, data is available in more points and the stress integration is more accurate. In the program both Gauss and the trapezoidal rule method is included.

3.2 Plasticity in FEM

3.2.1 Newton-Raphson iteration scheme

In nonlinear FE an iteration scheme is need to solve the FE model, in this section the modified Newton-Raphson scheme for displacement-based iteration is described.

The Newton-Raphson scheme consist of two loops, the inner loop which is the equilibrium loop, here iterations are done to obtain equilibrium between the outer and inner forces. In the outer loop, which is the load increment loop, an increment in force is applied. In the modified Newton-Raphson method the stiffness matrix is updated in the outer loop, which means that the same stiffness is used throughout a given equilibrium iteration.

The modified Newton-Raphson method is commonly used to avoid updating the stiffness matrix for each iteration step, as it is done in the Newton-Raphson method. Updating the stiffness matrix can take up a lot of computational time, so even though the modified Newton-Raphson method require more iterations to obtain equilibrium it can very well be faster [Krabbenhøft, 2002]. The two iteration methods are compared in a later section. An illustration of the two iterations schemes is shown in Figure 3.6.

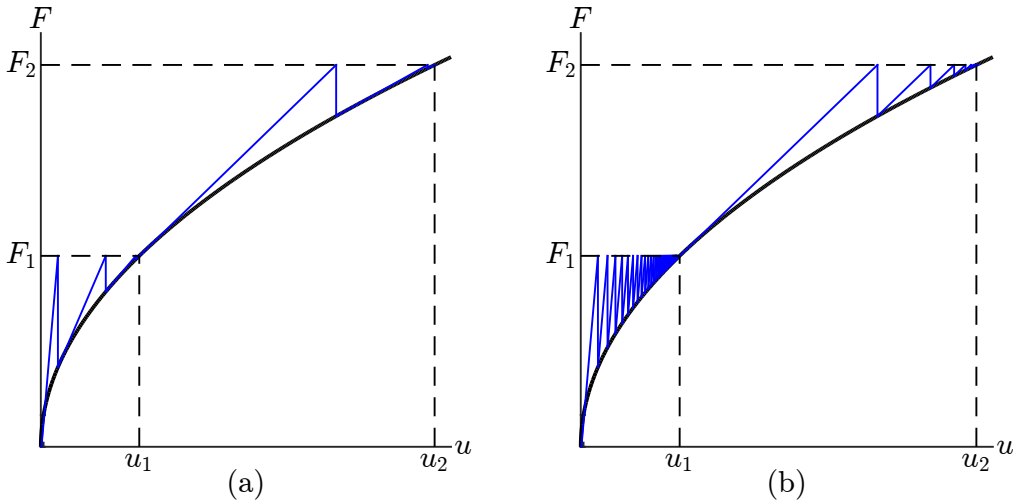

Figure 3.6: Convergence of load (a) Newton-Raphson iterations and (b) Modified Newton-Raphson iterations.

A description of the steps in the displacement based iteration scheme can be seen in table 3.1.

Table 3.1: Displacement iteration scheme using modified Newton-Raphson.

$[\mathbf{u}] = 0,\ [\sigma] = 0,\ [\mathbf{F}] = 0$	Initial state.
for $i = 1 : i_{max}$	Load/displacement increment loop.
$[\mathbf{k}]$ = function($[\mathbf{E}]$,$[\mathbf{A}]$)	Updating of stiffness matrix.
while $r >$ tolerance	The equilibrium loop runs while the residual force, r, is above a tolerance.
if $\text{it}_{\text{number}} > 1$ $[\Delta\varepsilon]$ = function($[\Delta\mathbf{u}]$) $[\sigma(i+1)]$ = function($[\Delta\varepsilon]$,$[\sigma(i)]$) $[\mathbf{F}_{int}]$ = function($[\sigma(i+1)]$) $r = [\mathbf{F}] - [\mathbf{F}_{int}]$ end	The residual force, r, is calculated after the first run through of the equilibrium loop.
if $\text{it}_{\text{number}} = 1$ $[\delta\mathbf{u}]$ = function($[\mathbf{k}]$,$[\mathbf{F}] = 0$,$[\mathbf{BC}]$) elseif $r >$ tolerance $[\delta\mathbf{u}]$ = function($[\mathbf{k}]$,r,$[\mathbf{BC}]$) else break end	In the first run through the displacement $[\delta\mathbf{u}]$ is calculated based on the boundary condition with a forced displacement. In in the following runs if the residual force is above the tolerance, $[\delta\mathbf{u}]$, is calculated based on the residual force and boundary conditions, $[\mathbf{BC}]$, where the forced displacement is not allowed to change. When equilibrium is obtained the loop is exited.
$[\Delta\mathbf{u}] = [\Delta\mathbf{u}] + [\delta\mathbf{u}]$ end	The displacement matrix is updated. End iterations.
$[\mathbf{u}] = [\mathbf{u}] + [\Delta\mathbf{u}]$ $[\varepsilon] = [\varepsilon] + [\Delta\varepsilon]$	The matrices are updated.
end	End of load step.

Table 3.1 is defined with matrices as it is done in the MatLab script.

3.2.2 Internal force

As mentioned in section Section 3.2.1 the residual force, r, is needed for the equilibrium iteration. In linear FE with rod elements the internal force is not calculated as it is not needed, the following describes how to calculate the internal force.

Based on the shape functions and the displacement, the strain can be obtained. The strains in a bar element and beam element is calculated in two different ways.

First the displacement vector in the global system is rotated to get the displacement vector in the local system.

$$\{d'\} = [\mathbf{T}]\,\{d\} \tag{3.25}$$

The transformation matrix is

$$[\mathbf{T}] = \begin{bmatrix} c & s & 0 & 0 & 0 & 0 \\ -s & c & 0 & 0 & 0 & 0 \\ 0 & 0 & 1 & 0 & 0 & 0 \\ 0 & 0 & 0 & c & s & 0 \\ 0 & 0 & 0 & -s & c & 0 \\ 0 & 0 & 0 & 0 & 0 & 1 \end{bmatrix}, \tag{3.26}$$

and

$$c = \frac{d'_4 - d'_1}{L_e}, \qquad s = \frac{d'_5 - d'_2}{L_e}. \tag{3.27}$$

The rotation of an element from global coordinates to local coordinates is illustrated in Figure 3.7.

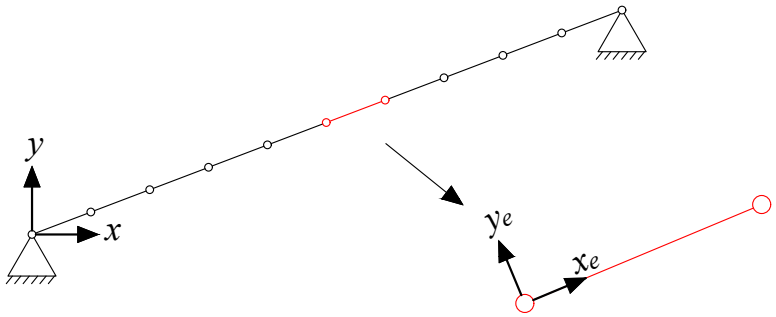

Figure 3.7: Rotation of beam element to local coordinates.

Here, y_e is the local y axis in the element. To obtain the strain in the bar element,

the shape function is differentiated and multiplied with the displacement as

$$\varepsilon_{\text{bar}} = \left\{ \frac{\mathrm{d}\Phi_1(x_e)}{\mathrm{d}x} \quad \frac{\mathrm{d}\Phi_4(x_e)}{\mathrm{d}x} \right\} \begin{Bmatrix} d'_1 \\ d'_4 \end{Bmatrix}. \tag{3.28}$$

For the continuum strain in the beam element, the curvature is first calculated by

$$\kappa(x_e) = \left\{ \frac{\mathrm{d}^2\Phi_2(x_e)}{\mathrm{d}x^2} \quad \frac{\mathrm{d}^2\Phi_3(x_e)}{\mathrm{d}x^2} \quad \frac{\mathrm{d}^2\Phi_5(x_e)}{\mathrm{d}x^2} \quad \frac{\mathrm{d}^2\Phi_6(x_e)}{\mathrm{d}x^2} \right\} \begin{Bmatrix} d'_2 \\ d'_3 \\ d'_5 \\ d'_6 \end{Bmatrix}. \tag{3.29}$$

The strain in the beam element can then be calculated as

$$\varepsilon_{\text{beam}} = -y_e \kappa. \tag{3.30}$$

To calculate the stress, the two strains are added together, stress in the rod element becomes

$$\sigma_x = (\varepsilon_{\text{bar}} + \varepsilon_{\text{beam}}) E(y_e). \tag{3.31}$$

The moment and normal force at each integration point is the calculated as

$$N(x_e) = \int_A \sigma_x \, \mathrm{d}A \tag{3.32}$$

$$M(x_e) = \int_A y_e \sigma_x \, \mathrm{d}A. \tag{3.33}$$

The internal force at each node in the element is then calculated as

$$\{F_N\} = \int_0^{x_e} \left\{ \frac{\mathrm{d}\Phi_1(x_e)}{\mathrm{d}x} \quad \frac{\mathrm{d}\Phi_4(x_e)}{\mathrm{d}x} \right\}^T N(x_e) \, \mathrm{d}x, \tag{3.34}$$

$$\{F_V\} = \int_0^{x_e} \left\{ \frac{\mathrm{d}^2\Phi_2(x_e)}{\mathrm{d}x^2} \quad \frac{\mathrm{d}^2\Phi_5(x_e)}{\mathrm{d}x^2} \right\}^T M(x_e) \, \mathrm{d}x, \tag{3.35}$$

$$\{F_M\} = \int_0^{x_e} \left\{ \frac{\mathrm{d}^2\Phi_3(x_e)}{\mathrm{d}x^2} \quad \frac{\mathrm{d}^2\Phi_6(x_e)}{\mathrm{d}x^2} \right\}^T M(x_e) \, \mathrm{d}x. \tag{3.36}$$

The internal force vector of the an element is then assembled, and rotated back to

global coordinates

$$\{F_e\} = T^{-1} \begin{Bmatrix} F_{N,1} \\ F_{V,1} \\ F_{M,1} \\ F_{N,2} \\ F_{V,2} \\ F_{M,2} \end{Bmatrix} \tag{3.37}$$

The internal force vector can then be assembled, and the residual force, $r = f - f_{int}$, calculated.

3.2.3 Elasto-plastic calculations on continuous cross section

Calculating a force/displacement curve for the beam model shows both the elastic region and the ultimate force capacity of the beam. In Section 2.2.1, the plastic moment was calculated. Using the plastic moment, the ultimate force capacity is found.

In Figure 3.8, the force/displacement curve shows the force going towards the ultimate analytically force capacity.

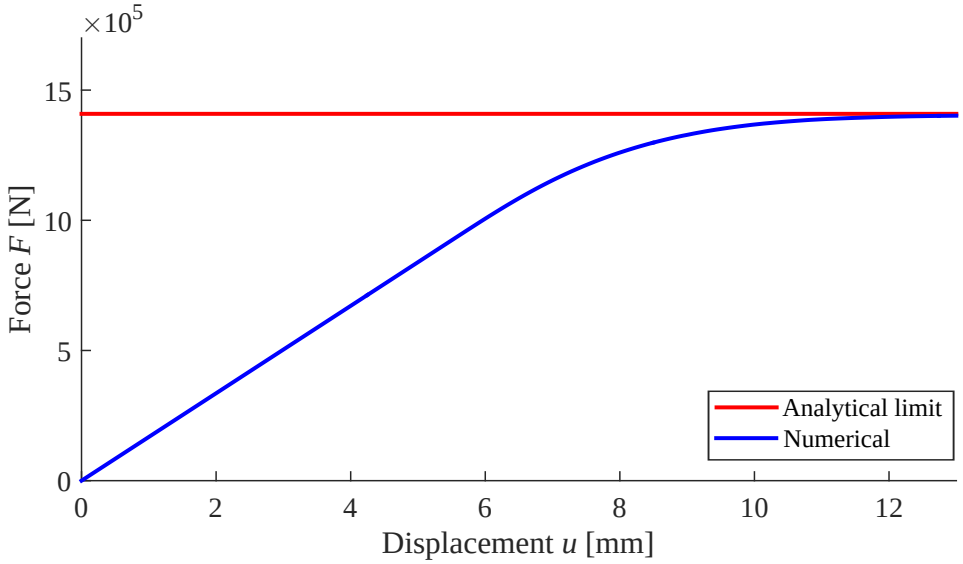

Figure 3.8: F-u curve.

The applied mesh in the numerical model is so fine, that the model is converged,

a convergence study is presented later in the report. As a result the deviation between the analytical solution and the numerical solution is very small. This proves, that it is possible to obtain the same result as the analytical solution, by applying the one-dimensional finite element method for an elasto-plastic beam.

3.2.4 Effects of plasticity

Neutral axis

In this section the moving of the neutral axis during bending is described, an analytical and a numerical solution to the problem are presented alongside with the theory.

The neutral axis will, during plastic deformation, move up or down when the beam is subjected to bending if the cross section is not symmetric or the yield stress is different for compression and tension. At pure bending, if the material is not yielding, the neutral axis is located at the point of zero stresses, see Figure 3.9.

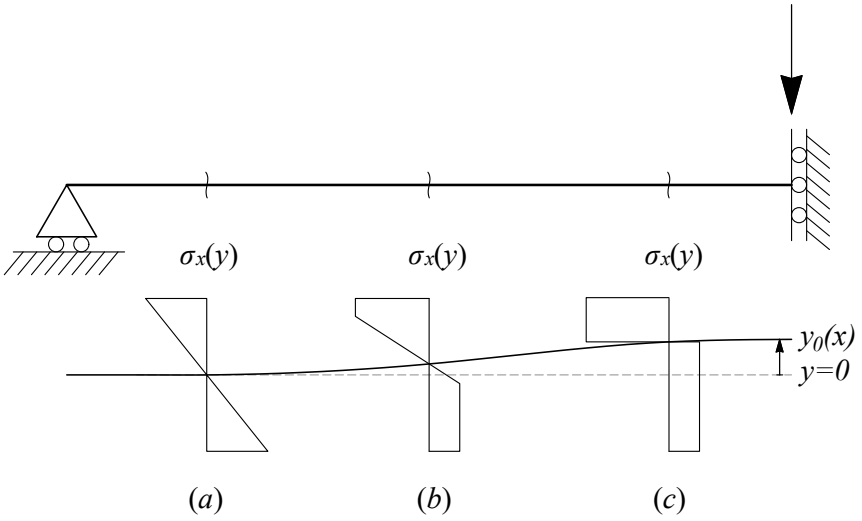

Figure 3.9: Sketch of neutral axis movement along beam.

At distribution (a), the material has not started to yield and the neutral axis is located at beam axis, $y = 0$. Moving along the beam axis, the neutral axis will move as the point of zero stress is moving to satisfy the normal force equilibrium:

$$\int_A \sigma_x(y)\, \mathrm{d}A = N. \tag{3.38}$$

In case of pure bending, $N = 0$, which implies that the neutral axis is located on

the beam axis. In Figure 3.9 it can be seen, that this is only true for elastic stress distributions, as the neutral axis moves when yielding is reached (b).

If the coordinate system is kept unchanged during bending, a beam strain at the original neutral axis may develop during yielding. The continuum strain in a cross section can be described as stated in Equation (2.7).

During elastic bending the neutral axis is located at the centroid, which is calculated as

$$C_y = \frac{\int \bar{y} f(\bar{y}) \mathrm{d}\bar{y}}{\int f(\bar{y}) \mathrm{d}\bar{y}} \Rightarrow \frac{\sum \bar{y} A_i}{\sum A_i}. \tag{3.39}$$

The y-axis is then defined as $y = 0 = \bar{y} - C_y$, for $\bar{y} = 0$ at the bottom of the profile.

For a cross section with a perfect elasto-plastic material that has the same strength characteristics in compression and tension, the neutral axis in pure bending at full plastic behaviour is located where the area above the neutral axis is equal to the area below.

Calculating the location of the neutral axis, in-between elastic and fully plastic is a bit more difficult. One way of doing it is by iteration, where the out of balance force is converted to a strain and then added to the beam strain as

$$\varepsilon_0^{(i+1)} = \frac{-\int_A \sigma_x \mathrm{d}A + N}{\int_A E(y)\, \mathrm{d}A} + \varepsilon_0^{(i)}. \tag{3.40}$$

1. Initial position of the neutral axis is assumed located in the beam axis i.e. $\varepsilon_0^{(1)} = 0$.
2. Normal stresses are calculated from $\varepsilon_x(y) = \varepsilon_0^{(i)} - \kappa y$.
3. Equation (3.40) is used to calculate a new $\varepsilon_0^{(i+1)}$.
4. The iteration is converged when the out of balance force, $\int_A \sigma_x \mathrm{d}A - N$, is negligible small. If this is not the case, step 2-4 are repeated.

Analytical solution for a T-profile

The analytical solution to the location of the neutral axis depends on which part of the profile is yielding. A T-profile subjected to pure bending, the bottom part starts yielding first if the material used is isotropic. The solution presented here is only valid for yielding at the bottom of the profile, and with an isotropic perfect elasto-plastic material.

The T-profile is divided into four zones as indicated in Figure 3.10.

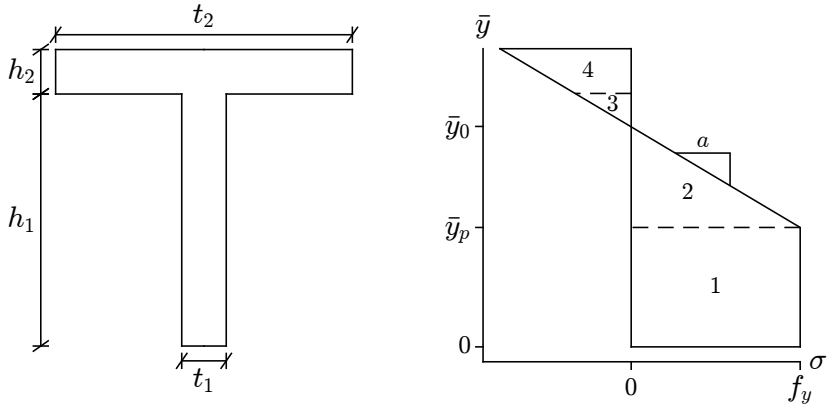

Figure 3.10: T-profile with arbitrary stress distribution.

The elastic stress can be formulated as a first order polynomial, $\sigma = a\bar{y} + b$, where $a = -\kappa E$ and $b = -a\bar{y}_0$. The intersection where yielding starts

$$f_y = a\bar{y}_p + b \;\Leftrightarrow\; \bar{y}_p = \frac{f_y - b}{a} \tag{3.41}$$

At the center of each zone the average stress is found, the location of each center is found as

$$\begin{aligned} \bar{y}_1 &= \tfrac{\bar{y}_p}{2}, & \bar{y}_2 &= \bar{y}_p + \tfrac{\bar{y}_0 - \bar{y}_p}{2}, \\ \bar{y}_3 &= \bar{y}_0 + \tfrac{h_1 - \bar{y}_0}{2}, & \bar{y}_4 &= h_1 + \tfrac{h_2}{2}. \end{aligned} \tag{3.42}$$

The area of each zone is then calculated as

$$\begin{aligned} A_1 &= \bar{y}_p t_1, & A_2 &= (\bar{y}_0 - \bar{y}_p) t_1, \\ A_3 &= (h_1 - \bar{y}_0) t_1, & A_4 &= h_2 t_2. \end{aligned} \tag{3.43}$$

The force in each zone is then

$$\begin{aligned} F_1 &= \sigma_y A_1, & F_2 &= (a\bar{y}_2 + b) A_2, \\ F_3 &= (a\bar{y}_3 + b) A_3, & F_4 &= (a\bar{y}_4 + b) A_4. \end{aligned} \tag{3.44}$$

The neutral axis can then be found by solving the equation $\sum F = 0$ for $\bar{y}_0$ due to pure bending.

Functions of curvature

As described in Section 3.2.4, the analytical solution is dependent on which section of the profile is yielding. In the following section the location of the neutral axis is calculated numerically, which gives the same result as long as enough points are used for the numerical integration.

For the numerical solution the iteration described earlier is used and Eq. (3.40) is numerical integrated. Given the same profile as in Section 3.2.4, the location of the neutral axis can be found for any given curvature. Figure 3.11 shows beam strain, neutral axis and moment as a function of curvature.

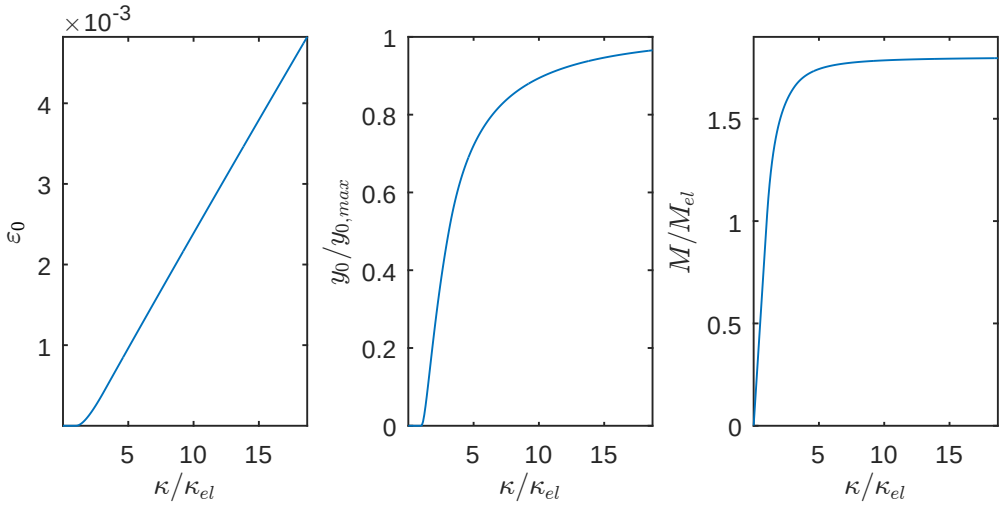

Figure 3.11: Curvature functions.

Here, κ_{el} is the curvature just before yielding.

3.2.5 Multi-material cross sections

Considering concretes ability to resist tensile stresses, it is necessary to have the possibility to insert reinforcement steel bars to increase the tensile strength of the beam. This is done by adding another set of calculations in the MatLab program running simultaneously with the primary material of the beam. Thus, the calculations can be described as illustrated in Figure 3.12.

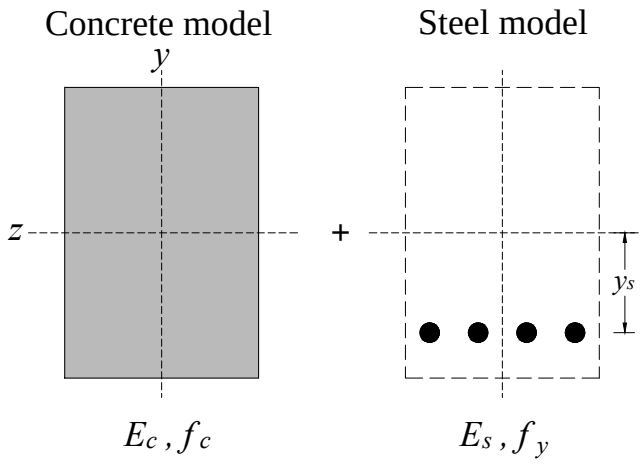

Figure 3.12: Concrete cross section divided into two parts.

The choice of material is not limited to concrete and steel, but as the focus of this project are steel reinforced concrete beams, this report will focus on these materials. It should be said, that the area of the concrete that disappears because of the steel bars are neglected. This causes a slightly larger area of concrete to contribute to the strength, but it is considered a minor increase in strength and is assumed to be acceptable. Thus the concrete area will be the entire cross section area A. For the reference beam used in this project, this corresponds to an increase in cross sectional area of 0.57%. This is assumed acceptable small to be neglected.

The main part of inserting a second material into the cross section is to run a second set of equations in the iteration loop described in Section 3.2.1. It is still a basic requirement that equilibrium is contained and therefore, the addition of contributions from concrete and steel must be done before the equilibrium loop is initiated.

As said, the same equations are used for the secondary material as for the primary material when considering stresses, strains and forces. These equations can be found in Section 3.2.2. The addition of primary and secondary material are done when calculating internal forces, leading to a second term in the equations for the internal forces, described in Section 2.1:

$$N = \int_A \sigma_{x,c} \, \mathrm{d}A + \int_{A_s} \sigma_{x,s} \, \mathrm{d}A_s \tag{3.45}$$

$$M = \int_A \sigma_{x,c} \, y \, \mathrm{d}A + \int_{A_s} \sigma_{x,s} \, y_s \, \mathrm{d}A_s \tag{3.46}$$

After adding the internal forces from the secondary material indicated by index s, the rest of the calculations remains unchanged, but now the strength from the

secondary material is included in the equilibrium loop, and the total strength will increase. The increase in strength can be illustrated by observing a beam displacement progress. For the geometry, the benchmark values are used, see table1.1 (p. 4).

An illustration of a multi-material cross section force/displacement curve can be seen in Figure 3.13.

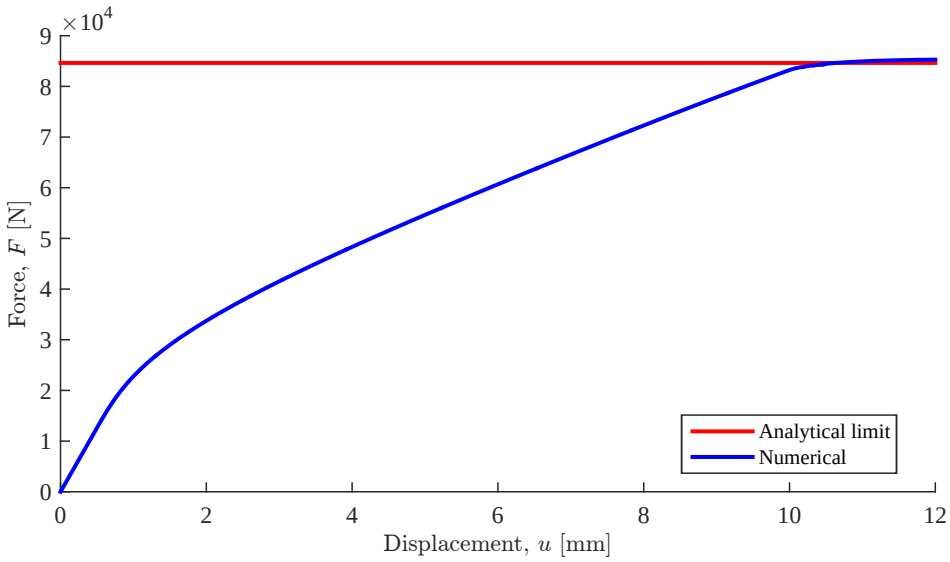

Figure 3.13: F-u curve for multi-material cross section.

It is seen that the multi-material cross section obtains a higher ultimate strength than the analytical benchmark solution, which the original perfect elasto-plastic material model for concrete with continuous material hit almost perfectly, see Figure 3.8.

The curve is seen to have two kinks, indicating beginning of yielding. The first kink is caused by tensile yielding of the primary material, which should simulate concrete. Then, a large part is seen to almost being linear, caused by the high strength of the reinforcement bars. Near the ultimate strength, the reinforcement bars then start yielding and the stiffness is almost lost completely and the cross section becomes fully plastic.

3.3 Concrete material model

In this section, the development of the material model used to simulate the behaviour of concrete is described. Earlier, it was stated that the Drucker-Prager

criterion could be used to describe the behaviour. In this case, the yield criterion can be simplified significantly, as the model is one-dimensional. The yield surface, described in Chapter 2, is boiled down to a "yield line" where the material becomes plastic when a yield point on the line is reached.

Earlier, the stress-strain curve for concrete was presented, see Chapter 1. Also, the use of linear elasto-plastic material model was presented in Chapter 2, which defined a point of yielding, where the material would go from linear elastic to perfect plastic.

Even though, the linear elasto-plastic model describes concrete fairly well, a further improved definition of the stress-strain curve is applied to describe the nonlinear behaviour of the real stress-strain curve for concrete, see Figure 3.14.

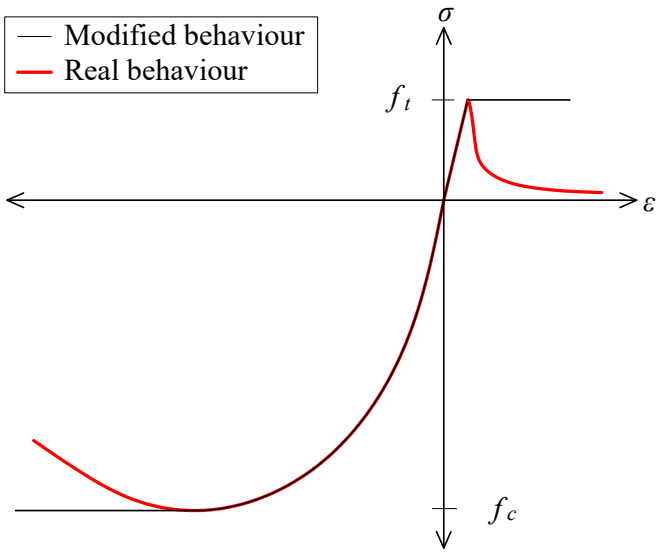

Figure 3.14: Nonlinear elasto-plastic material model.

The material is defined with a cut-off when the yield stress is reached. This excludes softening from the model and will not be included in the project. The nonlinear behaviour is described by Mohamad et al. [1990] as a third degree polynomial function, fitted to a series of uniaxial compression test results. The function states:

$$\frac{\sigma}{f_c} = 2.1\left(\frac{\varepsilon}{\varepsilon_c}\right) - 1.33\left(\frac{\varepsilon}{\varepsilon_c}\right)^2 + 0.2\left(\frac{\varepsilon}{\varepsilon_c}\right)^3. \tag{3.47}$$

Where σ is the current stress state, ε is the current strain state, f_c is the yield stress in compression and ε_c is the yield strain in compression. By means, this will only cover the nonlinear behaviour in compression. But the linear elastic definition of

the tensile behaviour is valid, so it is not necessary to improve further. The stress at a current state can now be found, only depending on the strain at this state.

Describing the compression in this way, it is fairly easy to evaluate the elastic modulus at the current stress-strain state, as the tangent to the stress-strain curve. This gives the distribution of the elastic modulus as seen in Figure 3.15.

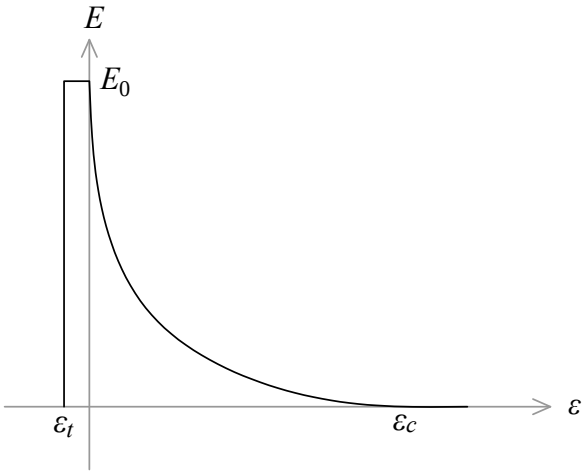

Figure 3.15: Elastic modulus in nonlinear elasticity.

The change in the elastic modulus in compression decreases as the strain goes towards the compressive yield strain. At yielding the elastic modulus becomes zero. In tension, the elastic modulus is constant until yielding as the definition is still linear elastic. When the tensile strain reaches the yield strain, the elastic modulus instantly becomes zero.

Chapter 4

One-dimensional FE analysis

In this chapter, the beam model is analysed and a number of convergence analysis is performed. Also, the beam model will be compared to a model designed in Abaqus. The structure is a simply supported beam, subjected to a forced displacement at the center of the beam. The system and cross section data are described in Chapter 1. Also, a concrete frame structure is analysed by using the MatLab script to test the MatLab script with a more complex structure.

4.1 Element convergence

In this section a convergence analysis will be performed for the different material models. The convergence analysis is based on the number of elements required to converge towards the exact solution. The convergences are shown in logarithmic plots. In logarithmic plots, the convergence is good if the curve comes out as a straight line.

Elasto-plastic beam with single material cross section

The beam is subjected to a forced displacement large enough to reach a fully plastic cross section. In Figure 4.1, the element convergence of the beam with an elasto-plastic material model with continuous cross section is shown.

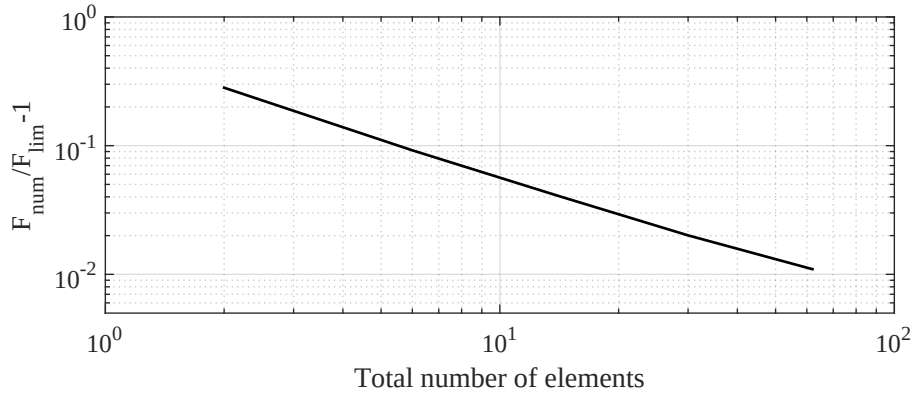

Figure 4.1: Convergence study of a beam with elasto-plastic material model.

Here, the number of integration points over the cross section and number of cross section integrations are kept constant to observe the effect of the total number of elements only. The *y* axis shows the numerical value calculated, divided by the analytical limit value minus one, which gives the error of numerical value compared to the analytical limit value. The line is almost completely straight, which means a good convergence.

To see what the gain in accuracy of using 60 elements rather than using 30 elements, the error for 30 and 60 elements are given in Table 4.1.

Table 4.1: Convergence of elasto-plastic beam with continuous material cross section.

No. elements	F_{num}	F_{num}/F_{lim}-1 [%]	Computational time [s]
30	14.383×10^5 N	2.0	6.33
60	14.255×10^5 N	1.1	12.92

Using 60 elements for the model will result in an error of 1.1%. Using 30 elements will increase the error of 0.9%, but in return the computation time is reduced by half.

Linear elasto-plastic beam with multi-material cross section

Next, the cross section properties is changed to match a reinforced concrete cross section with a linear elastic-perfect plastic material model. The dimensions are described in Chapter 1 and the material properties can be found in Table 2.2.

The element convergence is shown in Figure 4.2.

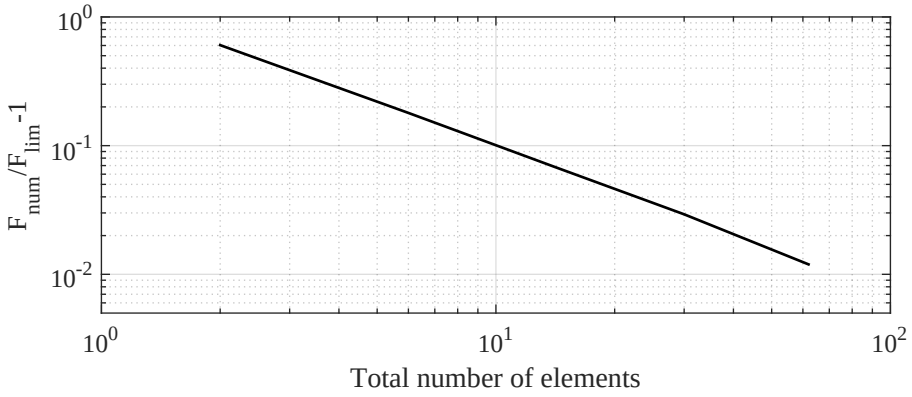

Figure 4.2: Convergence study of elasto-plastic concrete beam.

The convergence shows the same tendency as the elasto-plastic beam with a continuous cross section. Again, use of 30 elements could be defended as the difference is small. The convergence at 30 and 60 elements, are listed in Table 4.2.

Table 4.2: Convergence of elasto-plastic reinforced concrete beam.

No. elements	F_{num}	F_{num}/F_{lim}-1 [%]	Computational time [s]
30	8.75×10^4 N	2.99	7.77
60	8.61×10^4 N	1.27	14.54

The gain from using 60 elements in this case is greater than for the continuous cross section beam. The error is reduced with 1.72% by using 60 elements, but the computational time is doubled up.

Nonlinear elasto-plastic beam with multi-material cross section

The material models is changed so that the elastic loading region becomes nonlinear. This material model is the most advanced material model used in this project. The convergence is shown in Figure 4.3.

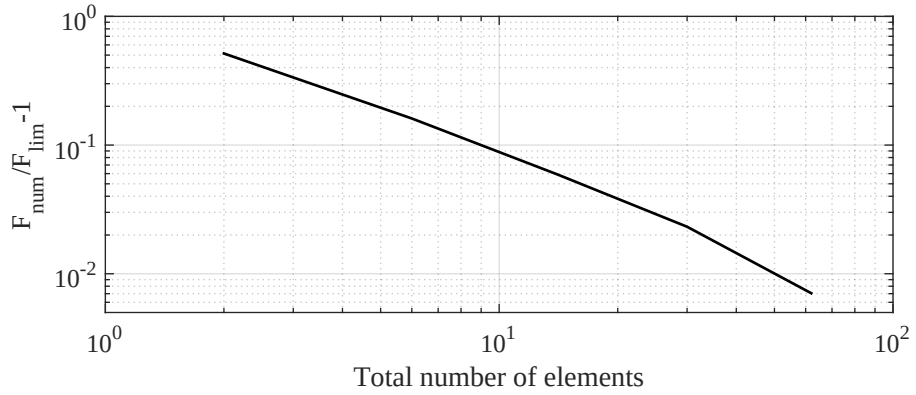

Figure 4.3: Convergence study of nonlinear elasto-plastic concrete beam.

The nonlinear material has a bit more curvature than the linear elasto-plastic material model, which implies a slightly weaker convergence. The convergence at 30 and 60 elements, are listed in Table 4.3.

Table 4.3: Convergence of nonlinear elasto-plastic reinforced concrete beam.

No. elements	F_{num}	F_{num}/F_{lim}-1 [%]	Computational time [s]
30	8.70×10^4 N	2.36	9.75
60	8.57×10^4 N	0.78	19.32

Convergence summary

The models are all converging good, but the continuous cross section model is converging a bit better than the rest in this analysis. This is seen in the line, which is more straight. All convergences of the material models are shown in Figure 4.4.

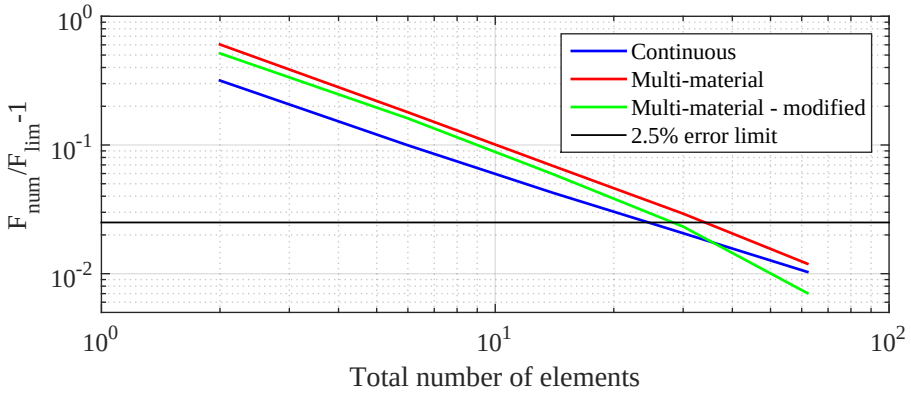

Figure 4.4: Convergence of all models.

The conclusion is, that use of 60 elements of course is better than using 30 elements, but the error of using 30 elements is not significantly bigger than using 60 elements. In the nonlinear material model, the error deviation between 30 and 60 elements is 1.58%, which is acceptable if the computational time on the other hand is decreased to about half of what is required, when using 60 elements.

4.2 Elements versus integration points

In this section the use of more elements compared the use of more integration nodes within each element is analysed. For this analysis one model is chosen, in this case the nonlinear elasto-plastic material model is applied. First the Trapezoidal rule is applied, then the Gauss integration method. The difference in integration method is compared in the end of this section.

The model element convergence, with a constant number of integration points, is already presented. The convergence when increasing the number of cross section integrations for an increasing number of elements used can be seen in Figure 4.5.

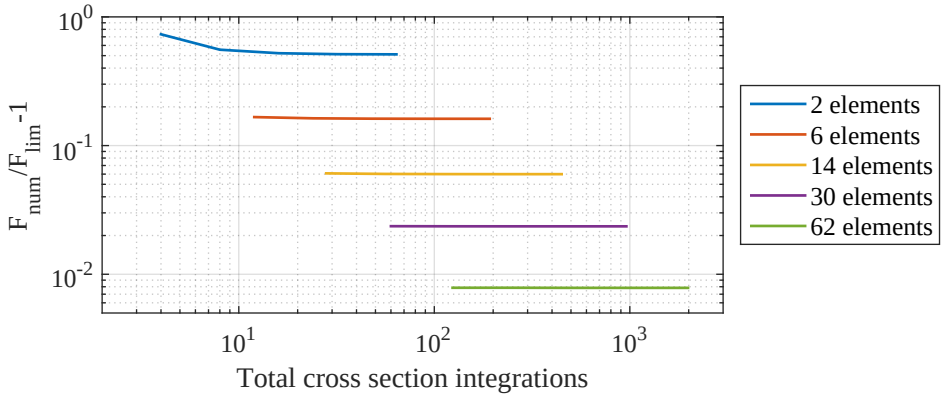

Figure 4.5: Integration points over beam length - Trapezoidal rule.

In Figure 4.6 the number of integration points over the cross section height vary together with the number of elements.

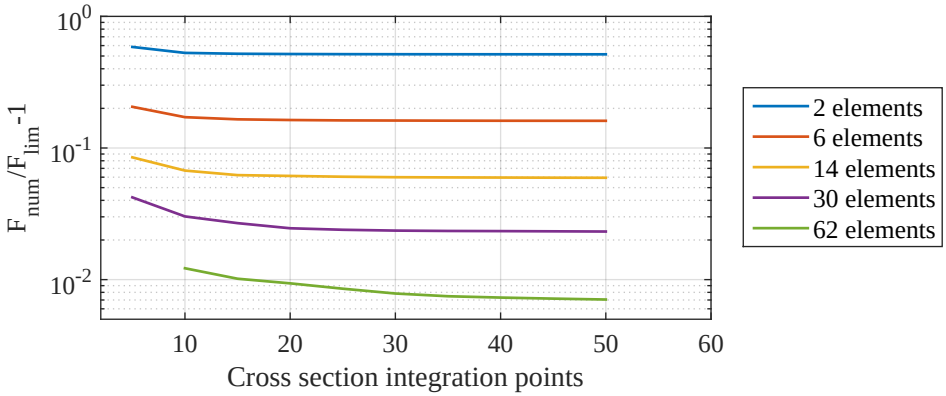

Figure 4.6: Integration points over cross section height - Trapezoidal rule.

It is seen, that the number of cross section integrations only influence the convergence when using 2 elements. When the number of elements is increased, the importance of the number of elements is greater than the number of cross section integrations and there is no further gain from using more cross section integrations.

Observing the number of integration points over the cross section height, the opposite tendency is seen. Here, the number of integration points is more important when the number of elements is increasing.

Now the integration method is changed to Gauss integration. First, the analysis is carried out for the total number of cross section integrations. The results is shown in Figure 4.7

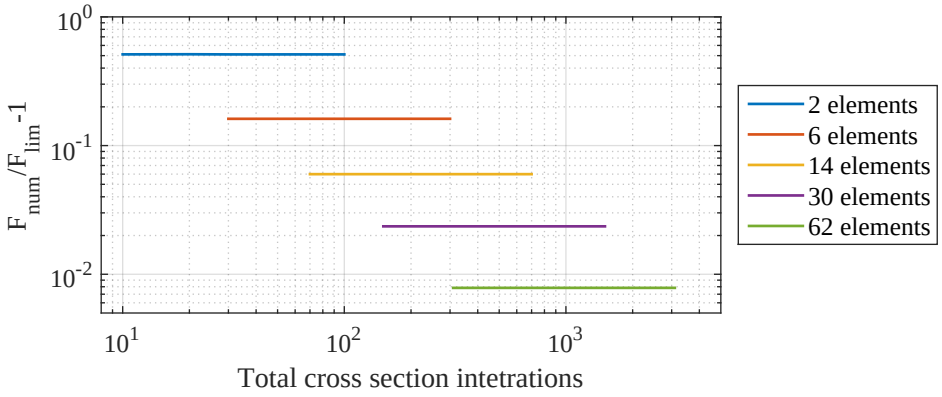

Figure 4.7: Integration points over beam length - Gauss integration.

The convergence study shows even less influence from the number of cross section integrations, when the Gauss quadrature is applied. This shows, that the Gauss quadrature might be better fitted to use when considering the integration over length.

The analysis is now carried out for the integration points over the beam cross section height. The results is shown in Figure 4.8

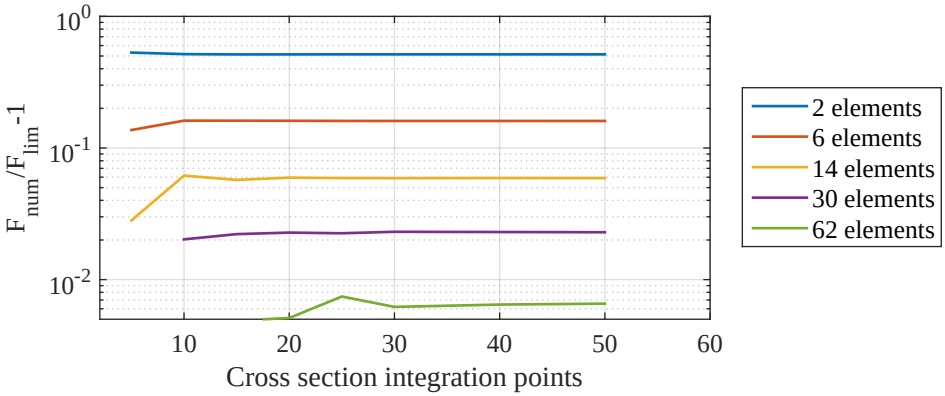

Figure 4.8: Integration points over cross section height - Gauss integration.

Here, the same tendency as for the trapezoidal rule. The more elements used, the more influence the number of integration points over the cross section height has. Gauss integration seems to be a worse fit for the integration over the cross section height as the convergence lines has irregularities when more elements are used.

When observing the influence of the integration method, it could be interesting to observe the stress distribution over the cross section height. At the point of first yield, the plastic strains will occur at the top or bottom of the beam first. As the

difference between the trapezoidal rule and Gauss integration is the location of the integration points near the edges, a change might be found in the distribution of stresses.

In Figure 4.9 and Figure 4.10, the stress distribution for the beam at some point of loading are shown.

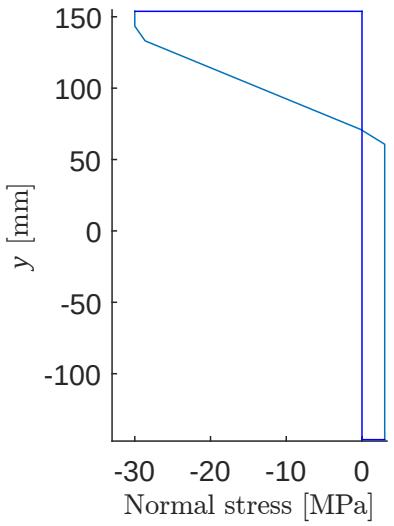

Figure 4.9: Stress distribution with trapezoidal rule over cross section height.

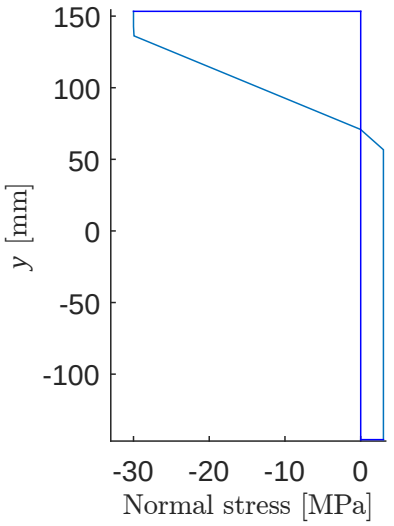

Figure 4.10: Stress distribution with gauss integration over cross section height.

It is seen, that the gauss integration points are suited better when observing yielding at the edge. But, the trapezoidal rule is more accurate in the middle of the cross section. The difference is so small, that the choice of integration method is unimportant. The choice may therefore be the trapezoidal rule, as the convergence study showed this to be better suited for cross section integration.

4.3 Iteration scheme methods

The iteration schemes should not cause any difference in the convergence. But, an improved iteration scheme could decrease the computational time. In this analysis, the modified Newton-Raphson scheme is compared to the full Newton-Raphson scheme. The difference is as described earlier, that the modified Newton-Raphson only updates the stiffness for every load increment, where the full Newton-Raphson scheme updates the stiffness for every iteration. In this comparison, the interesting parameters are total number of iterations used and computational time

used on calculations. The analysis is done for a fully converged model loaded to a fully plastic cross section. The results can be found in Table 4.4.

Table 4.4: Iteration scheme comparison.

	Total number of iterations	Elapsed time
Modified Newton-Raphson	302	20.6 s
Full Newton-Raphson	64	6.2 s

The results shows a significant reduction in both amount of iterations needed and in computational time. The update of the stiffness is very beneficial, and the computational time of setting up the stiffness matrix for each iteration is much faster than iterating to the correct value with an initial stiffness of the given load increment.

Summary

From previous analysis, regarding the different calculation methods used in the MatLab program, it can be concluded that the convergence is highly depending on the number of elements used, not only is this the most contributing factor to the convergence, but the integration over height and length is also depending on the number of elements. The choice of scheme method only have influence on the calculation time. Here, the full Newton-Raphson was the fastest and most effective.

4.4 Concrete beam analysis

In this section, a beam subjected to a forced displacement is analysed. As said earlier, the results will be compared to other solutions from different methods and programs. For the material model, the nonlinear elasto-plastic material model is applied. This is the most advanced and accurate material model for concrete used in this project and will give the best results for concrete structures. The beam dimensions are given in Table 4.5.

Table 4.5: Concrete beam properties.

Geometry	
Cross section	300 mm × 200 mm
Length	3000 mm
Rebars	3×12 mm
Rebar distance from bottom	50 mm
Concrete	
Yield stress (f_t/f_c)	3 MPa/30 MPa
Initial Young's modulus	30×10^3 MPa
Reinforcement steel	
Yield stress (f_y)	550 MPa
Young's modulus	210×10^3 MPa

Modelling

For the calculations, the number of elements are chosen so the model is converged. From the elements convergence section, it was concluded that the model converged with an acceptable accuracy at 30 elements. The model is shown in Figure 4.11.

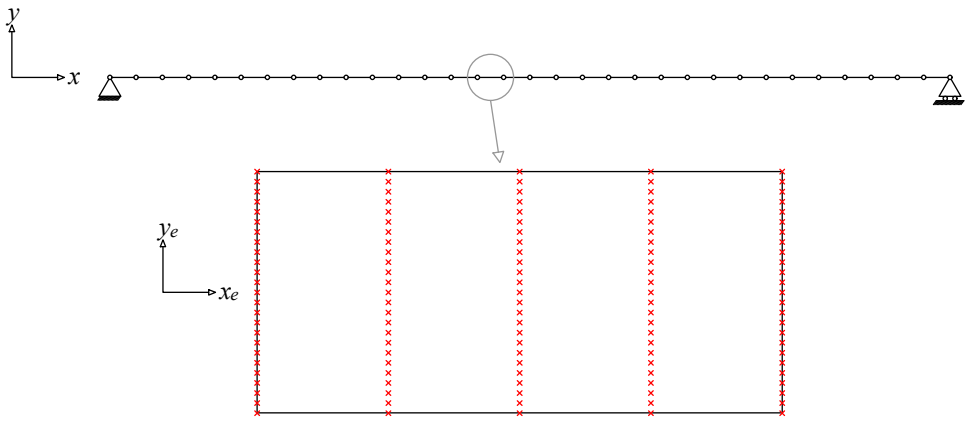

Figure 4.11: Sketch of 1D beam model and integration points in a beam element.

The supports are placed at the elastic neutral axis. Thus, the beam axis will be located in $y = 0$,$z = 0$. As to the analysis regarding number of cross section integrations, these have no influence on the accuracy when the number of elements is set higher than 2. Thus, the points in the x direction are set to 5 per element uniformly distributed and the points in the y-y direction is set to 50 per element as

the number of elements used requires that the number of integration points over the cross section height is set this high. The beam element can be seen in Figure 4.11.

The forced displacement is done at the center of the beam at the beam axis. The maximum displacement is set to 20 mm. Here the cross section becomes fully plastic.

Results

The analytical solution was presented in Chapter 2. The numerical one dimensional finite element model in MatLab resulted in the force/displacement curve shown in Figure 4.12.

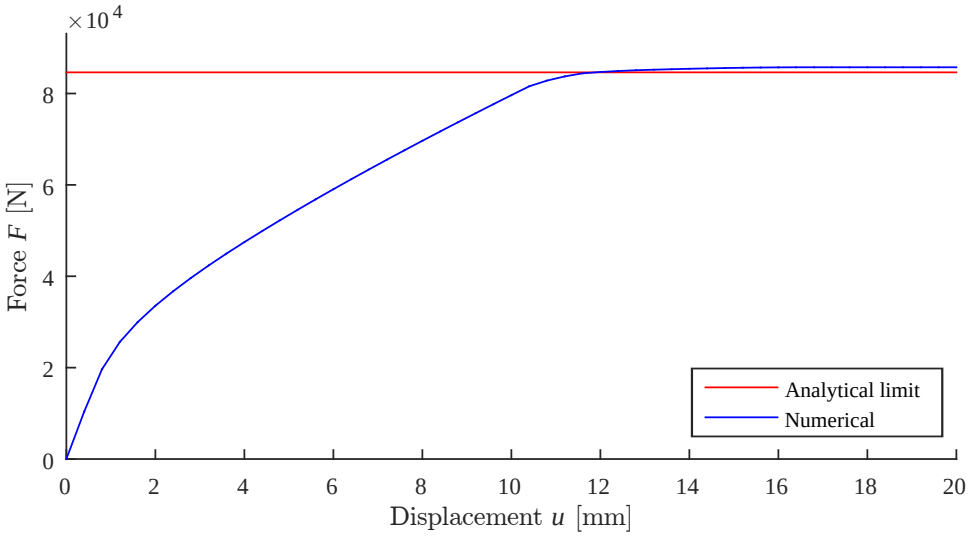

Figure 4.12: Force/displacement curve - Nonlinear concrete material model.

The final maximum force found from numerical calculations and the analytical fully plastic maximum force is compared in Table 4.6.

Table 4.6: Comparison of analytical and numerical solutions.

	Maximum force capacity
Analytical limit value	8.50×10^4 N
Numerical max value	8.69×10^4 N
F_{num}/F_{lim}-1 [%]	2.32 %

A deviation of 2.32 % is acceptable, considering the big difference in complexity

and time consummation between the two methods. The stress and strain distribution over the cross section height at the center of the beam, is shown in Figure 4.13.

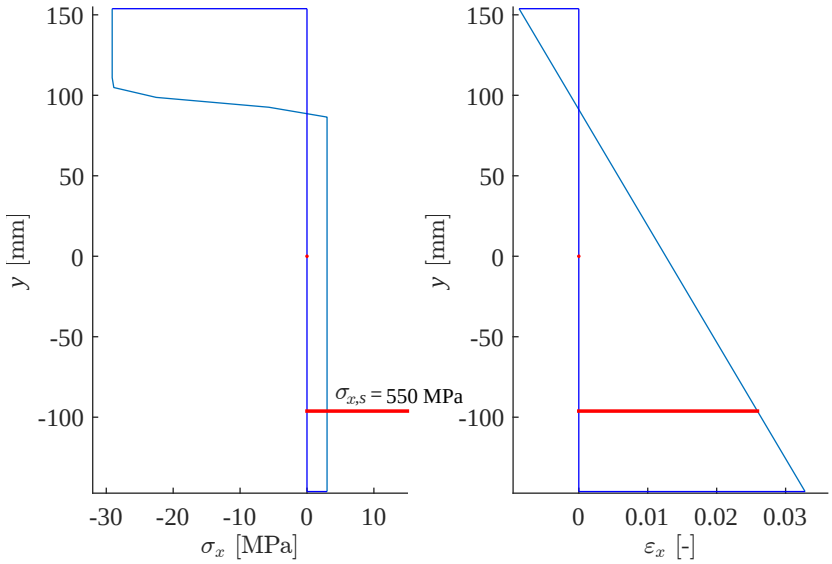

Figure 4.13: Stress and strain distribution - with rebar stress cut-off.

The cross section is almost fully plastic. The remaining part which seems to be elastic, is caused by an insufficient amount of integration points over the cross section height. Comparing the stress distribution with the analytical stress distribution gives a deviation as shown in Figure 4.14 and Figure 4.15.

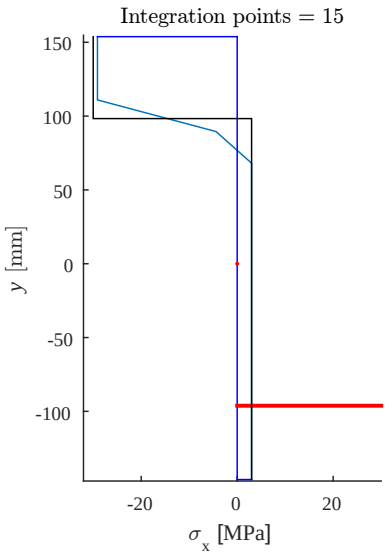

Figure 4.14: Stress distribution with 15 integration points over cross section height.

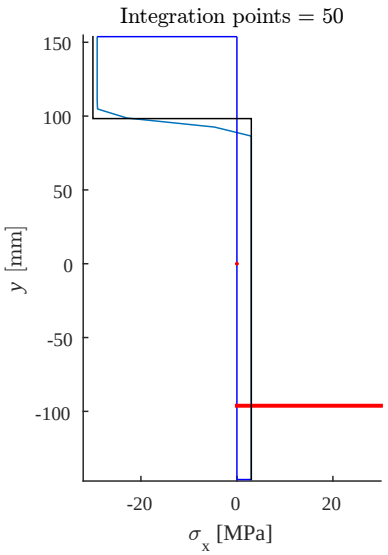

Figure 4.15: Stress distribution with 50 integration points over cross section height.

The black line indicates the analytical stress distribution. It is observed that the numerical model deviates from the exact solution, but goes towards the exact solution when more integration points are used to distribute the stresses over the cross section height.

Also, in Figure 4.14 and Figure 4.15, it can be seen that the increase in integration points leads to a change in the position of the neutral axis. The position of the neutral axis is shown in Figure 4.16.

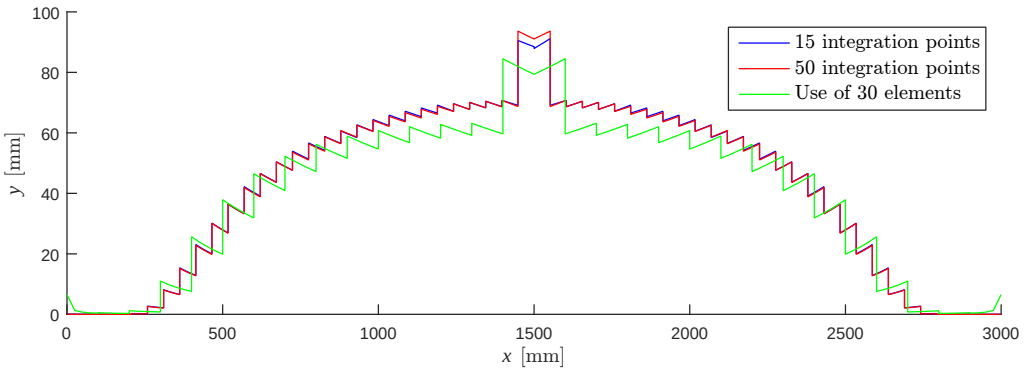

Figure 4.16: Position of the neutral axis.

The neutral axis has a lot of kinks. This is caused by discontinuity in stress between the elements. The neutral axis is found from the point of zero stresses on the y-axis, so if discontinuity exist in the stresses, it will also be the case with the neutral axis. It is seen, that the difference between using 15 and 50 integration points over the cross section height is minor, when considering the movement of the neutral axis. The difference in using 30 and 60 elements is significant, especially at the center of the beam where the deviation is large.

When the point of zero stresses moves away from the beam axis, see Figure 4.16, it creates an extra beam strain at the beam axis. This beam strain creates a residual force, which depend on the boundary conditions, will lead to either internal normal force or longitudinal displacement. As the boundary conditions are simple supported, see Figure 4.11, this will lead to longitudinal displacement. The deformation of the beam is shown in Figure 4.17.

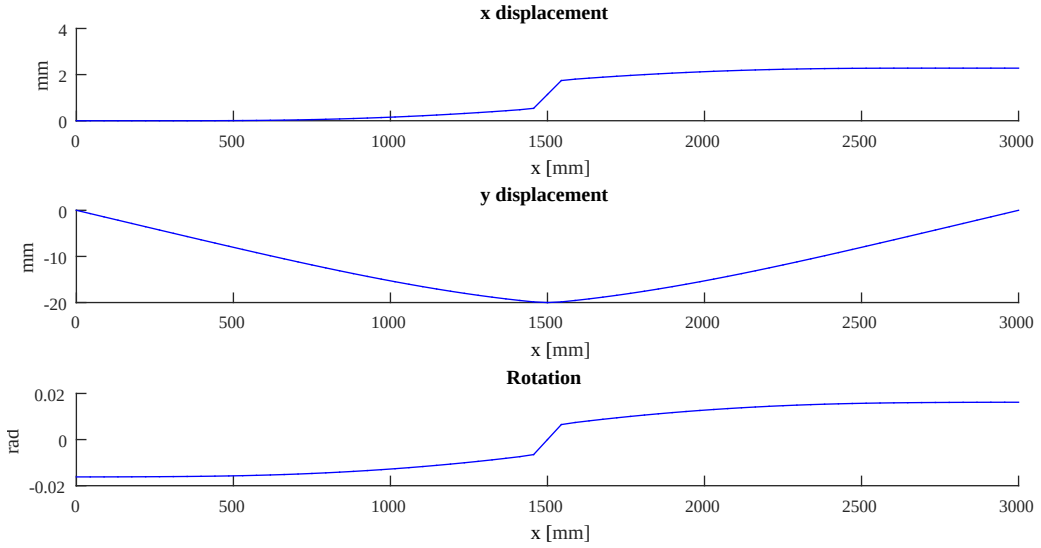

Figure 4.17: Beam deformation.

In the x deformation it is seen that the deformation increases a lot over a small distance at the center of the beam, which is caused be large plastic deformation. Observing the y deformation, the very center of the beam has developed a plastic hinge where the cross section is fully yielded. This is also visualized in the rotation, where the rotation change quite a lot over a small part of the beam. The internal forces should only consist of a shear force and a moment as the right support is equipped with a roller. The internal forces are shown in Figure 4.18.

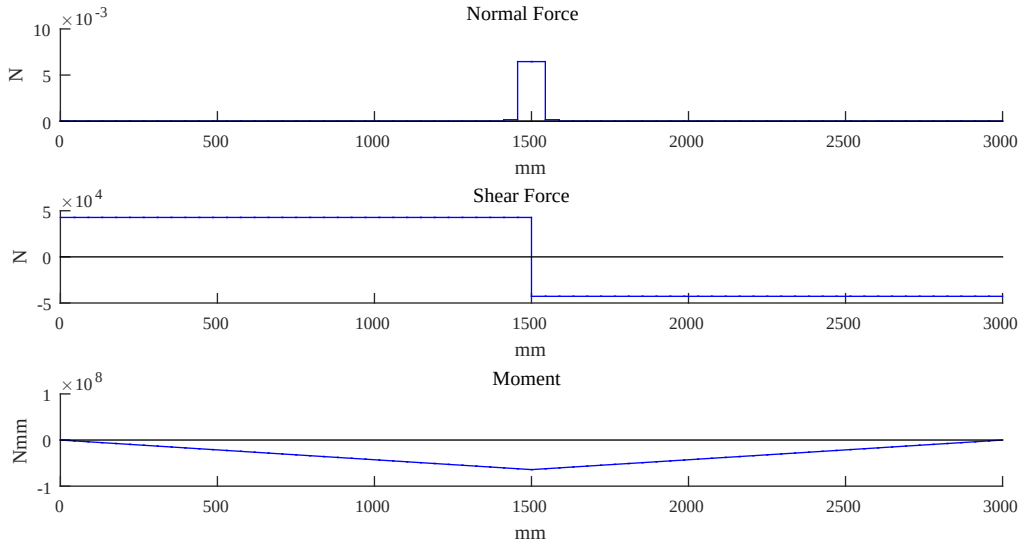

Figure 4.18: Beam internal forces.

The normal force is very close to zero, and is only present due the the tolerance restriction in the calculations. It is though acceptable small to be considered as zero.

It is now clear, that the MatLab script is capable of analysing reinforced concrete beams with random cross sections, also after the material is yielding. The next interesting part, is to compare the finite element calculations with a model made in a different software. The results will now be compared to a three dimensional model made in Abaqus.

Comparison with Abaqus model

A description of the Abaqus model can be found in Appendix A. The comparison is made to evaluate the MatLab script, when it is put up against a more complex model from a widely used and acknowledged software as Abaqus. An analysis of the beam is performed in Abaqus in 3D using a material model called Concrete damaged plasticity (CDP).

Results

Plotting the force/displacement curve shows the behaviour of the beam and the maximum force capacity of the beam. The force/displacement curves for the analytical, 1D MatLab and 3D Abaqus model are shown in Figure 4.19.

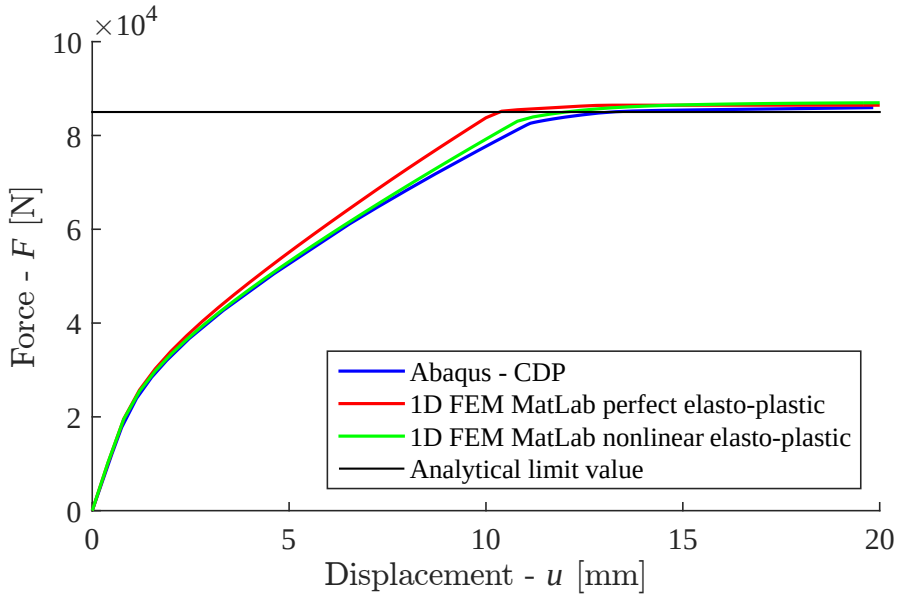

Figure 4.19: Force displacement curve comparison.

The curves show a clear similarity. The MatLab model seems to be slightly stronger, which makes sense, as this model does not include any kind of softening or damage and Abaqus does take softening/damage into account. The conclusion would be that the MatLab model is evaluating the behaviour of the reinforced concrete beam quite well, taken into consideration that the complexity of this model is limited. Especially the nonlinear material model lies very close to the Abaqus result.

Another way to compare models is through comparison of stresses. As the MatLab model is based on Bernoulli-Euler beam theory, it do not take shear into account. Thus, only normal stresses are usable to compare. In Figure 4.20, the normal stress distributions over the cross section at the center of the beam, are shown.

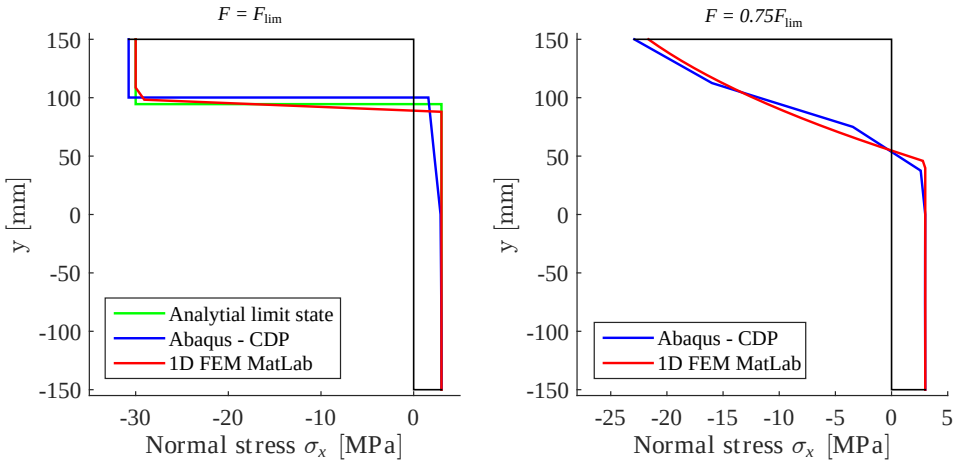

Figure 4.20: Normal stress distribution comparison.

The stress distributions are very similar and shows good stress estimations from the 1D MatLab model. Deviation between the models are expected due to the difference in complexity, but the models gives more comparable results than expected. The Abaqus model, which perform heavy calculations with a large amount of elements, is possible to be challenged by a far more simple finite element model, which do not require the same computation time or modelling time. The Abaqus model took 288 s to calculate. Compared with the MatLab computational of maximum 20 s is much more profitable when it comes to computational time.

The final comparison is due to the normal stresses in the entire beam. This is illustrated for the Matlab model in Figure 4.21.

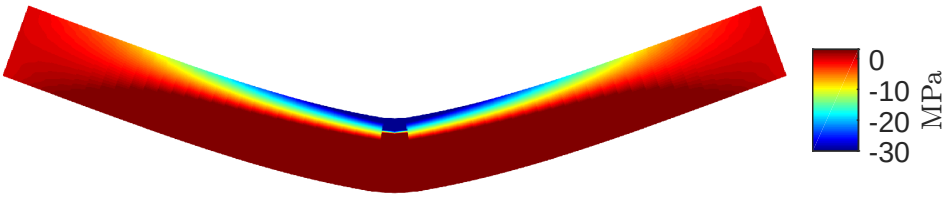

Figure 4.21: Normal stress distribution comparison.

The normal stresses calculated in Abaqus are shown in Figure 4.22.

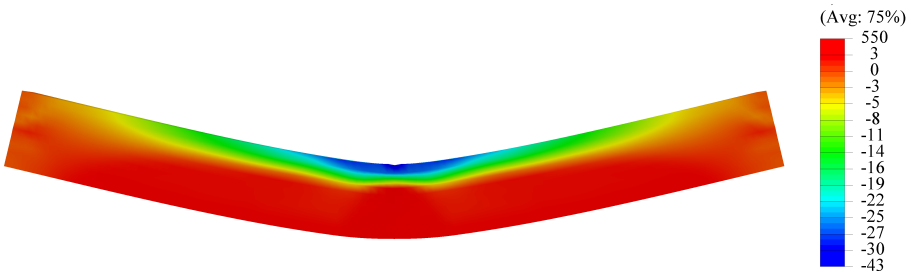

Figure 4.22: Normal stress distribution comparison. Units in MPa.

The stress distributions are again very similar. The Abaqus model has a smaller and more concentrated compressive yield zone, where the MatLab model has a wider span of plastic strains in the compressive yield region.

It can be concluded, that 1D MatLab model is capable of simulating the behaviour of beams in plasticity quite well.

4.4.1 Concrete frame

To evaluate the MatLab program's ability to analyse systems more complex than a simple beam, a frame model is constructed in reinforced concrete. The frame is illustrated in Figure 4.23. The frame analysis is conducted to check the MatLab scripts ability to handle more advanced structures.

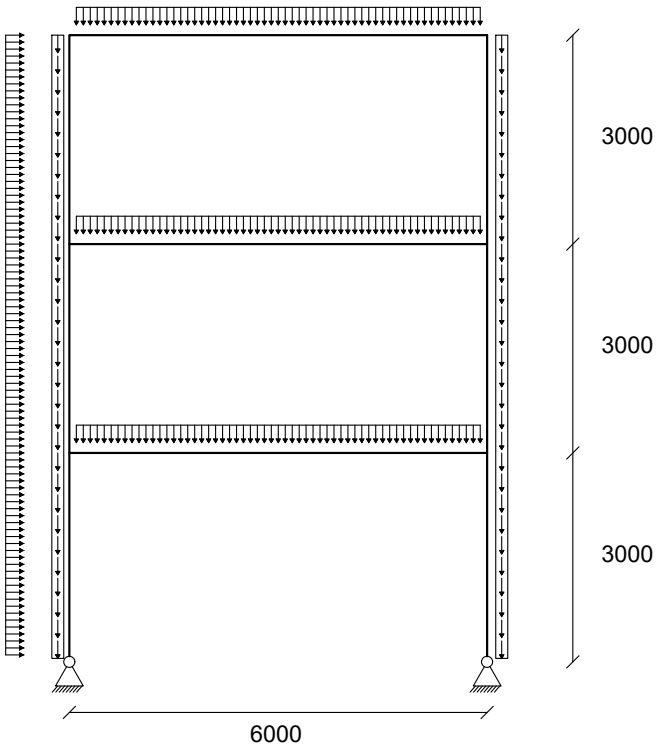

Figure 4.23: Frame structure. Units in mm.

The frame is subjected to static loads on each floor and a horizontal static wind load. The supports are pinned, which implies that all moment must be handled in the frame corners, calculations with fixed supports will also be shown to compare. The size of the wind load is arbitrary, but is set large enough to elicit yielding. Beside the wind loads and live loads, the structure is subjected to the self weight from the structure. The column and beam cross sections are illustrated in Figure 4.24 and the properties listed in Table 4.7.

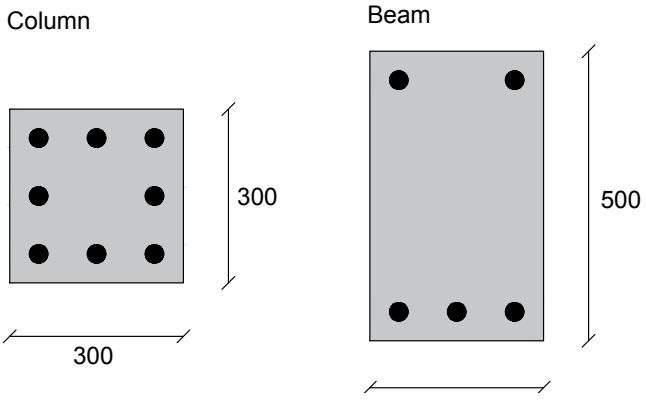

Figure 4.24: Frame cross sections. Units in mm.

Table 4.7: Frame cross section properties.

	Concrete	Reinforcement steel
Column	3/30 MPa	ø16 mm - f_y = 550 MPa
Beam	3/30 MPa	ø16 mm - f_y = 550 MPa

The analysis will show the total structure deformation and the stress distribution in each element. Also the internal force is found from the calculations.

Results

First, the deformation from the wind load and self weight is found. The total structure deformation is shown in Figure 4.25 and Figure 4.26.

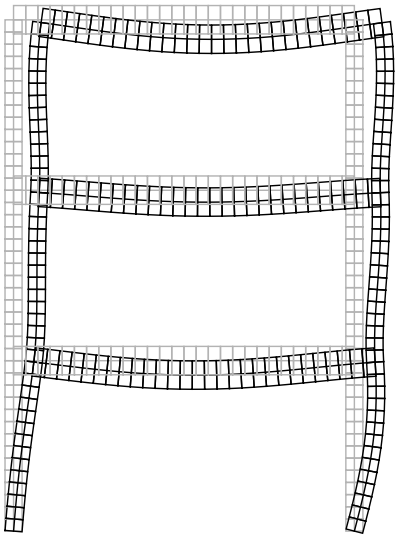

Figure 4.25: Scaled frame deformation with pinned supports.

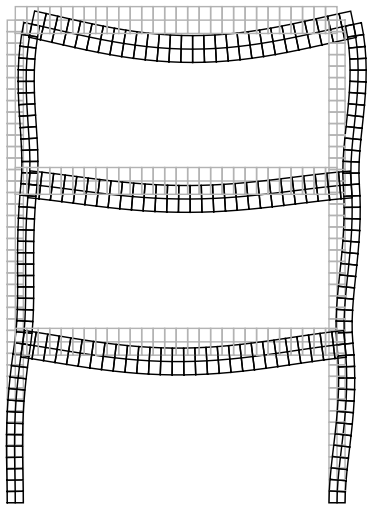

Figure 4.26: Scaled frame deformation with fixed supports.

The pinned support structure, is more exposed to lateral displacement than the structure with fixed supports. But, in the fixed support system, the beam bending is greater. To see the response of the structures when a region starts yielding the stresses are plotted, see Figure 4.27 and Figure 4.28.

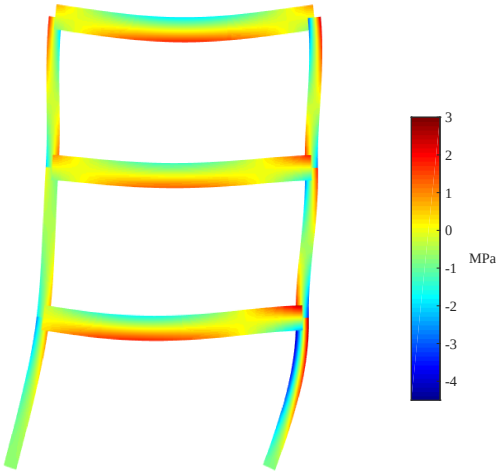

Figure 4.27: Frame normal stress distribution with pinned supports.

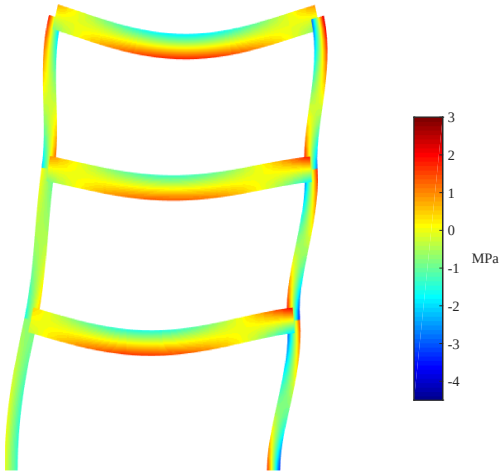

Figure 4.28: Frame normal stress distribution fixed supports.

From the stress plot, it is seen that the frame with pinned supports starts yielding first. Specially, the bottom right column starts yielding at the current loads, if the structure is pinned supported. The elements must contain more moment, as the supports are transferring less moment to the foundation. This is seen on the internal force plots in Figure 4.29 and Figure 4.30.

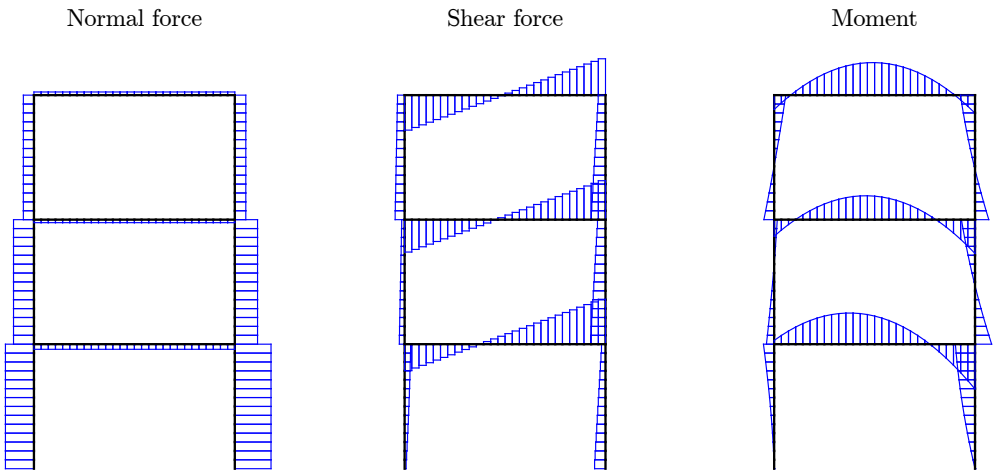

Figure 4.29: Frame internal forces with pinned supports.

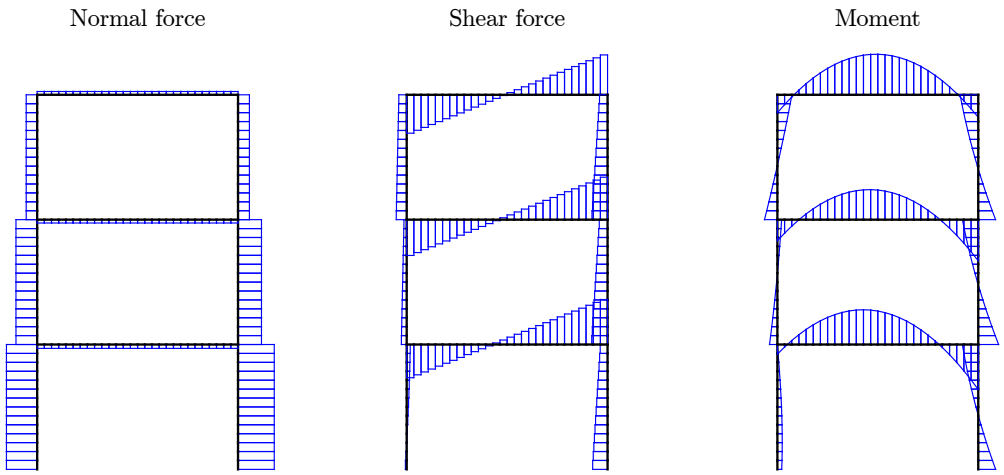

Figure 4.30: Frame internal forces with fixed supports.

The only significant difference in the internal forces in the moment distribution in the bottom columns. The fixed supported frame has an internal moment at the support, whereas the pinned supported frame is only transferring normal and shear force directly from each support to the foundation.

To check if the script calculations are correct. The total wind pressure is compared to the reaction force, see Table 4.8.

Table 4.8: Lateral force comparison.

Total wind pressure	10650 N
Total reaction force	−10639 N
Deviation	0.1 %

A deviation of 0.1 % is acceptable, as it most likely is caused by rounding errors.

To evaluate the behaviour of a structure subjected to a load series, the behaviour during unloading and reloading are the first steps toward dynamic excitation and response.

4.5 Unloading and reloading stress/strain curves

In this section the perfect elasto-plastic material model and the nonlinear elasto-plastic material model is expanded to include elastic unloading/reloading.

The perfect elasto-plastic material model with unloading/reloading is showed in Figure 4.31.

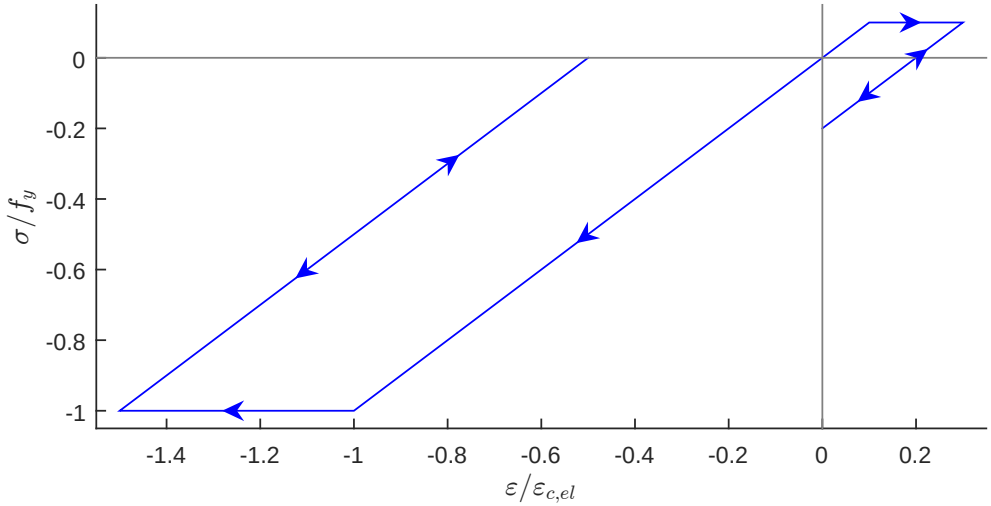

Figure 4.31: Perfect elasto-plastic material with unloading/reloading.

In Abaqus there is a smeared crack model, which is used as a basis for how the material behave during unloading/reloading. In the smeared crack model, the tensile stresses during unloading, goes directly towards zero [SIMULIA, 2014]. This principle is used to model material behaviour during unloading as well in this project. The nonlinear elasto-plastic material model with unloading/reloading, inspired by the smeared crack model, is shown in Figure 4.32.

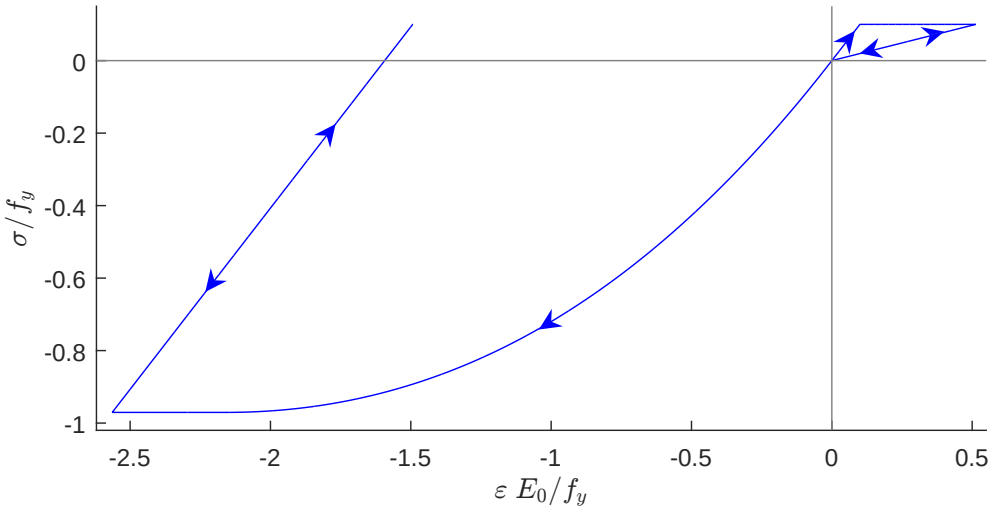

Figure 4.32: Nonlinear elasto-plastic material with unloading/reloading, strain normalized with respect to initial elasticity, E_0.

For both material models it is assumed that the materials act perfectly plastic if the yield stress is reached during unloading.

4.6 Unloading and reloading of reinforced concrete beam

In this section the permanent deformation resulting from plastic strains is examined. The reference beam is loaded close to the maximum capacity and then unloaded. A force based iteration scheme is used, which makes it impossible to achieve fully plastic behaviour. The force displacement curve is shown in Figure 4.33.

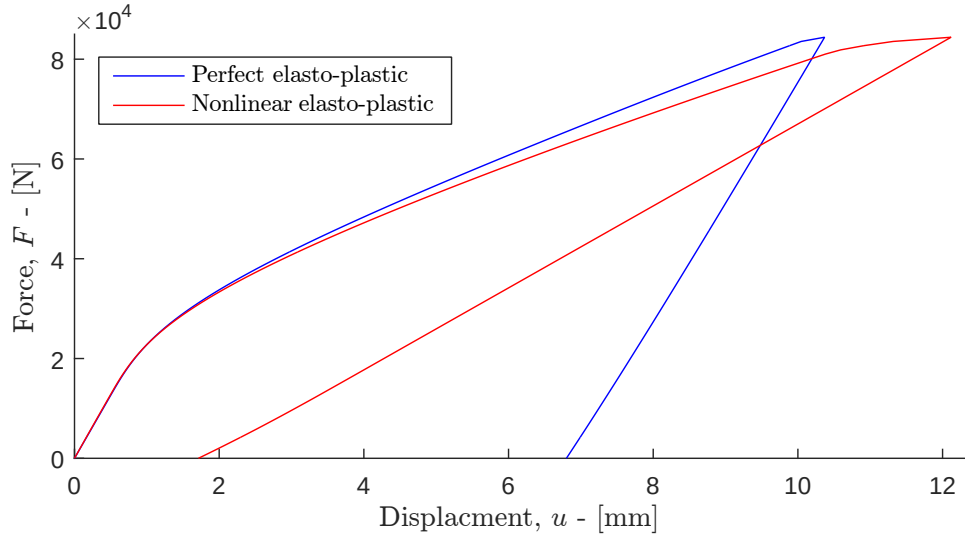

Figure 4.33: Force displacement curve for load/unloading.

It can be seen, that the nonlinear elasto-plastic material model is recovering more than the perfect elasto-plastic material model. This is also seen in the following stress plots.

The stress state at the maximum force/displacement with a perfect elasto-plastic material is shown in Figure 4.34.

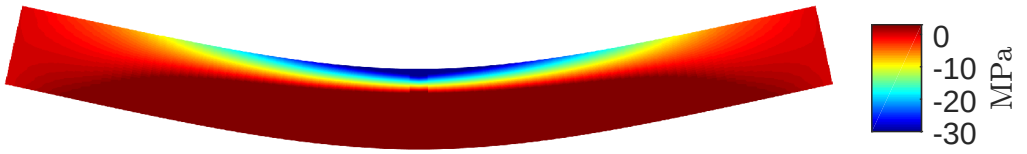

Figure 4.34: Stress state at maximum displacement with scaled deformation and perfect elasto-plastic material.

After complete unloading there is a permanent deformation and residual stresses, as shown in Figure 4.35.

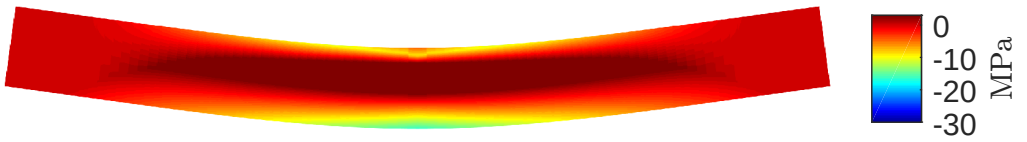

Figure 4.35: Residual stress state with scaled deformation and perfect elasto-plastic material.

The stress plots show that residual compressive stresses are created in the bottom of the beam and tensile residual stresses are formed in the middle of the beam together with a small part of the top edge. The stress state at the maximum force/displacement with a nonlinear elasto-plastic material is shown in Figure 4.36.

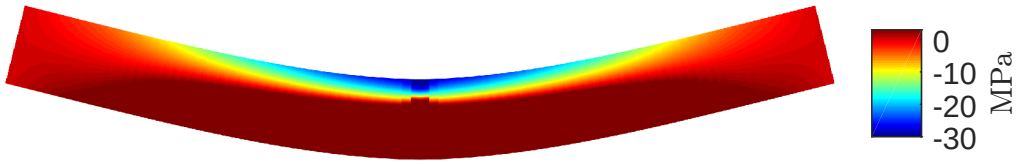

Figure 4.36: Stress state at maximum displacement with scaled deformation and nonlinear elasto-plastic material.

After complete unloading there is a permanent deformation and residual stress's, as shown in Figure 4.37.

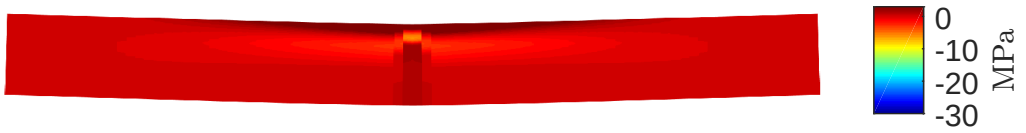

Figure 4.37: Residual stress state with scaled deformation and nonlinear elasto-plastic material.

The residual stress state for the nonlinear elasto-plastic material model shows a smaller permanent displacement and less residual stresses.

Reloading is examined, where the beam is loaded until yielding, then loaded in the opposite direction until some yielding is observed and then reloaded. After reloading the force displacement curve returns to follow the same line as before the unloading as shown in Figure 4.38.

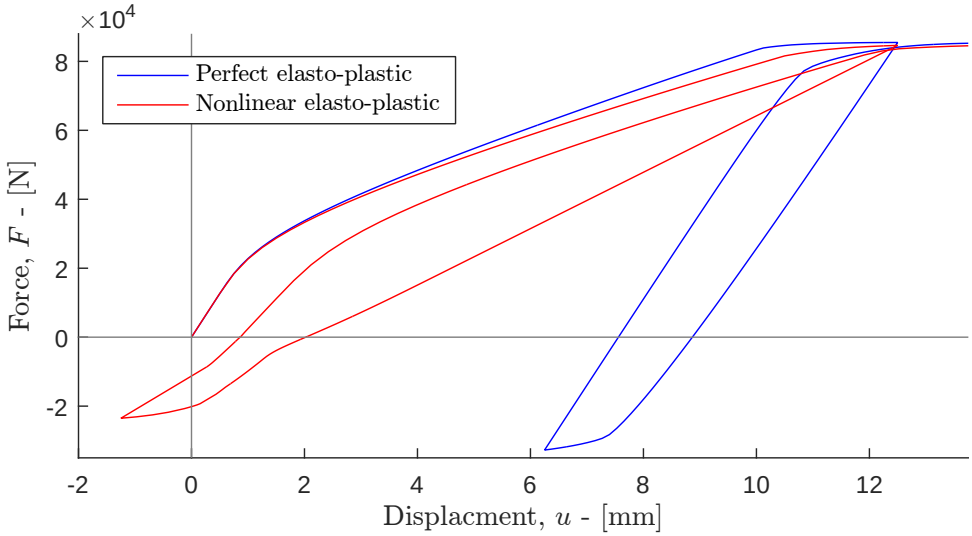

Figure 4.38: Force displacement curve for reloading.

It is seen, that both material models reach the same curve again after unloading and reloading, even though the unloading and reloading curves are widely different.

4.7 Static part summary

The static part is now done and sets the foundation for the coming part. The analysis conducted with static loads on a simple supported beam and a frame structure showed that it indeed is possible to perform plastic analysis using one

dimensional finite element modelling. A MatLab script was developed, capable of performing gradual loading or increasing a forced displacement in increments so that the plastic behaviour during yielding could be described.

The analysis showed fair comparisons between an analytical solution to a simple supported beam with a point load on the middle and the one-dimensional finite element solution performed in the MatLab script. Also, the Abaqus model gave similar results to the MatLab script.

The frame structure analysis showed that the MatLab script is able to handle more complex structures as well, also including plastic deformation.

Considering unloading and reloading, the MatLab script is definitely capable of both monotonic unloading and reloading of structures using both perfect elasto-plastic material behaviour and nonlinear elasto-plastic material behaviour. Here, the nonlinear material showed a larger recovered displacement, where the perfect elasto-plastic material has a steeper unloading/reloading curve. Though, the result after unloading and reloading was the same for both material models.

Part II

Dynamic finite-element analysis

Chapter 5

Introduction to dynamics

In this chapter the dynamic part of the MatLab script is introduced and the necessary preparations are done to enable dynamics in the MatLab script. Dynamic finite element models are often applied in earthquake engineering and when modelling traffic loads. The goal with this part of the MatLab script, is for it to be able to simulate the response of a reinforced concrete structure. A frame structure subjected to ground accelerations recorded from a real earthquake and a railway bridge subjected to a moving train is analysed.

Earlier, the material models where updated to handle unloading and reloading. This is necessary when considering plastic material, as the behaviour after plastic deformation is reached, is crucial to the dynamic response of the system.

Solving dynamic problems require a nonlinear differential equation solver. Solvers like this could be a Runge-Kutta method, HHT-α or a Newmark-β method. Applying schemes like these, the script becomes capable of numerical time integrate the dynamic response of a structure subjected to a load or displacement time series. The dynamic theory is based the equation of motion as the governing equilibrium equation. The equation of motion is defined on the form:

$$[\mathbf{m}]\{\ddot{u}(t)\} = \{f^{ext}(t)\} - \{f^{int}(t)\} - \{f^{damp}(t)\}. \tag{5.1}$$

Where $[\mathbf{m}]$ is the mass stiffness matrix and $\{\ddot{u}(t)\}$ is the acceleration vector. $\{f^{ext}(t)\}$ is the external forces acting on the system, $\{f^{int}(t)\}$ is the internal forces and $\{f^{damp}(t)\}$ is the damping forces.

The internal forces and the damping forces can be found from

$$\{f^{int}(t)\} = [\mathbf{k}]\{u(t)\} - \{R\}, \tag{5.2}$$

$$\{f^{damp}(t)\} = [\mathbf{c}]\{\dot{u}(t)\}. \tag{5.3}$$

Here, $\{R\}$ is a nonlinear restoring force, $[\mathbf{c}]$ is the damping matrix, $\{\dot{u}(t)\}$ is the

velocity vector and $\{u(t)\}$ is the displacement vector.

In this project, the Newmark-β scheme is applied to numerical time integrate the dynamic response. As the material behaviour is elasto-plastic, the original Newmark-β scheme is not sufficient. A incremental formulation of the Newmark-β method is used instead, which suits the plastic behaviour better.

5.1 Newmark-β method - Incremental formulation

The dynamic analysis is conducted using the an nonlinear solver, in this case the Newmark-β method. The dynamic forces are creating nonlinear behaviour of the material, which is modelled by the equation of motion combined from Equation (5.1), Equation (5.2) and Equation (5.3).

$$[\mathbf{m}]\{\ddot{u}(t)\} + [\mathbf{c}]\{\dot{u}(t)\} + [\mathbf{k}]\{u(t)\} - \{R(u(t),\dot{u}(t))\} = \{f^{ext}(t)\}. \tag{5.4}$$

Here u is the displacement vector, $\dot{u}$ is the velocity vector and $\ddot{u}$ is the acceleration vector. $R(u(t),\dot{u}(t))$ denotes the difference between the linear elastic internal force and the real nonlinear internal force, see Figure 5.1.

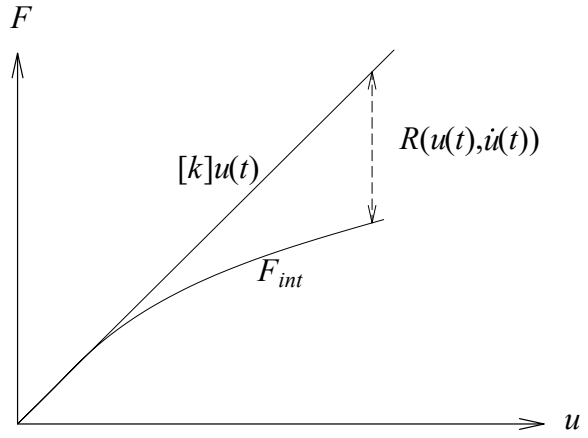

Figure 5.1: Illustration of nonlinear restoring force R.

The stability of the Newmark-β method depends on the parameters γ and β. If $(\beta,\gamma) = (1/4,1/2)$ the solution is unconditionally stable, and the acceleration is constant within each time step. If $(\beta,\gamma) = (1/6,1/2)$ the acceleration is linear interpolated. If $(\beta,\gamma) = (0,1/2)$ the method becomes identical to the central difference method. $(\beta,\gamma) = (1/4,1/2)$ is frequently used, as it result in a uncondi-

tional stable solution, however the result is not especial accurate. In Figure 5.2 the stability conditions for the Newmark-β method is shown, where $\xi = \beta + \frac{1}{(\omega_{\max}\Delta t)^2}$.

[Gavin, 2014]

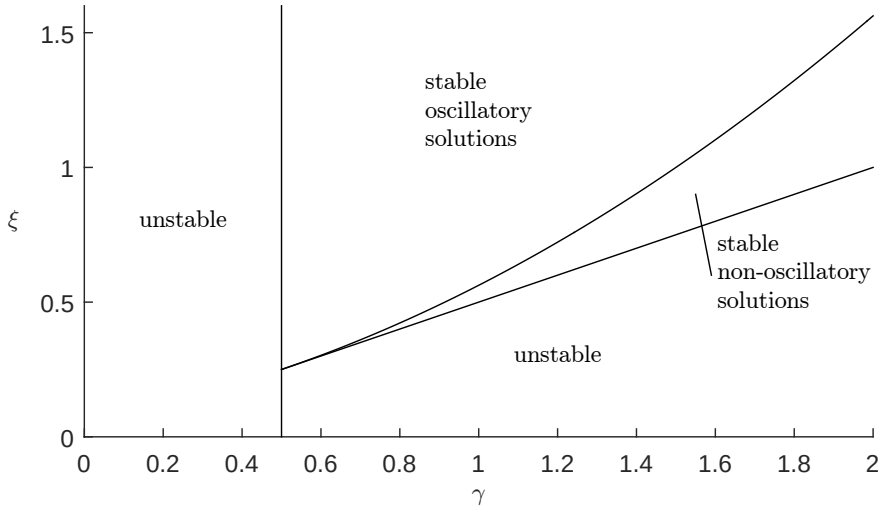

Figure 5.2: Stability conditions for the Newmark-β method. [Andersen, 2014]

For the Newmark-β method the inverse of two matrices is needed, this being the mass matrix and

$$[\tilde{\mathbf{k}}] = (\frac{1}{\beta\Delta t^2}[\mathbf{m}] + \frac{\gamma}{\beta\Delta t}[\mathbf{c}] + [\mathbf{k}]). \tag{5.5}$$

This is done one time in the begin of the calculation, as taking the inverse of a matrix takes alot of computational time.

The incremental equilibrium is found as

$$[\mathbf{m}]\{\delta\ddot{u}\} + [\mathbf{c}]\{\delta\dot{u}\} + [\mathbf{k}]\{\delta u\} = \{f_{i+1}^{\text{ext}}\} - \{f_i^{\text{ext}}\} = \{\delta f_i^{\text{ext}}\}. \tag{5.6}$$

The Newton-Raphson algorithm is used to solve the nonlinear equations, the algorithm is as followed:

1. First the initial value of the displacement increment $\delta x_i^{(0)}$ is set to zero, and the initial $\tilde{f}_i$ is calculated as

$$\{\tilde{f}_i(\delta u_i^{(0)})\} = \{\delta f_i^{\text{ext}}\} + \left(\frac{1}{2\beta}[\mathbf{m}] - \Delta t\left(1 - \frac{\gamma}{2\beta}\right)[\mathbf{c}]\right)\{\ddot{u}\} + \left(\frac{1}{\beta\Delta t}[\mathbf{m}] + \frac{\gamma}{\beta}[\mathbf{c}]\right)\{\dot{u}\}. \tag{5.7}$$

2. The displacement increment is updated with

$$\{\delta u_i^{(n+1)}\} = [\tilde{\mathbf{k}}]^{-1}\{\tilde{f}_i(\delta u_i^{(n)})\}, \tag{5.8}$$

where

$$\{\tilde{f}_i(\delta u_i^{(n)})\} = \{\tilde{f}_i(\delta u_i^0)\} - \{R_{i+1}^{(n)}\} + \{R_i\}, \tag{5.9}$$

and the restoring force is updated with

$$\{R_{i+1}^{(n)}\} = [\mathbf{k}](\{u_i\} + \{\delta u_i^{(n)}\}) - \{f^{\text{int}}\}. \tag{5.10}$$

3. Step two is iterated upon until it converges, i.e. $|\{\delta u_i^{(n+1)}\} - \{\delta u_i^{(n)}\}| < \varepsilon$, where ε is the tolerance.

The displacements are updated with

$$\{u_{i+1}\} = \{u_i\} + \{\delta u_i\}, \tag{5.11}$$

the velocities are updated with

$$\{\dot{u}_{i+1}\} = (1 - \frac{\gamma}{\beta})\{\dot{u}_i\} - \Delta t(1 - \frac{\gamma}{2\beta})\{\ddot{u}_i\} + \frac{\gamma}{\beta\Delta t}\{\delta u_i\}, \tag{5.12}$$

and the accelerations are calculated as

$$\{\ddot{u}_{i+1}\} = -[\mathbf{m}]^{-1}([\mathbf{c}]\{\dot{u}_{i+1}\} + [\mathbf{k}]\{u_{i+1}\} - \{R_{i+1}\} - \{f_{i+1}^{\text{ext}}\}). \tag{5.13}$$

This integration scheme, creates the basis for the dynamic calculations of a structure with an elasto-plastic material model.

5.2 Free vibration

In this section the free vibration of a reinforced concrete beam is analysed. Free vibration can be forced by giving the beam an initial displacement and then releasing it to vibrate freely. The free vibration can be used to find the natural frequencies of the system, by the acceleration spectrum.

5.2.1 Release from forced displacement

The beam is monotonically loaded until a displacement of 10 mm, which will cause some yielding, see Figure 4.12. The displacement is subjected at the center of the beam, see Figure 5.3.

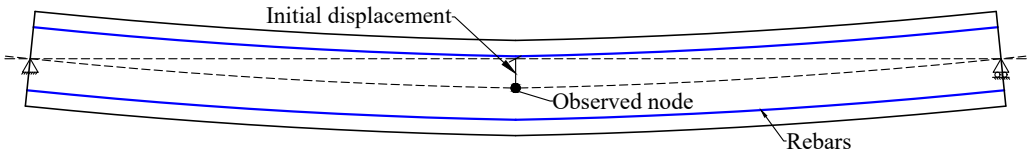

Figure 5.3: Beam for free vibration analysis.

The beam cross section is shown in Figure 5.4, where h = 300 mm, b = 200 mm, c = 50 mm and the rebars have a diameter of 12 mm.

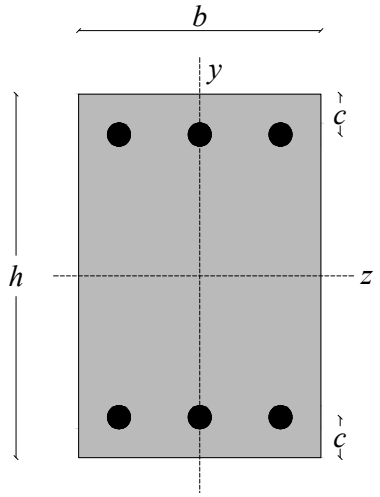

Figure 5.4: Cross section of reinforced concrete beam.

In Figure 5.5, the displacement, velocity and acceleration for both elastic vibration and elasto-plastic vibration without any form of damping, are shown.

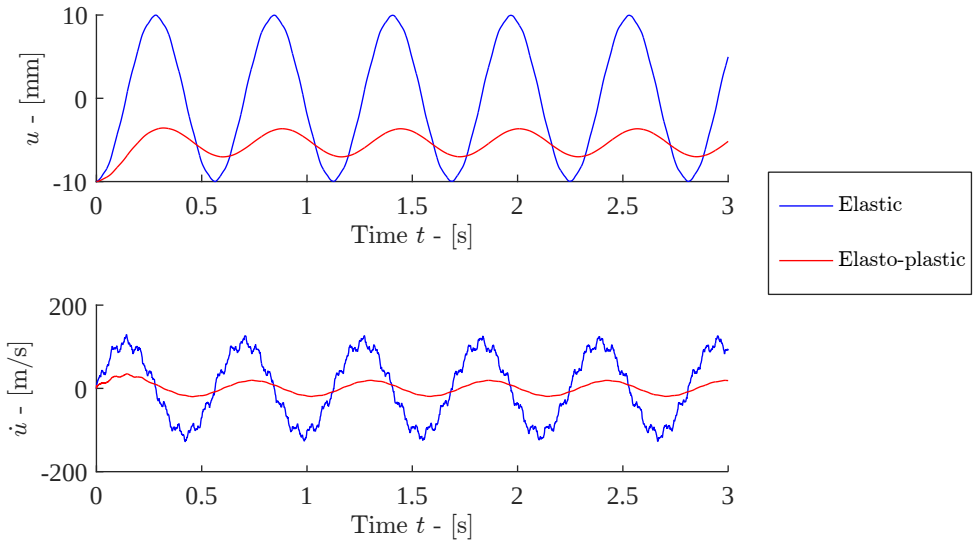

Figure 5.5: Free vibration from initial displacement release.

The elasto-plastic beam has some energy loss due to the plasticity, causing the beam not to vibrate as powerful as the elastic beam, which clearly is behaving purely elastic as the displacement is moving around zero with the same amplitude.

Observing the velocity of the two beams, the elastic beam obtains higher velocities and has some smaller and more frequent deviations. This indicates that the elastic beam has more than one eigenmode activated. The elasto-plastic beam on the other hand, seems to only activate the first eigenmode.

5.2.2 Evaluation of eigenfrequencies by acceleration spectrum

Applying the Fourier transformation of the beam accelerations and obtaining the Fourier coefficients, the acceleration spectrum is found, see Figure 5.6.

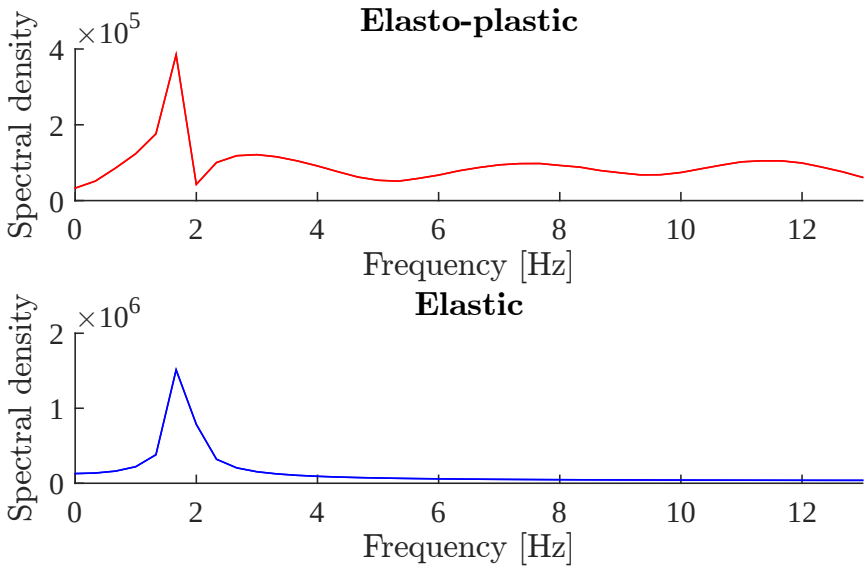

Figure 5.6: Acceleration spectrum for elastic and elasto-plastic beam.

In the spectrum, a peak indicates a frequency where an eigenmode is activated and the thereby the natural frequency for the given eigenmode is found.

The natural frequencies of the elastic and elasto-plastic beam are given in table 5.1.

Table 5.1: Beam natural frequencies form acceleration spectrum.

Mode	Elastic [Hz]	Elasto-plastic [Hz]
1	1.67	1.67

Natural frequency by stiffness and mass matrix

The model properties for evaluating the eigenfrequencies of the beam are given in table 5.2.

Table 5.2: Beam mass and volume properties.

	Volume	Mass
Concrete - $\rho = 2400\,\mathrm{kg/m^3}$	$1.79 \times 10^{-2}\,\mathrm{m^3}$	430 kg
Rebars - $\rho = 7800\,\mathrm{kg/m^3}$	$1.0 \times 10^{-3}\,\mathrm{m^3}$	8 kg
Total	$1.8 \times 10^{-2}\,\mathrm{m^3}$	438 kg

The eigenfrequencies can be found from the stiffness matrix and mass matrix.

Earlier, the stiffness matrix was defined as

$$[\mathbf{k}] = \int_0^{L_e} [\mathbf{B}]^T [\mathbf{D}][\mathbf{B}] \, \mathrm{d}x. \tag{5.14}$$

When dynamics are considered, the mass of the structure is just as important as the stiffness. The mass matrix is defined as

$$[\mathbf{m}] = \int_0^{L_e} \{\Phi(x_e)\}^T \rho A \{\Phi(x_e)\} \, \mathrm{d}x. \tag{5.15}$$

For undamped vibrations, the eigenfrequency can be found from an eigenvalue problem

$$([\mathbf{k}] - \omega_0^2 \cdot [\mathbf{m}])\{\Phi\} = 0. \tag{5.16}$$

And a non-trivial solution will yield

$$\det([\mathbf{k}] - \omega_0^2 \cdot [\mathbf{m}]) = 0. \tag{5.17}$$

Here ω_0 is the angular eigenfrequency, where only the positive roots are considered. The eigenfrequency f can be found from the following relation between angular eigenfrequency and the eigenfrequency

$$\omega_0 = 2 \cdot \pi \cdot f. \tag{5.18}$$

First five eigenfrequencies are listed in table 5.3.

Table 5.3: Beam undamped eigenfrequencies.

Mode	Natural frequency f_i [Hz]
1	1.779
2	7.115
3	9.697
4	16.009
5	28.462

Comparing the natural frequencies with the ones found from the acceleration spectrum it is seen, that beam released from a forced displacement, in the frequency interval 1-12 Hz, only activates mode one.

The first five eigenmodes are illustrated in Figure 5.7.

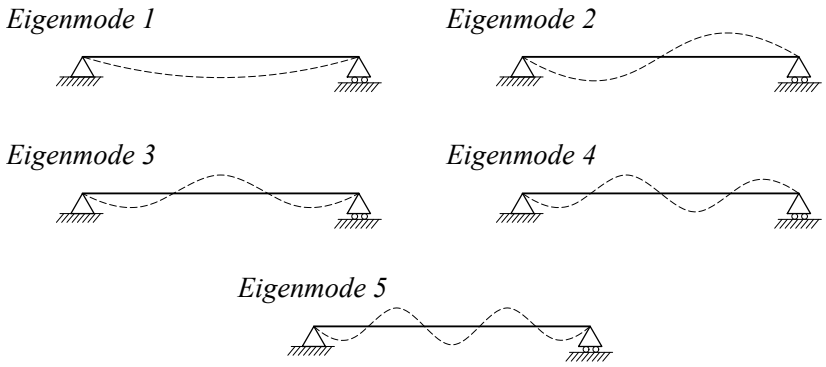

Figure 5.7: Different eigenmodes for a simple supported beam.

The mode shapes found by use of the MatLab script, are given in Appendix B. Here, the modes shapes are compared with the mode shapes found in Abaqus.

5.3 Damping

If no damping are defined for the system, the system will keep vibrating forever. To damp the system, a method called Rayleigh damping is applied. Rayleigh damping applies the mass and stiffness together with two coefficients a and b. The Rayleigh damping are found from

$$[\mathbf{c}] = a[\mathbf{k}] + b[\mathbf{m}]. \tag{5.19}$$

The Rayleigh coefficients a and b are found by

$$\begin{bmatrix} a \\ b \end{bmatrix} = \begin{bmatrix} \frac{0.5}{\omega_0(1)} & 0.5\omega_0(1) \\ \frac{0.5}{\omega_0(2)} & 0.5\omega_0(2) \end{bmatrix} \{\eta\}. \tag{5.20}$$

Where $\omega_0(i)$ is the angular frequency corresponding to mode i and $\{\eta\}$ is a vector containing the modal damping ratio for mode one and two. The modal damping ratios are for uncracked concrete structures around 4-7%. [Lee, 2007]

The free vibration without applying damping leads to infinite vibration, as seen in Figure 5.8.

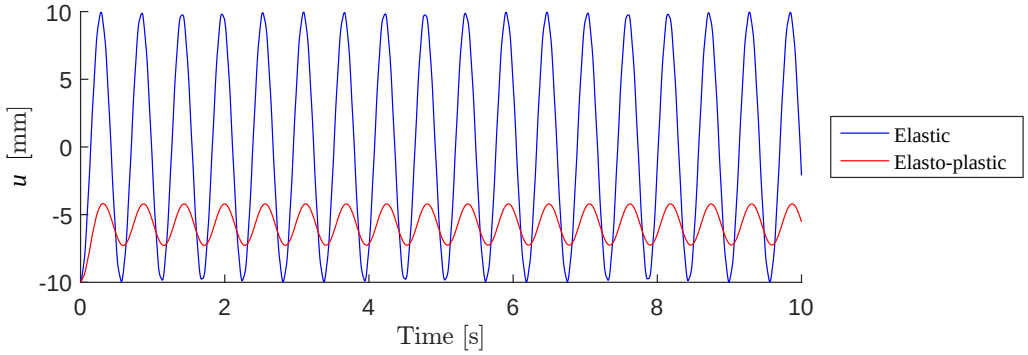

Figure 5.8: Beam displacement from free vibration without damping.

In Figure 5.9, Rayleigh damping is applied with a damping ratio of 0.05. This corresponds to 5% damping.

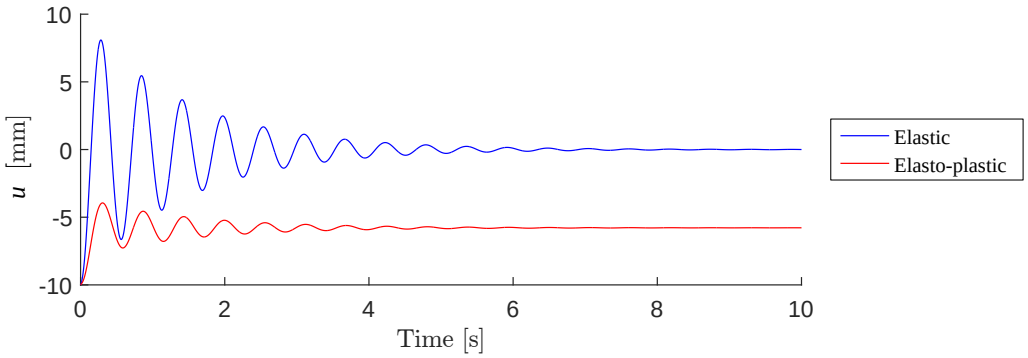

Figure 5.9: Beam displacement from free vibration with Rayleigh damping.

The difference is significant. Not only will the beam stop vibrating when damping is considered, but the elasto-plastic beam vibration is damped out earlier than the pure elastic beam vibration. This is due to the plasticity reducing the amplitude of the fluctuations and the vibrations are therefore damped out earlier.

5.4 Effects of plasticity in cyclic loading

In this section the effect of plasticity with cyclic loading is analysed, a load series with the same frequency as the first eigenfreuency is applied to the middle of the beam. The load is slowly increased to avoid exciting other modes, the load series is shown in Figure 5.10.

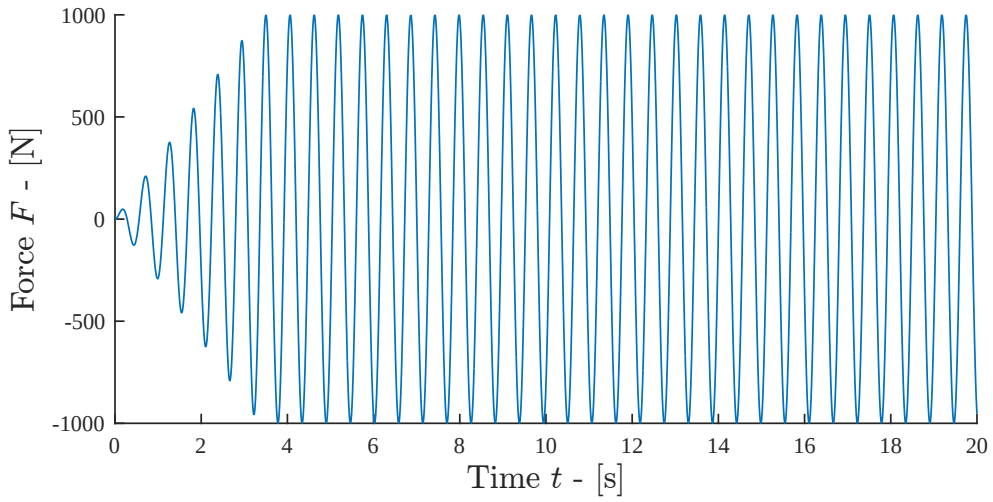

Figure 5.10: First 10 sec of load series used for analysing the effects of plasticity.

The first eigenfrequency is excited which causes resonance to occur, this leads to an increase in the amplitude of the vibrations. At some point the vibrations becomes large enough for plasticity to develop, at that point some of the energy is dissipated. This result in lower amplitude of vibrations in the elasto-plastic system than the elastic system, as is shown in Figure 5.11.

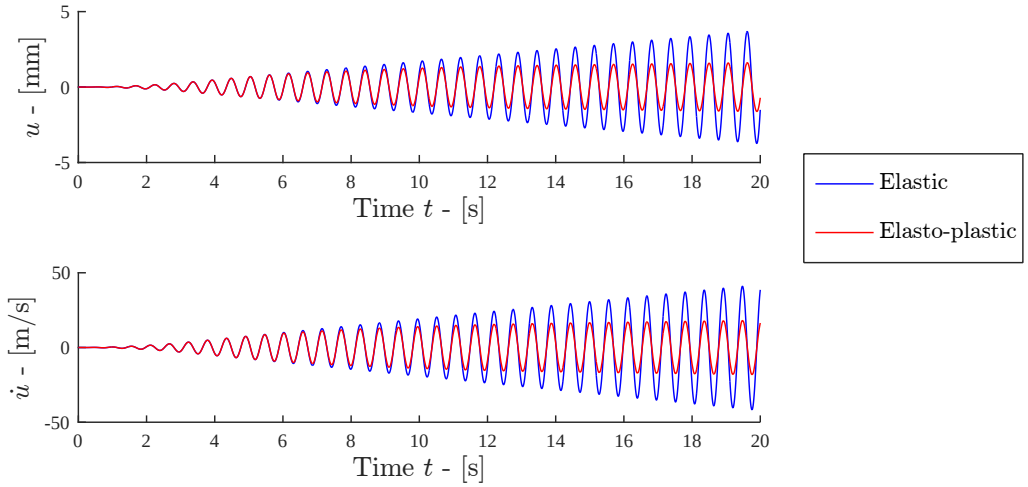

Figure 5.11: Elastic and plastic respond of the beam.

After a number of cycles the elasto-plastic beam obtain a constant amplitude of vibrations, where as the elastic beam vibrations continues to increase in amplitude.

Figure 5.11 clearly shows, that by including plasticity energy is dissipated which is why the vibrations are smaller for the elasto-plastic system.

5.5 Frame structure subjected to earthquake excitation

This section contains an analysis of a three story reinforced concrete frame subjected to an excitation series. The frame dimensions and properties are given in Section 4.4.1, but frame is constructed with fixed supports. The nodes and element division are shown in Figure 5.12, only the main nodes are shown. Between each main node, a number of sub nodes are used.

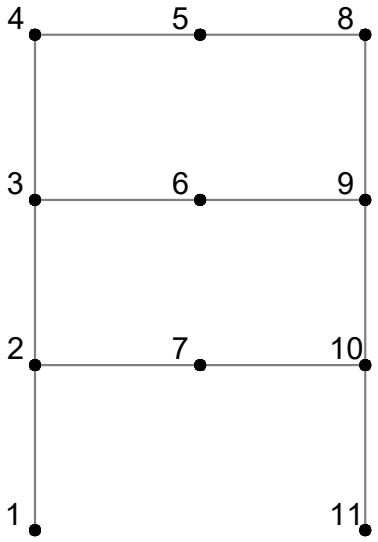

Figure 5.12: Frame nodes and element division.

The excitation is a recording from a real earthquake called *El Centro*. The data recorded, is the ground acceleration over a period of 30 s. Trailing zeroes are added to see the aftermath of the excitation on the structure. The *El Centro* ground acceleration is shown in Figure 5.13.

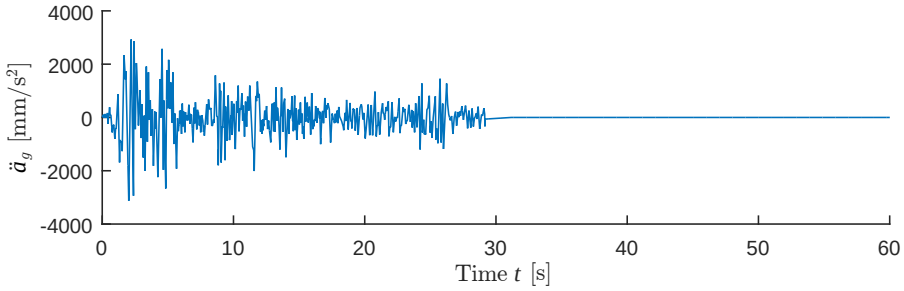

Figure 5.13: *El Centro* earthquake ground acceleration series.

As the structure is fixed to the ground, the ground acceleration is directly transferred to the foundation nodes 1 and 11. To apply the ground acceleration in the Newmark scheme, the force equivalent to the ground acceleration is calculated by use of the mass. The external force is calculated as

$$\{f^{ext}(t)\} = -[\mathbf{m}]\ddot{a}_g(t)\{\mathbf{1}\}. \tag{5.21}$$

Where $\{\mathbf{1}\}$ is a vector containing the value one at all horizontal degree of freedoms and zero at the rest.

The external force is then applied in the incremental Newmark-β scheme to evaluate the response of the frame structure. To evaluate where in the frame the largest plastic deformation occur, the relative displacement between the main nodes is calculated and shown in Figure 5.14.

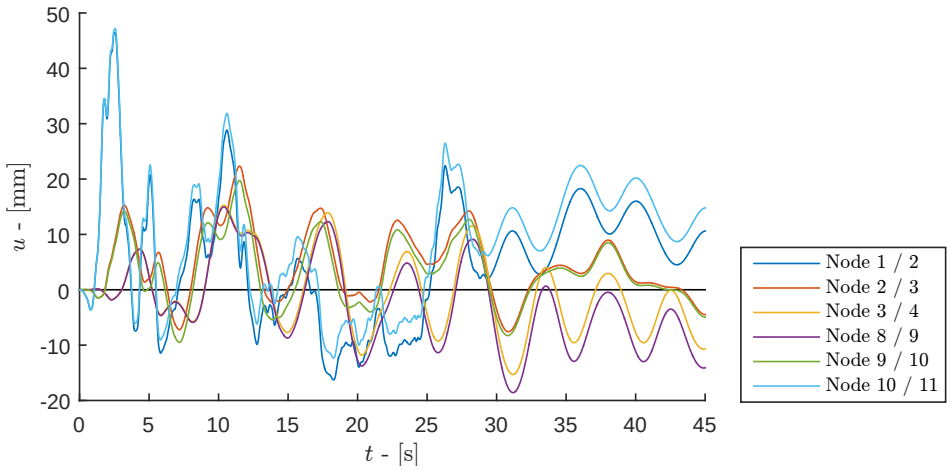

Figure 5.14: Relative displacement in the elasto-plastic system.

From Figure 5.14 it can be seen that the most deformation occurs between the main elements in the bottom of the frame, and the least at the top.

The relative displacement for the elastic system is shown in Figure 5.15.

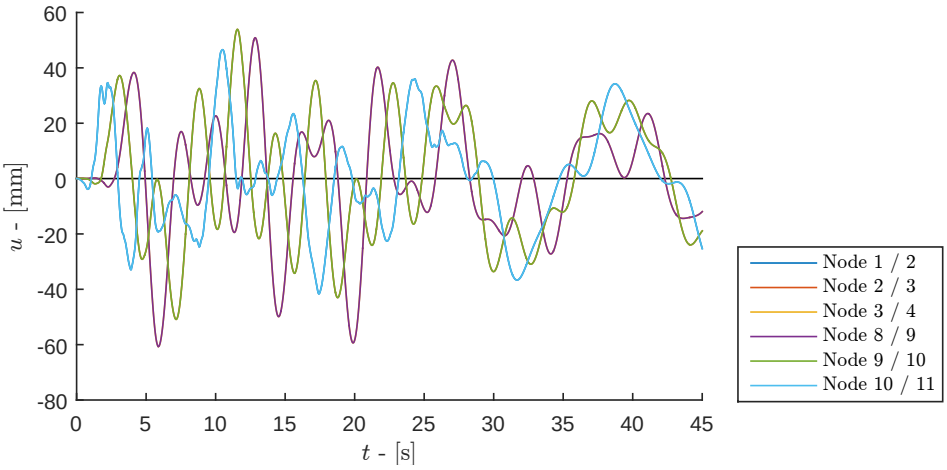

Figure 5.15: Relative displacement in the elastic system.

By comparing the elasto-plastic system with the elastic system, as seen in Figure 5.14 and Figure 5.15. It can be seen that the elasto-plastic system has smaller vibrations than the elastic, which is caused by the energy leaving the elasto-plastic system as plasticity occurs.

After the vibrations have damped out, the permanent deformation of the elasto-plastic system is shown in Figure 5.16. It can be seen that the moving of the neutral axis due to plastic deformation has caused an elongation of the beam elements.

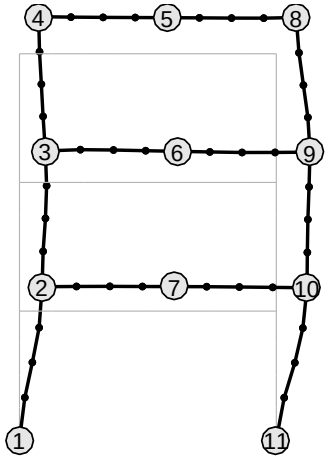

Figure 5.16: Permanent deformation of the frame.

Another application of dynamics could be moving traffic loads on a railway bridge. This scenario is analysed in the following section.

5.6 Railway bridge

In this section a small bridge carrying a railway is analysed. The bridge is subjected to dynamic loads as a moving train passes the bridge. The bridge is sketched in Figure 5.17.

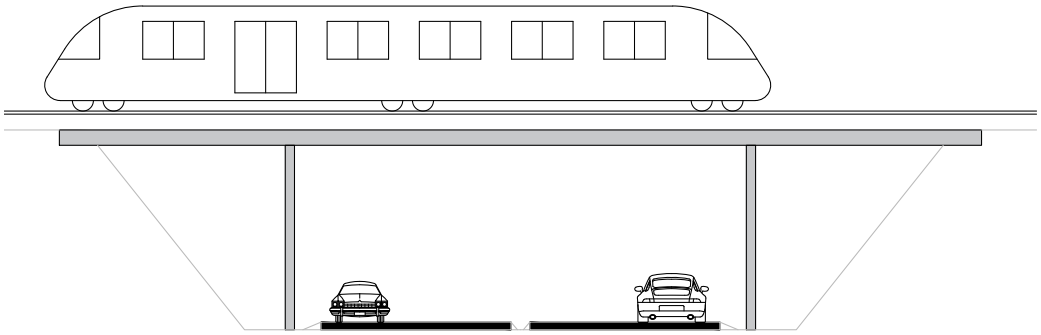

Figure 5.17: Railway bridge.

The beam and column cross sections in the bridge structure are given in Figure 5.18.

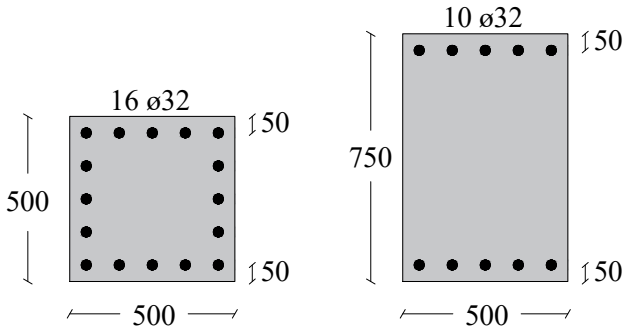

Figure 5.18: Bridge column and beam cross sections. Units in mm.

The train will cause a moving vertical load on the structure transferred at the train wheels. Thus, the load will be subjected as point loads in pairs at each shaft. This is illustrated in Figure 5.19.

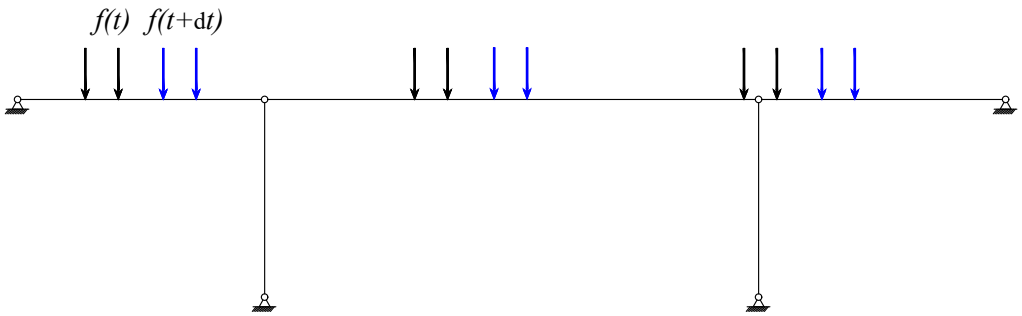

Figure 5.19: Sketch of time depending load on bridge.

The moving loads from the train will cause the bridge to vibrate. If the train is sufficiently long the load series could cause the bridge to go into resonance, which of course is critical. The resonance state and the corresponding load causing resonance is therefore interesting to investigate. Observing the node located in the middle of the bridge span, a train with two wheels per shaft and an arbitrary distance between both wheels and shafts, the external force in the middle node will be as shown in Figure 5.20.

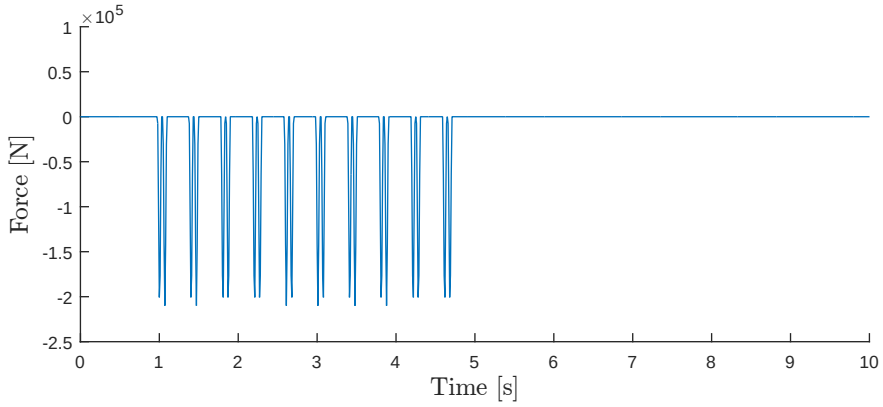

Figure 5.20: Load series for one node.

The external force is zero until the wheel is sufficiently close the node will start to detect the load. As the train is moving relatively fast the force increase and decrease quickly. This sudden load and reload will definitely cause activation of higher modes of vibration.

5.6.1 Resonance analysis

In this section, three kinds of train with different weight, shaft and wheel distance are driving across the bridge. The speed of the trains are increasing from

a fairly slow speed to a high speeding train. As the trains passes the bridge, the displacement is observed in five points shown in Figure 5.21.

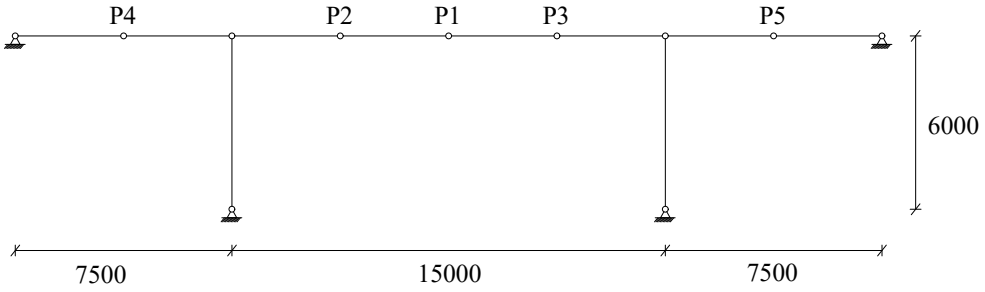

Figure 5.21: Dimensions and observed nodes on bridge during train pass. Units in mm.

The three kinds of trains used are shown in the following figures. For train 1, the dimensions and loads are given in Figure 5.22.

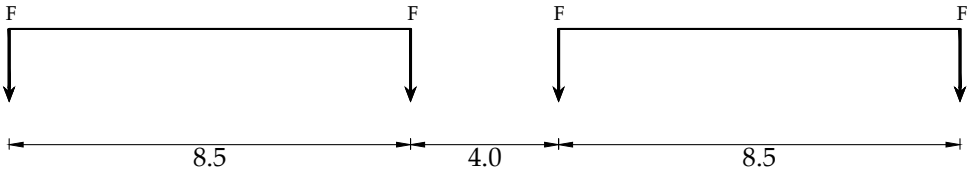

Figure 5.22: Train 1 dimensions and loads. Dimensions in m.

For train 2 the dimensions and loads are given in Figure 5.23.

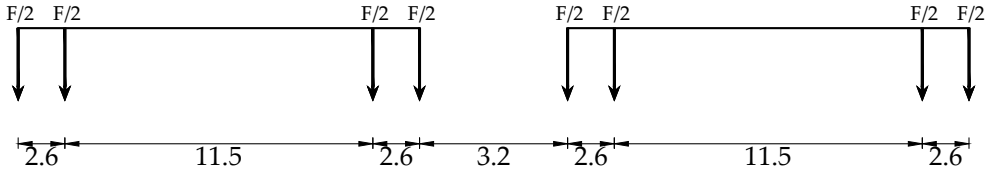

Figure 5.23: Train 2 dimensions and loads. Dimensions in m.

For train 3 the dimensions and loads are given in Figure 5.24.

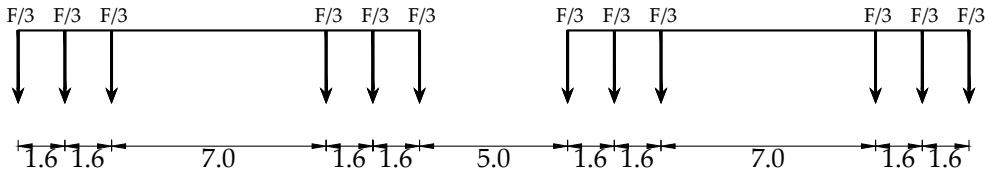

Figure 5.24: Train 3 dimensions and loads. Dimensions in m.

The load F corresponds to a shaft load of 21 ton, thus $F = 210$ kN. The load will be distributed over the number of wheel on the shaft. This is done to see the effect of distributing the load over an area or length, instead of applying the load in a point. Figure 5.22, Figure 5.23 and Figure 5.24 shows two carts for each train, in the analysis 5 carts are used.

The bridge is subjected to load series from all three trains. The train speed is increasing and the maximum displacement is plotted for each speed level for the given nodes shown in Figure 5.21. In Figure 5.25 and Figure 5.26 the maximum displacement is plotted against the train speed, for train 1, to see which speed of the train that will give the most vibration of the bridge.

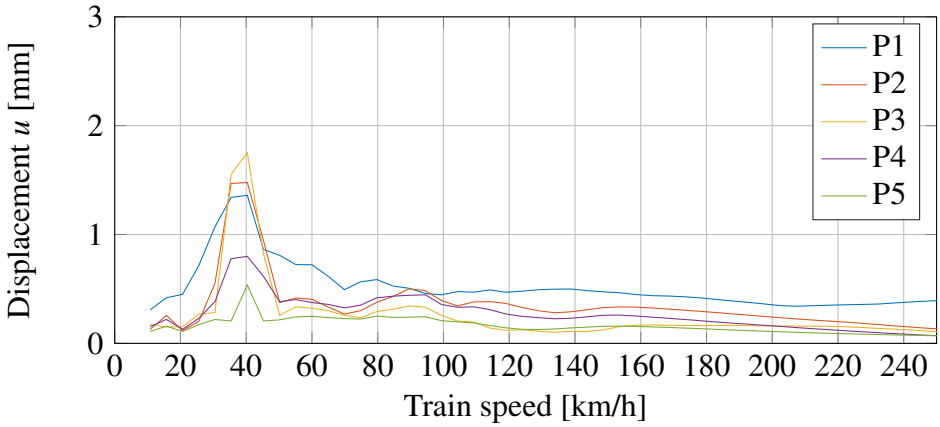

Figure 5.25: Train 1 speed/displacement diagram - linear elasto-plastic material model.

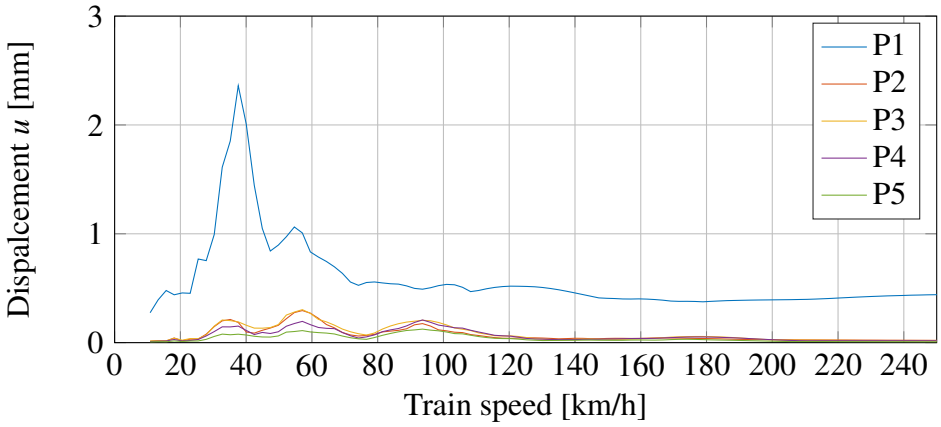

Figure 5.26: Train 1 speed/displacement diagram - linear elastic material model.

A clear peak is seen at approximately 38 km/h for both the elastic system and the elasto-plastic system. At this speed the load from the wheels seems to be in phase

with the bridge vibration, which causes the displacement to increase further. The main difference is, that the train passing by only activates one node on the elastic system, but activates all nodes in the elasto-plastic system.

The second train has two wheels per shaft. This is expected to give a less concentrated speed interval where the bridge will go into resonance. The speed/displacement curves are given in Figure 5.27 and Figure 5.28.

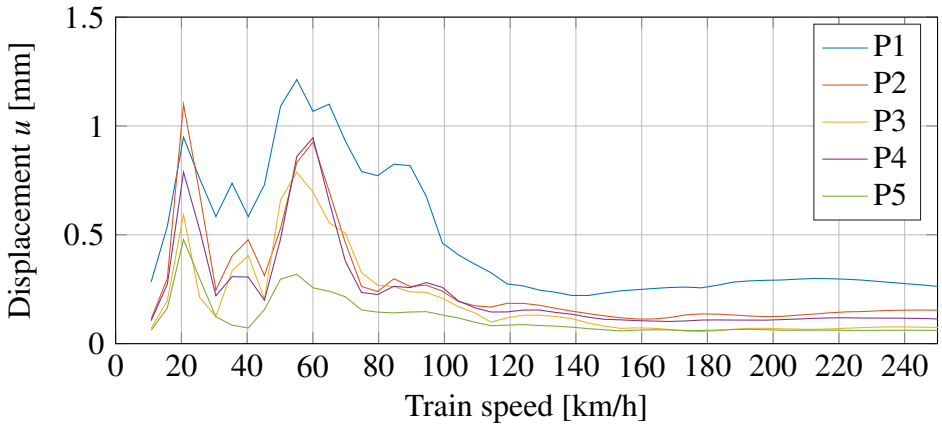

Figure 5.27: Train 2 speed/displacement diagram - linear elasto-plastic material model.

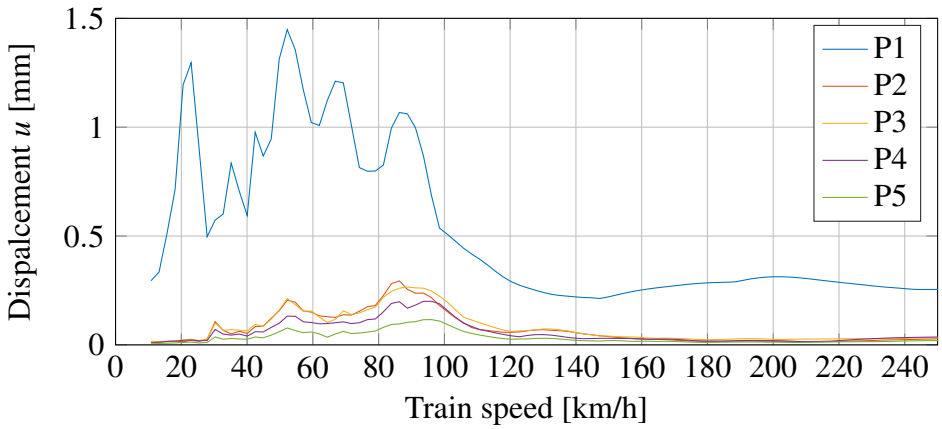

Figure 5.28: Train 2 speed/displacement diagram - linear elastic material model.

For train 2, there are a lot of peaks. Speeds from approx. 25 km/h to 90 km/h seems to give rise to a lot of vibration in P1, which is the node located at the middle of the bridge, see Figure 5.21. The speeds which makes the bridge vibrate is definitely distributed over a larger span of speeds in the elasto-plastic system. But the same tendency as for train 1 is observed. In the elastic system only one

node seems to be really activated, where the in the elasto-plastic system, all nodes along the bridge deck are vibrating.

In Figure 5.29 and Figure 5.30, the speed/displacement curves for train type 3 are shown.

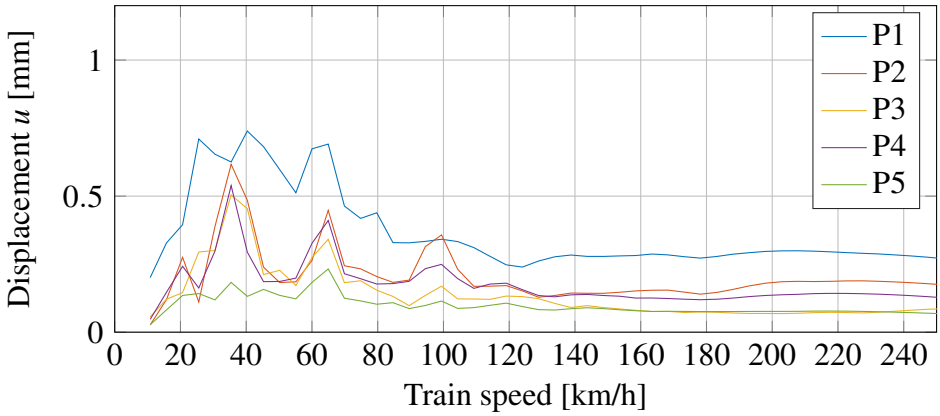

Figure 5.29: Train 3 speed/displacement diagram - linear elasto-plastic material model.

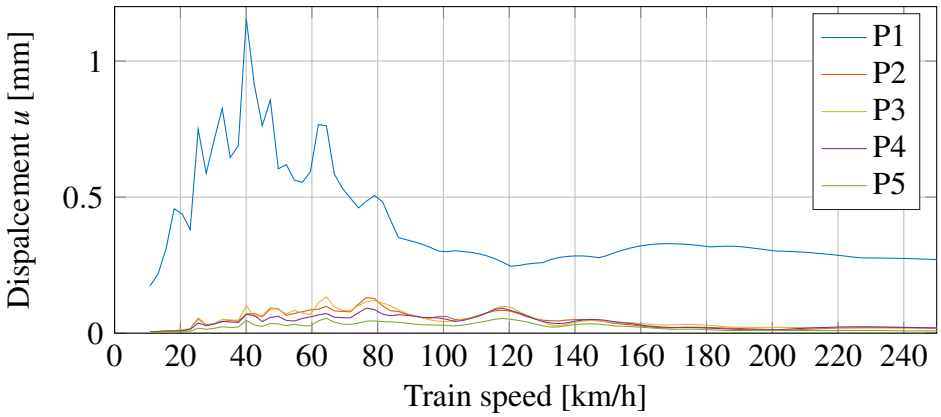

Figure 5.30: Train 3 speed/displacement diagram - linear elastic material model.

It is seen, that some train speeds are causing the bridge to fluctuate more. It is also clear, from the results, that the vibration of the bridge is hitting a sort of stable level when the train speed exceeds about 100 km/h. Hereafter, the train speed seems to be out of phase with the bridge vibration and will therefore not cause resonance.

The resonance analysis shows, that the response of the bridge follows the concentration of the force applied. When a concentrated force as train 1 with one wheel per shaft drives across the bridge with different speeds, the bridge responds to a

narrow interval of the train speeds. When the load is distributed over two or three wheels per shaft, as train 2 and train 3 does, the response of the bridge can be seen over a larger span of speeds and the fluctuations are smaller when the load is distributed over more wheels.

Summary

From the resonance study, it can be concluded that no matter which load series applied, the structure will go into resonance when the load is travelling with a given speed. This result is also found by Liu et al. [2013], who showed that when a train passes a bridge with a speed parameter corresponding to $\frac{v}{f_b d} = 1$, the bridge will hit resonance. Here, v is the train speed, d is the length of the train and f_b is the fundamental natural frequency of the bridge.

The span of speeds, where resonance is reached, vary with the concentration of the load. It is seen, that with a single wheel per shaft, the speeds where the structure will hit resonance, are limited to a more narrow spectrum than if the load is applied over two or three wheels per shaft. Here the span of train speeds are more spread, but still with significant peaks, where the response is substantial.

The difference between the elastic and elasto-plastic system is quite significant. The plasticity gives rise to some dissipation of energy leading to smaller fluctuations in the middle node, P1, but bigger fluctuations in all other nodes. This is continuous for train 1, 2 and 3.

Chapter 6

Conclusion

The goal of this project, was to develop a one-dimensional finite element program and implement plasticity. Furthermore, the program should be able to handle dynamic analysis as well.

The one-dimensional finite element program was used in an static analysis of a reinforced concrete beam and a reinforced concrete frame structure. The results were good, when compared with commercial software Abaqus. The comparison showed high resemblance between the one-dimensional finite element code and a three-dimensional model created in Abaqus.

The concrete material model started out as perfect elasto-plastic, but the behaviour was improved by adding nonlinear loading characteristics to the stress-strain curve for the concrete. This gave a slightly weaker concrete material, but ended up giving even better results, compared to the results from the Abaqus model.

A convergence study showed, that the number of elements is the most important parameter when it comes to convergence. The total number of cross section integrations and number of integration points over the cross section height, are somehow depending on the number of elements used. The choice of integration method showed, that the trapezoidal rule converged the best when observing the number of integration points over the cross section height. For integration over the beam length, the Gauss integration was independent of the number of points and the number of elements, and is therefore better suited for the task.

It can be concluded from the results obtained, that the shape functions could be improved. This would help reduce the discontinuity issues in the stresses and position of the neutral axis. The shape functions in their current form, are defining the longitudinal elongation as constant over the cross section, which is not the case. When the neutral axis position change, the longitudinal elongation will vary through the beam.

Inspired by the smeared crack model, the stress-strain relation was improved to handle unloading and reloading. This made it possible to expand the program to

include elasto-plastic dynamic analysis as well.

The free vibration study showed, that the plasticity will lead to some dissipation in energy. This energy dissipation will cause the beam to fluctuate less than a beam which is purely elastic.

The earthquake study of a frame structure showed the same behaviour. The energy dissipation will cause the frame structure to have smaller vibrations and damp out earlier.

The train bridge study showed larger vibration in the middle of the bridge for the elastic case, however the elasto-plastic system showed more vibration further away form the middle. Also, the bridge study showed, that more concentrated loads, e.g. Train 1, will cause bigger displacements and a more clear peak when the train speed cause the bridge to go into resonance. Including plasticity, will lead to a build up in displacement in the bridge deck. Including plasticity, will give a more realistic response of the system, as the energy dissipation will lead to more authentic vibrations.

Chapter 7

Reference Lists

Bibliography

Andersen, **2014**. Lars Andersen. *Structural mechanics and dynamics*. Course material and MATLAB codes, 2014.

Gavin, **2014**. Henri P. Gavin. *Numerical Integration in Structural Dynamics*. URL : http://people.duke.edu/h̃pgavin/cee541/NumericalIntegration.pdf, 2014. 24-05-2016.

Jensen, **2012**. Bjarne Chr. Jensen. *Betonkonstruktioner efter DS/EN 1992-1-1*. ISBN-13: 9788757127669, Handbook. Nyt teknisk forlag, 2012.

Krabbenhøft, **2002**. Kristian Krabbenhøft. *Basic Computational Plasticity*. Department of Civil Engineering - Technical University of Denmark, 2002.

Lee, **2007**. Yi-Kuen Lee. *DAMPING CROSS-REFERENCE*. URL : http://teaching.ust.hk/mech300/mech300_7_1_damping_ref.pdf, 2007. 16-05-2016.

Liu, Zhou, Shi, Wang, Shi, og Roeck, **2013**. K. Liu, H. Zhou, G. Shi, Y.Q. Wang, Y.J. Shi, og G. De Roeck. *Fatigue assessment of a composite railway bridge for high speed trains. Part II: Conditions for which a dynamic analysis is needed*. Journal of Constructional Steel Research, 82, 246 – 254, 2013. ISSN 0143-974X. doi: http://dx.doi.org/10.1016/j.jcsr.2012.11.014. URL `http://www.sciencedirect.com/science/article/pii/S0143974X1200274X`.

Mohamad, Farid, og Al-Janabi, **1990**. Anis Mohamad, B.J. Farid, og A.J.M. Al-Janabi. *Stress-Strain Relationship for Concrete in Compression Made of Local Materials*. Department of Civil Engineering - University of Basrah, Iraq, 1990.

Poulsen og Olesen, **2015**. Peter Noe Poulsen og John Forbes Olesen. *Bærende konstruktioner 1 - Statisk bestemte stænger og bjælker*. ISBN: 978-87-502-1107-5, Handbook. Polyteknisk Forlag, 2015.

SIMULIA, **2014**. SIMULIA. *Abaqus Theory Guide*. URL : http://130.149.89.49:2080/v6.14/books/stm/default.htm?startat=ch04s05ath119.html, 2014. 31-05-2016.

Williams og Todd, **1999**. Martin S. Williams og J. D. Todd. *Structures: Theory and Analysis*. ISBN: 9780333677605. Palgrave Macmillan, 1999.

Part III

Appendix

Appendix A

Abaqus modelling

In this chapter a model is created in commercial software Abaqus. Abaqus is a widely used program for analysing complex structures in practise and will give results to compare the model created in MatLab.

Abaqus offers many choices regarding element types, geometry, boundary conditions and load apply etc. and can be modelled to match the model in MatLab. Though, Abaqus is not capable of analysing one dimensional reinforced concrete models, the comparison with the MatLab program will not be entirely fair. Thus, the boundary conditions, element type and apply of load must be set up equally for both models.

A.1 Model

For the Abaqus model, a 3D model is chosen. This is done to compare the MatLab script against a model with a much higher complexity.

A.1.1 Boundary conditions

The boundary conditions is simple supports, implying pinned support at one edge and roller support at the second edge. The model boundary conditions are illustrated in Figure A.1.

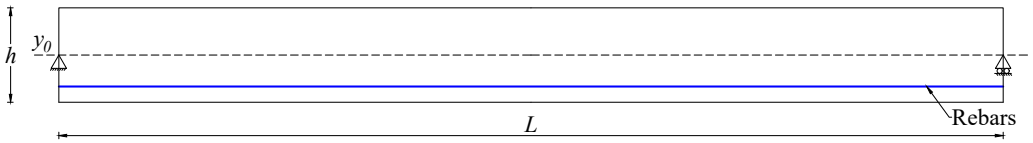

Figure A.1: Abaqus statical system.

At the right edge a support with roller is applied along the z axis to prevent displacement in the transversal directions. The roller is important to make the system statically determined.

At the left edge pinned supports are applied at the elastic neutral axis along the z axis. This is also the case with the roller support. In this case, this should give no axial deformations as the beam theory implies small displacements.

A.1.2 Loading

As the MatLab model is loaded by forced displacement, the Abaqus model should be loaded likewise. The forced displacement is modelled as an additional boundary condition. Figure A.2 illustrates the deformed model after applying forced displacement u at the top of the beam.

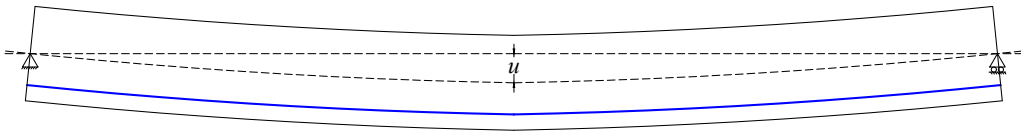

Figure A.2: Forced displacement.

A.1.3 Modelling reinforced concrete beam

The complete model will consist of a concrete block and reinforcement bars. The concrete block is modelled as a solid with $h = 300\,\text{mm}$, $b = 200\,\text{mm}$ and $L = 3000\,\text{mm}$. The reinforcement bars are modelled as trusses and assigned a cross sectional area $A_s = 339\,\text{mm}^2$ responding to 3 bars with a diameter of 12 mm.

To make the to elements interact, an embedded region constraint is applied to constrain the translational degrees of freedom of the embedded nodes. The concrete block will act as the host as this is the main region. The reinforcement bars are then embedded in the concrete block.

Element type

For the concrete block 8-node linear brick elements are used. Further, these elements use reduced integration and hourglass control. For the reinforcement bars 2-node linear 3-D truss elements are applied.

Material setup

To model a concrete beam plasticity has to be included in the material model. Thus, an elastic property is not sufficient to simulate the behaviour of concrete

to a satisfying degree. To include plasticity after yielding, a mechanical material property called Concrete Damaged Plasticity (CDP) is applied together with an elastic material property. The elastic and CDP properties are given in table A.1.

Table A.1: Elastic and CDP parameters used for concrete material model.

Parameter	**Value**
Elastic modulus, E	30×10^3 MPa
Poissons ratio, ν	0.2
Dilation angle	31 °
Eccentricity	0.1
f_{b0}/f_{c0}	1.16
K	0.6667
Viscosity parameter	0
Compression strength	30 MPa
Tensile strength	3 MPa

The reinforcement bars are modelled as elastic steel with an additional plastic feature that includes yielding. The steel material are given in table A.2.

Table A.2: Elastic and plastic parameters used for steel material model.

Parameter	**Value**
Elastic modulus, E	210×10^3 MPa
Poissons ration, ν	0.3
Yield strength, f_y	550 MPa

Appendix B

Mode shapes

The vibration of a beam in its natural frequencies causes resonance. The shape of the beam during resonance depends on the natural frequency that the beam is subjected to. The prediction of the first five mode shapes was shown in earlier in Figure 5.7. The calculated mode shapes from the MatLab script are illustrated in Figure B.1, Figure B.2, Figure B.3, Figure B.4 and Figure B.5.

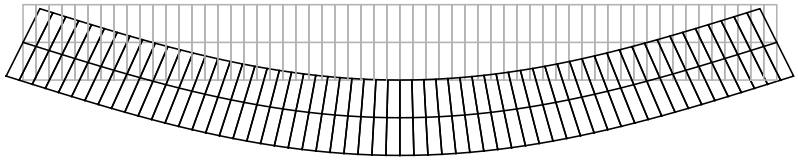

Figure B.1: Mode shape 1.

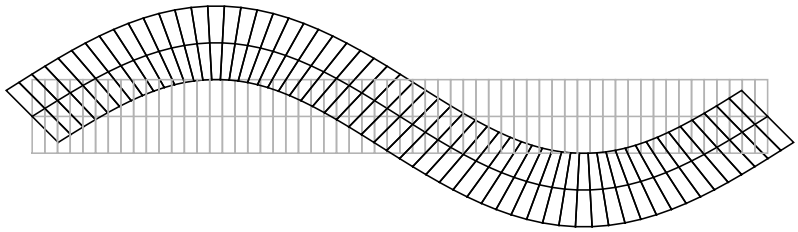

Figure B.2: Mode shape 2.

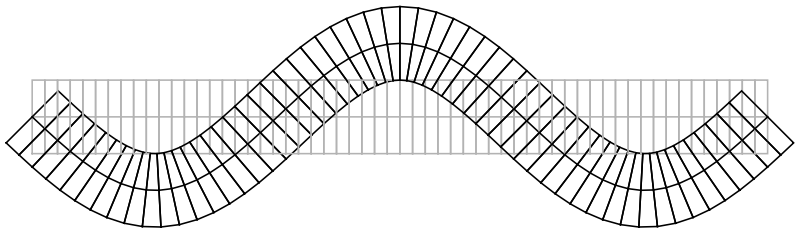

Figure B.3: Mode shape 3.

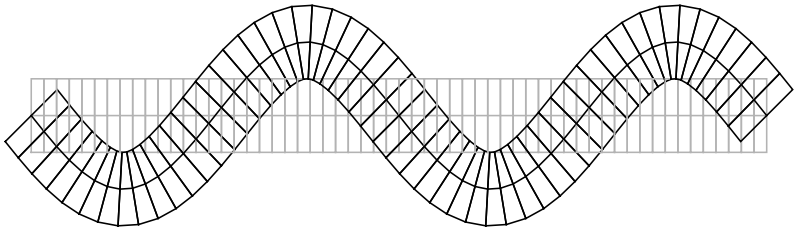

Figure B.4: Mode shape 4.

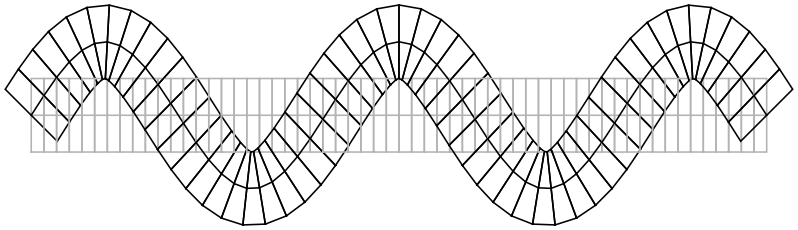

Figure B.5: Mode shape 5.

The mode shapes are close exactly the same as predicted. The mode shapes found in Abaqus is illustrated in Figure B.6, Figure B.7, Figure B.8, Figure B.9 and Figure B.10.

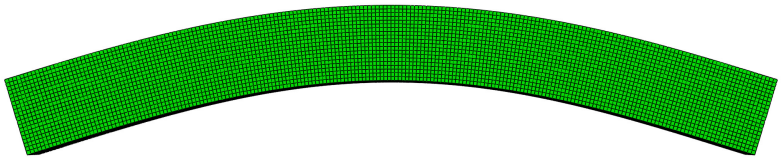

Figure B.6: Mode shape 1 - Abaqus.

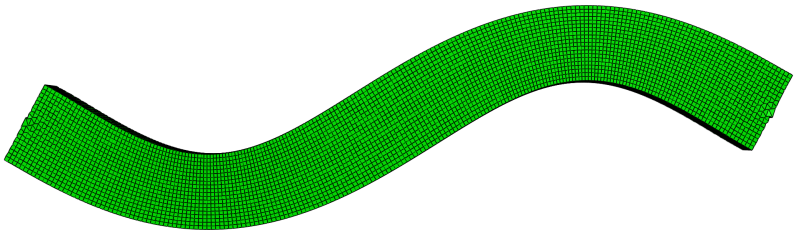

Figure B.7: Mode shape 2 - Abaqus.

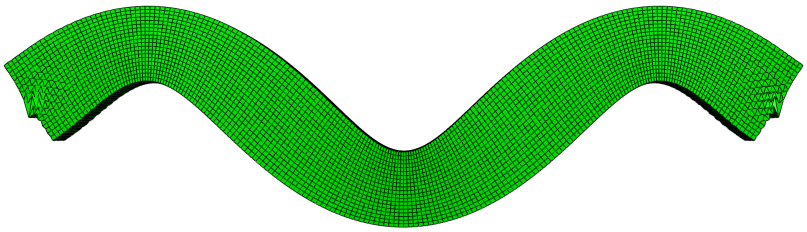

Figure B.8: Mode shape 3 - Abaqus.

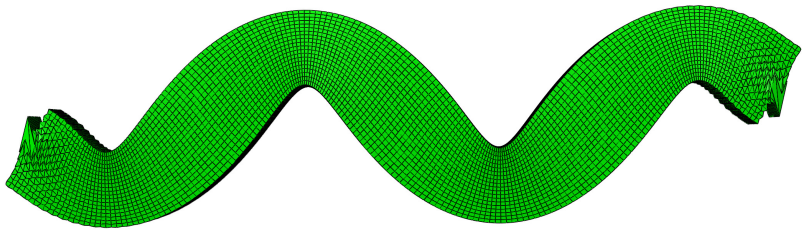

Figure B.9: Mode shape 4 - Abaqus.

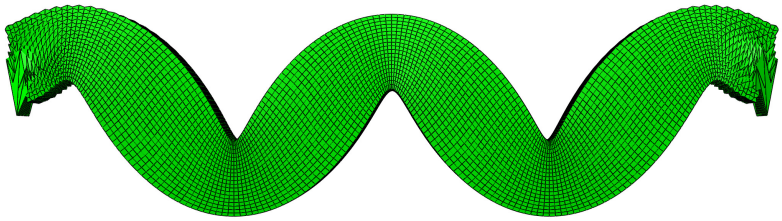

Figure B.10: Mode shape 5 - Abaqus.

Appendix C

Digital appendix

C.1 MatLab scripts

- Functions
- Graph
- Beam_1D_Dynamic_beam.m
- Beam_1D_Dynamic_bridge.m
- Beam_1D_Dynamic_frame.m
- Beam_1D_Static_Disp.m
- Beam_1D_Static_force.m
- elcentro.dat
- input_beam.m
- input_beam_force.m
- input_bridge.m
- input_frame.m

C.2 Abaqus model

- RC_beam.cae